THE DETERMINATION OF HYDROGEN EMBRITTLEMENT BEHAVIOR OF ARMOR STEELS BY EXPERIMENTAL METHODS AND THE OPTIMIZATION OF HYDROGEN BACK-DIFFUSION OPERATION

A THESIS
SUBMITTED TO THE DEPARTMENT OF ADVANCED MATERIALS AND
NANOTECHNOLOGY
AND THE GRADUATE SCHOOL OF ENGINEERING AND SCIENCE OF
ABDULLAH GUL UNIVERSITY
IN PARTIAL FULFILLMENT OF THE REQUIREMENTS
FOR THE DEGREE OF
MASTER OF SCIENCE

By
Ferdi Caner BAYRAM
May 2021

THE DETERMINATION OF HYDROGEN EMBRITTLEMENT BEHAVIOR OF ARMOR STEELS BY EXPERIMENTAL METHODS AND THE OPTIMIZATION OF HYDROGEN BACK-DIFFUSION OPERATION

A THESIS
SUBMITTED TO THE DEPARTMENT OF ADVANCED MATERIALS AND NANOTECHNOLOGY
AND THE GRADUATE SCHOOL OF ENGINEERING AND SCIENCE OF ABDULLAH GUL UNIVERSITY
IN PARTIAL FULFILLMENT OF THE REQUIREMENTS
FOR THE DEGREE OF
MASTER OF SCIENCE

By
Ferdi Caner BAYRAM
May 2021

SCIENTIFIC ETHICS COMPLIANCE

I hereby declare that all information in this document has been obtained in accordance with academic rules and ethical conduct. I also declare that, as required by these rules and conduct, I have fully cited and referenced all materials and results that are not original to this work.

Name-Surname: Ferdi Caner BAYRAM

Signature :

REGULATORY COMPLIANCE

M.Sc. thesis titled "The Determination of Hydrogen Embrittlement Behavior of Armor Steels by Experimental Methods and the Optimization of Back-Diffusion Operation" has been prepared in accordance with the Thesis Writing Guidelines of the Abdullah Gul University, Graduate School of Engineering & Science.

Prepared By   Advisor
Ferdi Caner BAYRAM   Burak BAL
Signature   Signature

Head of the Advanced Materials and Nanotechnology Program
Prof. Dr. Murat DURANDURDU
Signature

ACCEPTANCE AND APPROVAL

M.Sc. thesis titled "The Determination of Hydrogen Embrittlement Behavior of Armor Steels by Experimental Methods and the Optimization of Back-Diffusion Operation" and prepared by Ferdi Caner BAYRAM has been accepted by the jury in the Advanced Materials and Nanotechnology Graduate Program at Abdullah Gül University, Graduate School of Engineering & Science.

21/05/2021

(Thesis Defense Exam Date)

JURY:

Advisor: Doç. Dr. Burak BAL ....

Member: Dr. Öğr. Üyesi Çağatay YILMAZ ....

Member: Dr. Öğr. Üyesi Murat AYDIN ....

APPROVAL:

The acceptance of this M.Sc. thesis has been approved by the decision of the Abdullah Gül University, Graduate School of Engineering & Science, Executive Board dated ….. /….. / ……….. and numbered ……………..……… .

……….. /……….. / ………..

(Date)

Graduate School Dean
Prof. Dr. Hakan USTA

ABSTRACT

THE DETERMINATION OF HYDROGEN EMBRITTLEMENT BEHAVIOR OF ARMOR STEELS BY EXPERIMENTAL METHODS AND THE OPTIMIZATION OF BACK-DIFFUSION OPERATION

Ferdi Caner BAYRAM

MSc in Advanced Materials and Nanotechnology

Advisor: Assoc. Prof. Dr. Burak BAL

May 2021

Hydrogen embrittlement, also known as hydrogen attack or hydrogen-assisted cracking, is a process whereby metallic materials (i.e., high-strength steels, titanium alloys and aluminum alloys) become brittle or fractures due to the exposure, introduction and diffusion of hydrogen atoms through the microstructure of metals. It is a serious matter that drastically degrades the mechanical properties (e.g., ductility and toughness) of a wide range of different structural materials which include pipeline steels, armor steels, advanced high strength steels, etc. This thesis study aims to investigate the hydrogen embrittlement behavior of armor steels that conform to MIL-DTL-12560 Class 4a and MIL-DTL-46100 military specifications used by FNSS Defense Systems Inc. and to optimize the temperature and duration parameters of hydrogen back-diffusion operation to reduce the risk of hydrogen embrittlement. To characterize the embrittlement behavior of armor steels used by FNSS, various mechanical tests, including tensile tests, compression tests, high strain rate tests, hardness tests, CVN impact tests and ballistic tests, were carried out with as-received and hydrogen-uncharged specimens in order to unveil the adverse effects of hydrogen embrittlement on the mechanical properties of these steels. A cathodic hydrogen charging system was used to charge the specimens with hydrogen for mechanical tests. The effects of microstructure on the mechanical response of materials were also investigated for deeper understanding.

Keywords: Hydrogen embrittlement, Hydrogen-induced cracking, advanced high strength steels, armor steels

ÖZET

ZIRH ÇELİKLERİNİN HİDROJEN GEVREKLİĞİ DAVRANIŞLARININ DENEYSEL YÖNTEMLERLE BELİRLENMESİ VE HİDROJEN GİDERME OPERASYONUNUN OPTİMİZASYONU

Ferdi Caner BAYRAM

İleri Malzemeler ve Nanoteknoloji Bölümü Yüksek Lisans

Tez Danışmanı: Doç. Dr. Burak BAL

Mayıs 2021

Hidrojen kırılganlığı veya hidrojen destekli çatlama olarak da bilinen hidrojen gevrekliği, hidrojen atomlarının metallerin kristal kafes yapısına girmesi, difüzyonu ve maruz kalması nedeniyle bazı metalik malzemelerin (yüksek mukavemetli çelikler, titanyum alaşımları, alüminyum alaşımları, vb.) kırılgan hale geldiği veya kırıldığı karmaşık bir süreçtir. Boru hattı çelikleri, zırh çelikleri, gelişmiş yüksek mukavemetli çelikler gibi çok çeşitli farklı yapısal malzemelerin mekanik özelliklerini (örneğin, süneklik ve/veya tokluk) belirgin şekilde düşüren ciddi bir konudur. Bu tez çalışmasının amacı, FNSS Savunma Sanayi Sistemleri tarafından kullanılan MIL-DTL-12560 Class-4a ve MIL-DTL-46100 askeri şartnamelerini sağlayan zırh çeliklerinin hidrojen gevrekleşme davranışlarını deneysel yöntemlerle araştırmak ve hidrojen geri difüzyon operasyonu için sıcaklık ve zaman parametrelerini optimize etmektir. Bu kapsamda, hidrojene maruz kaldığında mekanik özelliklerin olumsuz şekilde etkilendiğini tespit etmek için, iki farklı zırh çeliğinin hidrojen yüklü ve hidrojen yüklü olmayan numuneleri ile tek eksenli çekme, basma, yüksek gerinim hızı, sertlik, darbe ve balistik testler de dahil olmak üzere çeşitli mekanik testler gerçekleştirildi. Deneysel çalışmalarda kullanılmak üzere gerekli olan hidrojen yükleme işlemi, bir elektrokimyasal hidrojen sistemi kullanılarak gerçekleştirilmiştir. Son olarak, hidrojenli ve hidrojensiz numunelerin kırılma yüzeylerinde mikroyapısal analizler gerçekleştirilmiştir. Mikroyapının mekanik özelliklere etkisi ayrıca araştırılmıştır.

Anahtar kelimeler: Hidrojen gevrekleşmesi, Hidrojen kırılganlığı, İleri yüksek mukavemetli çelikler, Zırh çelikleri

Acknowledgments

Table of Contents

List of Figures

List of Tables

List of Abbreviations

HSS	High Strength Steels
AHSS	Advanced High Strength Steels
TWIP	Twinning-induced Plasticity Steels
DP	Dual-phase Steels
TRIP	Transformation-induced Plasticity Steels
MS	Martensitic Steels
HIC	Hydrogen-induced Cracking
HAC	Hydrogen-assisted Cracking
SEM	Scanning Electron Microscopy
UHSS	Ultra-High Strength Steels
QT	Quenching and Tempering
UTS	Ultimate Tensile Strength
RHA	Rolled Homogeneous Armor
HHA	High Hardness Armor
HE	Hydrogen Embrittlement
IHE	Internal Hydrogen Embrittlement
HEE	Hydrogen Environmental Embrittlement
TDS	Thermal Desorption Spectroscopy
HIE	Hydride-Induced Embrittlement
HEDE	Hydrogen-Induced Decohesion
HELP	Hydrogen-Enhanced Localized Plasticity
AIDE	Adsorption-Induced Dislocation Emission
SFE	Stacking Fault Energy
MVC	Micro-Void Coalescence
CVN	Charpy V-Notched
DIC	Digital Image Correlation
FEA	Finite Element Analysis
STF	Stress Triaxiality Factor
EFS	Equivalent Fracture Strain

…To My Wife and My Family…

Chapter 1

1. Introduction

The first chapter aims to inform the readers about the thesis presented herein titled "The Determination of Hydrogen Embrittlement Behavior of Armor Steels by Experimental Methods and the Optimization of Back-Diffusion Operation". In the beginning, the history of steel, its importance for humanity and its different categories including the armor steels used in this study were briefly mentioned. Later on, it was talked about why the security measures were increased in vehicles manufactured by the defense industry and, accordingly, the use of advanced high-strength steels became significantly important in this sector. Subsequently, information was given about hydrogen embrittlement, which is one of the biggest obstacles to the usage of armor steels. Finally, the aim and objectives of this thesis were indicated as a subsection to make it more understandable for the readers.

1.1 Motivation and Background

From ancient times, humans have been endeavoring for developing novel materials, discovering new metals and improving existing alloy systems which have been in great demand for more than thousands of years. The alloying strategy has been used since the Bronze Age to confer desired mechanical properties. The base-element paradigm strategy involves the addition of secondary elements in relatively small amounts to the primary element, such as iron in steels and nickel in superalloys, to form new alloys. It is also widely used in metallurgy to manipulate the mechanical properties by adding some alloying elements, such as chromium for improving the corrosion resistance and manganese for enhancing the formability of steel plates. One of the most prominent additions of humankind to Earth is undoubtedly steel, which is the most popular, most important and widely used engineering and structural material. The underlying reason why it has actively been used for years in almost all applications is that it possesses remarkable mechanical properties such as high strength, good ductility, durability and most importantly low prime cost with various production methods. The banana diagram of steel

grades is given in Figure 1.1. They can be classified within three different sub-groups by their tensile strength as follows;

- ➢ Mild Steels, tensile strength is less than 300 MPa
- ➢ High Strength Steels (HSS), tensile strength is between 300 MPa and 700 MPa
- ➢ Advanced High Strength Steels (AHSS), tensile strength is bigger than 700 Mpa

The demand for HSS increased due to the developing technology and the globalizing world towards the end of the last century because they were extensively used in a wide variety of applications such as automotive, defense, marine, transportation, etc. As the practicability of these steels was increased, modification on existing high strength steels was performed and a new steel category has come to the forefront namely AHSS [1].
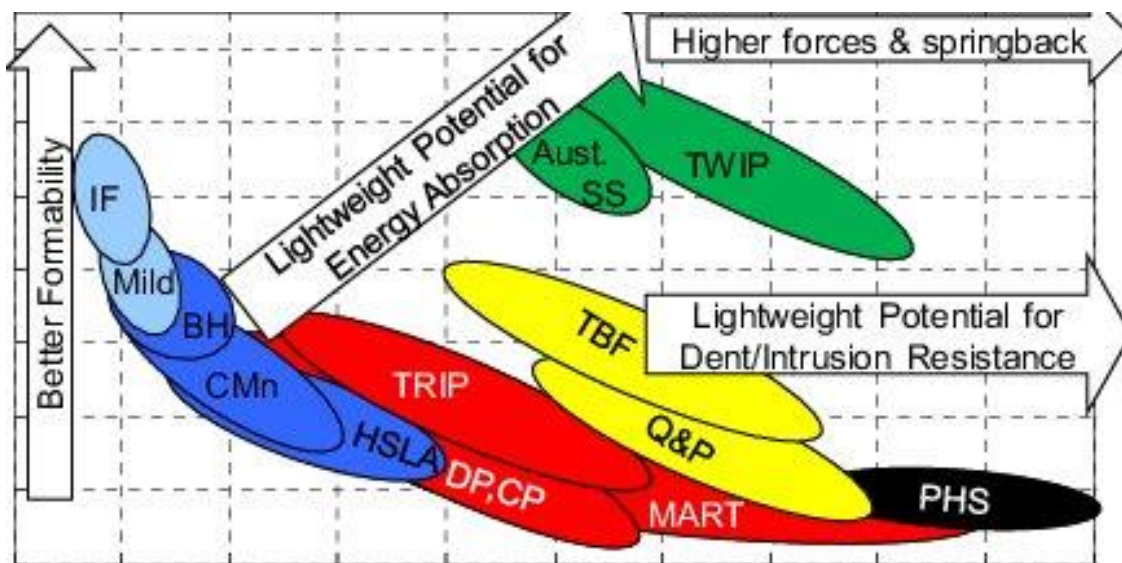
Figure 1.1 The banana diagram of steel grades [2]

The biggest advantage of using AHSSs is their formability and good strength-ductility trade-off when compared to conventional HSS and mild steels. Some of the well-known AHSS are Twinning-induced plasticity (TWIP) steels, Dual-phase (DP) steels, Transformation-induced plasticity (TRIP) steels and Martensitic steels (MS). MS shows remarkable strength and moderate ductility. Therefore, it is commonly used and preferred in the defense industry which requires high strength values to confer ballistic requirements in case of danger.

The defense industry is an industrial sector that can manufacture and maintain the tools, equipment and weapons, ammunition required for the defense of the country. It has an important role for countries in terms of better defense integrity, economic independence and reducing external dependency. The ability to manufacture all kinds of tools and types of equipment by private or public institutions constitutes the defense industry. The main purpose of the defense industry is to eliminate threats in the shortest time, most effectively and with the minimum cost.

Therefore, advanced technology is used most intensively in this sector. The technological developments reached in this age and the diversity of internal-external attack threats make it necessary to give importance to defense products based on advanced technology and the level of development. Since the defense industry uses very advanced technologies, research and development activities are carried out in a very intense way. The emergence and development of the defense industry have been due to the necessity of countries' need to defend themselves because an effective defense mechanism is an important guarantee for the future of countries. Terror-related activities and cases, which started to operate especially during the cold war period, started to increase all over the world after the September 11 attacks on the twin towers. Considering the current records as of 2020, terrorist incidents have increased dramatically every year, especially in the Middle East.
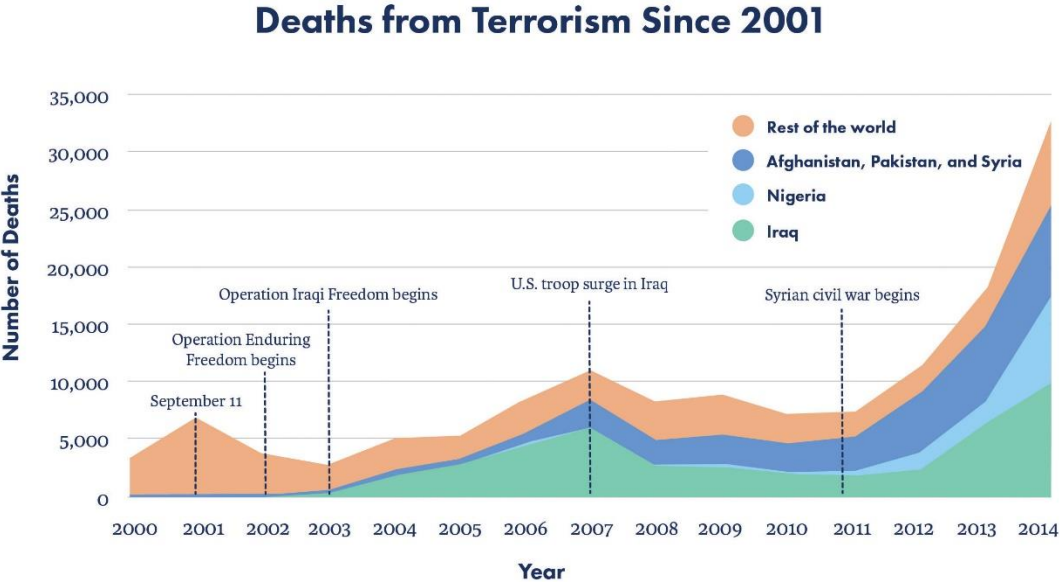
Figure 1.2 The number of deaths related to terror attacks from 2001 to 2014 [3]

Figure 1 shows the number of casualties from terrorism in the period of 2001 and 2014. Even after 2014, many terror incidents were seen including Europe and America. Therefore, terrorism and terrorist incidents, have pushed countries to be more meticulous in defense and open to strategic and technological developments to protect themselves from foreign powers. For this reason, developed and developing countries have significantly increased their investments in the defense industry in recent years in order to protect their territorial integrity and to make an economic contribution. To preserve their national sovereignty and economic independence and to have a say in world politics, military power should be more effective than other countries. Therefore, countries have increased the diversity of weapons and defense

industry products and the budgets spent on defense have increased significantly compared to previous years.

Military expenditures by country

- **38%** USA
- **14%** China
- **3.7%** India
- **3.4%** Russia
- **3.2%** Saudi Arabia
- **2.6%** France
- **2.6%** Germany
- **32.5%** Rest of the world

Legend:
- USA
- China
- India
- Russia
- Saudi Arabia
- France
- Germany
- Rest of the world

Source: Stockholm International Peace Research Institute (SIPRI), April 2020
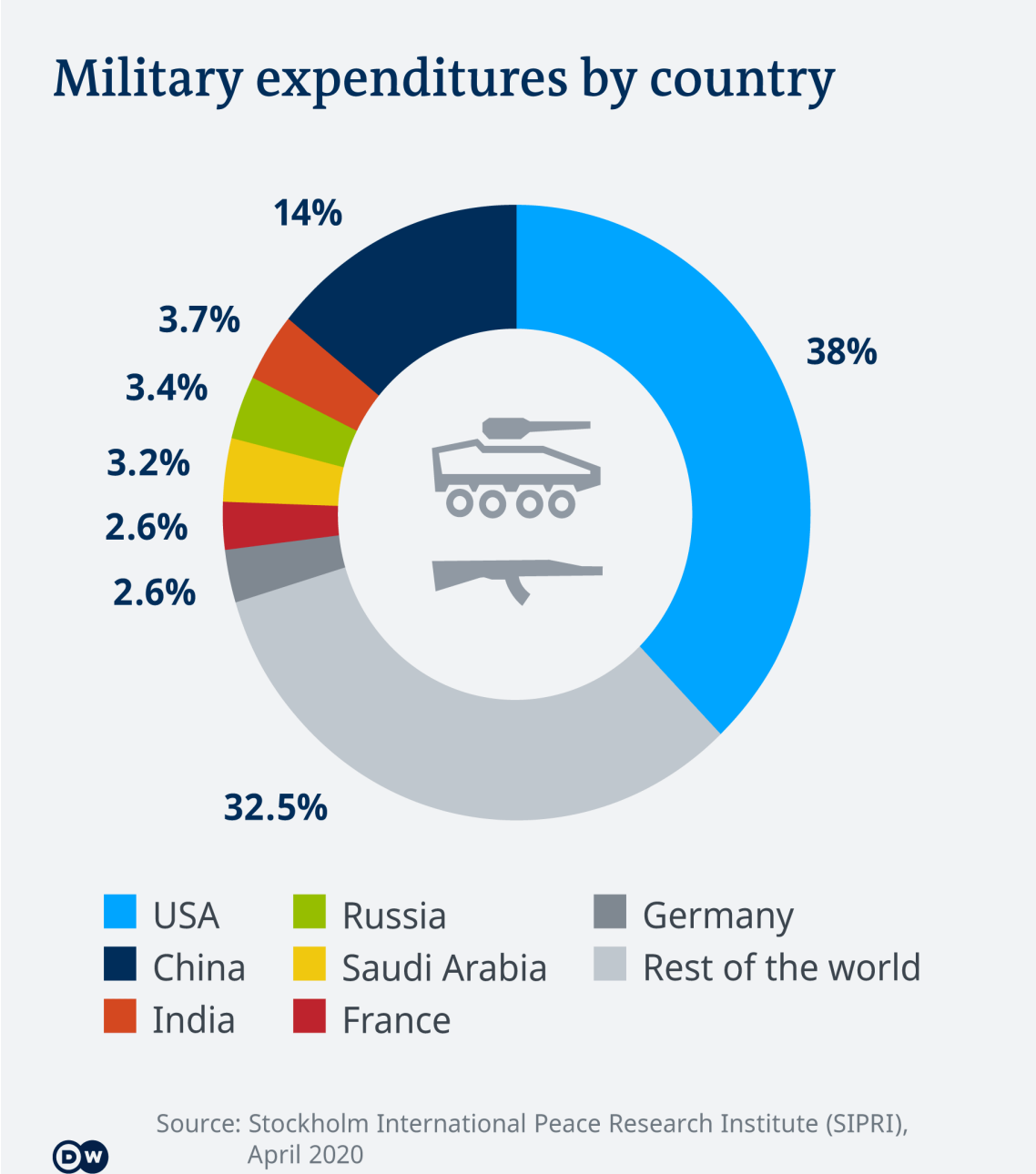
Figure 1.3 The military expenditures of countries according to SIPRI report [4]

These countries allocate billions of dollars from their budgets for the defense industry each year (as shown in Figure 1.2) and are among the countries that constitute the largest shares from their budgets. Despite spending billions of dollars every year, the sector has a positive effect on the budget, as a certain part of all these investments contribute to the economy through exports. Turkey is also one of those countries which have increased the defense expenditures in recent years. Turkey's military spending has increased 86 percent over the last 10 years and reached 20.4 billion dollars in 2019. Moreover, the domestic and international sales data of

Turkey's defense industry has reached up nearly 11 billion dollars, of which 3.1 billion dollars came from exportation. The defense industry sector has to keep up with constantly changing and developing technological developments. Countries that cannot catch up with the recent technological developments of the age have great difficulties both in terms of protecting themselves from external threats and at the point of a solid economy. For this reason, the countries that could not develop their skills in this field became more dependent on foreign countries since it is the sector most affected by the developments in technology and it is the driving force of the country's industry compared to other industrial sectors. To give an example, while Turkey cannot export unmanned aerial vehicles due to the various sanctions nearly ten years ago, it now produces its own armed/unmanned aerial vehicles and exports them all around the world. Besides, the reforms in the defense industry have brought Turkey to the position of exporting countries from the importing country. The defense industry should not be considered only as a commercial concern. Besides that, it is an industrial organization that considers essential criteria such as reliability, strategy, independence, low external dependency and technological issues. Since the most advanced technologies are used in the defense industry, system developments and Research and Development (R&D) studies are quite expensive compared to other sectors. Even if it is very costly to develop advanced technology, they convert a certain part of their investment into economic input through export. And these high-profit margins create a positive effect on the sector and encourage companies to invest.

The huge investments, which have been made by both public and private sector over the last fifteen years, in the defense industry has begun to bring some positive results economically and strategically [5,6]. In 2010, only ASELSAN appeared in the "defense news" article, where the top 100 defense industry companies were announced regularly every year. When it comes to 2020, Turkey has been involved with seven companies (ASELSAN, TAI, BMC, ROKETSAN, STM, FNSS, HAVELSAN) on the list [7]. This success achieved by Turkish defense industry companies is the most advanced technology and deep research and development phase used in products. The main purpose of defense industry companies is not to gain maximum profit with minimum cost compared to companies in other industries. The main goal is to have high performance and quality rather than minimum cost and maximum profit [8]. The defense industry sector operates to produce the necessary materials for military defense and offers a wide range of products including armored vehicles, tactical wheeled vehicles, unmanned aerial vehicles, helicopters, etc. [9]. Many different types of materials are used in these high-tech products such as metals, composites, plastics, and one of which is armor steels. Armor steels are classified under a special class of high strength steels. These armored steels

are widely used for the production of armored combat vehicles, tactical wheeled vehicles and weapon systems.

Figure 1.4 Armored combat vehicles produced by FNSS Defense Systems Inc.

The reason why armor steels are preferred is that they possess some excellent characteristics such as high resistance to bullet and explosive impacts, high strength and toughness [10,11]. Moreover, good weldability and low production costs also make them preferable candidates over aluminum alloys, ceramic, glass and fiber-reinforced composite materials. Even though these armor steels have remarkable mechanical properties and are widely used in the defense industry, AHSS are very susceptible to hydrogen embrittlement (also known as hydrogen-induced cracking (HIC) and hydrogen-assisted cracking (HAC)) [12,13]. Hydrogen embrittlement can be defined as the result of the diffusion of hydrogen atoms into metallic materials that cause loss of ductility and reduction of load-bearing capacity. This problem mainly arises from the fact that as the strength of the materials increase, they become more vulnerable to hydrogen embrittlement because the material turns into a harder and less ductile form. High-strength steels are extensively used in some critical applications such as marine, automotive, construction, defense industry and aerospace [14–16]. Considering the extremely costly usage areas and applications of high-strength steels, the prevention of hydrogen embrittlement phenomena has become a primary concern for manufacturers. Otherwise, it will cause unexpected catastrophic brittle failure and loss of millions of dollars. The nature of hydrogen embrittlement has not been fully understood yet [17–19]. Therefore, it is a potential risk factor for armor steels as well as other high-strength steels. While numerous studies have been conducted to improve the physical, mechanical, and ballistic properties of armor steels, there is only a limited number of studies to prevent the hydrogen-related cracks for armor steels. To fill this gap, this thesis focused on the determination of hydrogen embrittlement behavior of armor steels used by FNSS Defense Systems Inc. by different experimental methods and also

the optimization of hydrogen back-diffusion from armor steels investigated. In the following chapters, the topics will be covered as follows;

- ➢ The class of armor steels and specific armor steels used by FNSS
- ➢ hydrogen embrittlement phenomena and detrimental effects on high strength steels (specifically armor steels)
- ➢ The experimental studies performed to reveal the hydrogen effect on armor steels
- ➢ The hydrogen back-diffusion operations and the optimization of time and baking temperature parameters

1.2 The Aim and Objectives

Armor steel plates are commonly used in the body manufacturing of tracked and wheeled armored vehicles produced by FNSS Defense Industry Inc. They are commonly used as the main component of the hull in all armored combat vehicles. For this reason, large-scale experimental studies, including tensile/compression tests, Charpy impact test, high temperature and high strain rate tests and hardness test, are required on armor steels in order to determine the static, dynamic and ballistic and mine protection behaviors of the vehicle body. Mechanical characterization of armor steels to cover all operating conditions is mostly possible with these experimental studies. Experimental studies are also used to calculate the constitutional equations of the material and often the necessary coefficients of these equations. Later on, it is used in computer-based simulation studies. The mechanical behavior of the armor steels from which the bottom plate of the hull is produced is of great importance in terms of ballistic protection requirements and protection level against mine explosion, since it is clearly defined in the project contracts of FNSS Defense Industry Inc. Therefore, more detailed mechanical analysis is obligatory to satisfy the requirements for the armor steel material of the bottom plate. With the help of the ongoing studies (tensile /compression tests, micro/macro hardness tests, etc.) inside and outside of FNSS, highly developed material library knowledge is currently present especially for the armor steels it uses in the vehicles it designs. Numerous studies have been carried out to determine the material constitution equations and damage behaviors specific to armor steels. The samples used in experimental studies were tested before any manufacturing process such as laser cutting, welding, bending, etc. However, hydrogen atoms can be introduced into armor steels during these production processes by the effect of high temperature and pressure. Once the concentration of atomic hydrogen reaches a critical level within the microstructure, it may lead

to the embrittlement of material that is unwished for the sake of manufacturers. As it was aforementioned earlier, high-strength steels are a group of materials with high susceptibility to hydrogen embrittlement. Thus, the issue of hydrogen embrittlement emerges as a factor to be considered for armor steels. Armor steels are subjected to many manufacturing methods such as casting, heat treatment, rolling, laser cutting, welding, etc. During these operations, hydrogen can diffuse into microstructure and be trapped in vacancies, grain boundaries or dislocation sites. Therefore, it is essential to carry out detailed research which covers the detrimental effect of hydrogen presence within the material microstructure. Although numerous research studies to understand hydrogen embrittlement behavior of high strength steels were performed and found in the literature, no notable research for the hydrogen embrittlement behavior of armor steels in the literature is present. Hence, this thesis study presented herein is of great importance to shed new light on a vital but rarely studied important subject.

Figure 1.5 The cracks thought to be caused by hydrogen during production process a) after laser cutting, b) after welding, c) after bending process

This thesis aims to investigate the effects of the hydrogen embrittlement phenomenon on the armor steels used by FNSS, which may cause abrupt failures of structural components during both in the manufacturing processes or in-service environments and affect their ballistic and mine protection requirements. In this respect, an electrochemical hydrogen charging system was established to introduce hydrogen atoms into microstructure and the validation of this system was carried out to make sure that hydrogen is charged properly. Later on, various experimental methods which include tensile, compression, hardness, high strain rate, Charpy impact test, etc., were applied to characterize the behavior of abovesaid armor steels. Following this mechanical characterization part, the hydrogen bake-out process was employed to optimate the baking parameters of armor steels which are temperature and duration. To do this, specimens were charged with hydrogen and then baked at certain temperature and duration values in accordance with ASTM B850 – 98 standard. In addition, detailed microstructure studies (SEM, Optic Microscopy) were carried out on as-received and hydrogen charged specimens used in the mechanical tests. Finally, ballistic tests were performed for two different armor steels with and

without hydrogen charged specimens to observe the effect of hydrogen on the ballistic performance.

Chapter 2

2. Research Related to Armor Steels

This chapter aims to give a piece of detailed information about mechanical properties, production stages, heat treatment processes and chemical compositions of armor steels used in the defense industry. The content was enriched by giving comparative tables of mechanical properties, chemical compositions and alloying elements of armor steels in the subsections of this chapter. Moreover, this chapter was strengthened by providing information for the armor steels conforming to MIL-DTL-12560 Class 4a and MIL-DTL-46100 standards used by FNSS Defense Systems Inc. for the production of armored vehicles.

2.1 Armor Steels and Their Properties

Armor steel is also called protection steel or ballistic protection steel. They're classified in the class of AHSS (sometimes called ultra-high-strength steels (UHSS)) aimed to resist cracking, fragmentation and breakage against multiple impacts of bullets with different characteristics. Armored materials have been excessively used in many lands, air, sea and even spacecraft for both civilian and military purposes. For civilian purposes, armor materials are used for VIP cars and money transportation cars. On the other side, they are used to produce armored vehicles, helmets, armored vests, body-guard, etc. Steel and aluminum alloys, ceramics, glass and fiber-reinforced composite materials are used as armor materials. At present, the most common armor material used in tanks and similar defense vehicles is steel. Even under harsh conditions, armored combat vehicles must resist cracking, fragmentation and breakage against violent attacks such as highly explosive and disintegrating warheads. Therefore, structural armor steels ought to contain a high-quality homogeneous microstructure. The three most basic properties expected from armor steels are as follows;

- High resistance to ballistic impacts and perforation
- Convenience in manufacturing (cutting, welding, shaping, etc.)
- long service life such as high fatigue resistance

They possess remarkable mechanical properties such as high strength, prominent hardness and moderate ductility and these prominent features satisfy the demand of manufacturers and required ballistic performance in the field [20–22]. Protection of various surfaces (engine, underbody, crew, hull back compartment, ammunition and turret) and providing the highest protection against other ammunition is of great importance for armor steels. The desired properties of strength and hardness are achieved by choosing medium carbon steel. Because carbon needs to be limited for the sake of good weldability. The production of armor steels is carried through casting in ingots within standard compositions and produced in sheet metal form. However, the desired mechanical properties are not obtained at the end of casting. Therefore, austenitization, tempering and quenching processes should be applied to achieve martensitic microstructure to gain outstanding features satisfying ballistic performance. By doing so, the strength and toughness are balanced. The saturation of carbon and carbide forming alloy elements in austenitization and the precipitation of carbide depending on temperature and time in tempering is to play an active role in the balancing of mechanical properties. There are plenty of armor steels produced by different brands with different mechanical properties for different purposes in the market. SSAB, Swebis and Swebor are some of the well-known producers.

Table 2.1 The comparison of armor steels in the market [[23],SSAB, Arcelormittal]

Type of armor steel	Hardness	Toughness (Joule) (-40 °C)	Yield Strength (YS) (min MPa)	UTS (MPa)	Plate Thickness (mm)
MIL-A-12560 (Class I)	34-40 HRC	21.6	1150	1250	25.4
MIL-A-12560 (Class II)	29-34 HRC	28	1175	1350	25.4
MIL-A-46100	50-53 HRC	13.5	1100	1600	25.4
MIL-A-46173	477-601 HB	30	>1100	>1700	25.4
Armox 370 (Class II)	280-330 HBW	60	800	900-1100	6-59.9
Armox 500	480-540 HBW	32	1250	1450-1750	4-20
Ramor 400	360-460 HBW	-	-	-	2-30

Mars 300	578-655 HB	>8	>1300	>2000	3-25
MIL-DTL-12560 (Class 4a)	302-400 HB	30	1200	1450	5-40
MIL-DTL-46100	477-534 HB	20	1250	1600	2.5-40

In table 2.1, some of the armor steels purchased in the market with different hardness, toughness and plate thicknesses are tabulated. Most of the data were provided from the websites of producers. It is obvious that all these armor steels serve in different application areas due to their different mechanical properties. The purpose of the continuous progress and the development of protection levels in armor technology is that the ballistic protection resistance required to be created against the damage caused by changing weapon technology and ammunition must be kept at the highest level. The high strength values that armor steels possess, which can reach with high toughness, are possible by showing the same strength in every part of the material. This is accomplishable with the homogeneously distributed same toughness and hardness values in all parts of the structure to be formed [24]. During the penetration process, which starts with the ballistic destructor hitting the target, the mechanical strength properties of the target must be higher in order to minimize the damage level of the destroyer so that a high level of protection is provided. Thus, the progress in armor technology ought to be continuous to minimize the risks during the service.

2.2 Production of Armor Steels and Heat Treatment

Despite various materials (ceramic, composite, etc.) are used to manufacture armored products, steel is widely preferred as a common armor material for defense purposes because of its relatively easy manufacturability. The reason why steel materials are preferred is material properties such as high strength, toughness and combinability, which are indicative of the high material properties [25]. Armor steels are classified in the alloyed steel group in terms of their chemical composition. When examined metallurgically, it is known that martensitic structure is observed in their microstructure. As shown in Figure 2.1, melting, alloying, casting, hot rolling, heat treatment, sanding-painting and packaging operations are applied in the production process of armor steels.
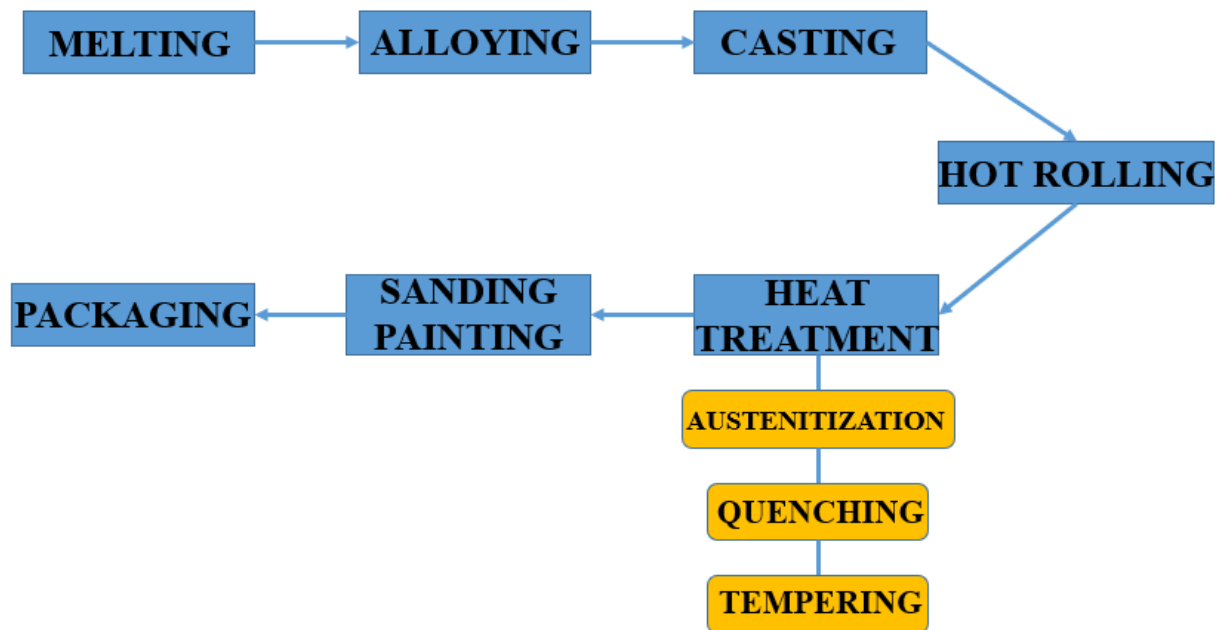
Figure 2.1 The production process of armor steels and applied heat treatment [25]

The alloyed steel, which is formed through the addition of Ni, Cr and Mo alloying elements into melted metal in the oxygen furnace, is made solid in slab form by applying a continuous casting process. After that, the hot rolling process is performed in usage dimensions. After the rolling process is completed, a couple of heat treatment series including austenitization, quenching and tempering is applied to the produced armor plates in order to achieve the targeted strength and toughness values and turned into a final product. Heat treatment is a widely utilized method to enhance the desired mechanical and metallurgical properties in steel. The microstructure of produced steel is saturated enough with both C element and carbide-forming alloy elements by the austenitization process performed at temperatures of 900-950 °C. The microstructure is transformed into martensite as a result of the subsequent quenching process. Martensitic steels provide the highest strength among all microstructures produced by heat treatment. Due to the excessive residual stresses associated with martensitic transformation, it is only used in such applications which require high strength and hardness. After quenching, tempering is applied to the armor steel in order to remove the rising hardness and gain the desired toughness. Tempering is typically applied to increase the impact of energy absorbed by the material. Controlling the temperature and time parameters in the tempering process also plays an important role in determining the mechanical properties of steel. Finally, the plates are packed after sandblasting and painting.

Table 2.2 Desired properties in line with manufacturing processes in armored steels

	Manufacturing Processes			
	Thermal Cutting	Welding	Machining	Shaping
Essential Metallurgical Properties	*low carbon equivalent *limited segregation *very low hydrogen content	*low carbon equivalent *limited *very low hydrogen content *low residual stress	*limited harness	*high ductility

Suitable metallurgical properties should be provided to minimize manufacturing difficulties during application. The most suitable metallurgical conditions for various production stages are illustrated in Table 2.2. Since the movements of light or heavy vehicles in different rough terrain and heavy weapon hits are inevitable, high fatigue resistance in the welding areas is a necessity for armor steels. Stress corrosion problems may arise in hard armor steels over time (HB> 500). When exposed to a corrosive environment, corrosion increases, especially in the stressed areas. With the development of technology, hardness values in armor steels are in the increasing trend over years. In order to minimize the loss in toughness values due to the increased strength and hardness, the amount of sulfur and phosphorus elements was decreased by secondary metallurgical processes [23].

2.3 Alloying of Armor Steels

Steels made by adding one or more alloying elements are called alloy steels. They are used in order to provide unique properties which cannot normally obtain from carbon steels. The main alloying elements found in steels are Carbon, Manganese, Silicon, Sulphur, Phosphor, Chrome, Nickel, Molybdenum (Mo), Vanadium (V), Wolfram (W), Niobium (Nb), Titanium (Ti), Cobalt (Co), Aluminum (Al), Boron (B), Copper (Cu) and Nitrogen (N). The effect of alloying elements on determining of mechanical properties of steels is incontrovertibly high. For example, the carbon content up to 0,8% increase the tensile strength and yield point. However, the brittleness increases above this value. The role and contribution of each alloying element to the mechanical properties are different from each other. Therefore, the usage and the content of alloying elements are highly dependable on applications.

Table 2.3 The chemical composition (%) of alloying elements in different armored steels[[26],SSAB, Arcelormittal]

Chemical [%] Composition	MIL-A-12560	MIL-A-46100	MIL-A-46173	Armox 500	Mars 300	MIL-DTL-12560	MIL-DTL-46100
Carbon	<0.30	<0.30	0.37 max	0.32 max	<0.55	0.26	0.3
Manganese	1.20	0.95	0.90	1.2 max	<0.7	1.5	1.7
Sulphur	0.005	0.005	0.005	.003 max	<.002	-	-
Phosphor	0.012	0.012	0.012	.010 max	<.010	0.030	0.030
Silicon	0.2-0.4	0.2-0.4	0.2-0.4	0.4 max	<1	0.015	0.015
Nickel	1.8 max	1.85 max	3.0 min	1.81 max	2.4	0.7	0.8
Chrome	1.0	1.6	1.9 max	1.01 max	<0.4	1.50	1.50
Molybdenum	0.3-0.5	0.5	0.3-0.5	0.7 max	<0.5	0.5	0.5

The classification of armor steels varies by their composition and usage areas. The chemical composition of several armor plates of steel is given in Table 2.3. In addition to the main alloying elements seen in the table, elements such as vanadium, titanium, niobium, aluminum, boron are also available, albeit a little. When armor steels are classified according to the American standard, they receive the MIL code. On the other hand, Mars is the code that corresponds to the French military standard. Armor steels generally possess low carbon percentages within the microstructure. It is important to note that the 3% carbon value is an important limit in terms of weldability because the optimal balance of toughness and hardness is negatively affected after 3% and thus the weldability decreases. Moreover, the amount of molybdenum remains between 0.3-0.7% and prevents the grain growth and brittleness in the microstructure by avoiding carbide precipitation at the grain boundaries. Molybdenum, vanadium, titanium, niobium alloying elements have a grain refining effect which is important to improve mechanical properties.

2.4 Armor Steels Used in Experimental Studies

The production techniques of UHSS steel plates could be classified under two different sub-groups which are pronounced as thermo-mechanical control process (TMCP) and quenching and tempering (QT) process. TMCP is a steelmaking technique developed by

Japanese scientists in the 1980's which is comprised of controlled rolling and controlled cooling processes [27]. It was designed to enhance the mechanical properties (high strength, weldability and toughness) of steel plates [28]. The second sub-group of the UHSS steel production technique is the QT process which consists of quenching and tempering two-stage of heat treatment processes. This technique is too often used in order to produce high-quality heavy plates and armor steels could be considered as a member of QT steels. As its name signifies, the quenching process is the very rapid cooling of the metallic material somewhere from above its recrystallization temperature to room conditions which induces a martensitic transformation from the austenite phase. In order to improve the characteristics of steels, the tempering process is applied to obtain greater toughness and ductility properties in a trade-off with hardness [29,30]. The quenched steel is heated to below the critical point for a length of time, then allowing it to cool by air. Tempering parameters, temperature and heating time, are highly dependent on the composition of steel which will decide the amount of hardness removed. As might be expected, armor steels possess an almost fully martensitic microstructure [31,32]. A small amount of austenite phase would be retained during the rapid cooling and existed in the microstructure. The ultimate tensile strength (UTS) of UHSS could exceed 2000 MPa owing to the martensite microstructure which is known as a very hard and very brittle phase with needle-shaped features [33,34]. To achieve remarkable mechanical properties in the production of armored and wheeled combat vehicles, FNSS procures and uses two different armor steel grades which conform to MIL-DTL-12560 Class 4a (will be mentioned as Armor Steel-1 in this thesis) and MIL-DTL-46100 (will be mentioned as Armor Steel-2 in this thesis) U.S. military specifications. While Armor Steel-1 is a member of rolled homogeneous armor (RHA), Armor Steel-2 is studied in the group of high hardness armor (HHA). RHA is obtained by rolling cast homogeneous armor plates to the desired thickness. During the hot rolling process, the grain structure of armor steels is homogenized and helps to remove the imperfections which may reduce the strength of materials. Moreover, it also provides the advantage of elongating the grain structures within microstructure to form long lines which assist to resist higher stresses when in service. On the other hand, HHA is the name of another group of armor steel with hardness values exceeding 430 BHN and is also homogeneous armor steel [35]. These are widely preferred all around the world due to its reliability, remarkable mechanical properties and easy to manufacture. Lastly, their microstructures possess tempered martensite with homogeneously distributed and retained austenite in small quantities. Detailed information about Armor Steel-1 and Armor Steel-2 is given in Table 2.4. Since Armor Steel-2 has higher

16

YS and UTS values, it is reasonable to obtain different mechanical properties during experimental studies.

Table 2.4 Approximate mechanical properties of studied UHS armor steels

	Approximate YS (MPa)	Approximate UTS (MPa)	Approximate Tensile El (%)	Hardness (HBW)
Armor Steel-1	1200	1450	8	420-480
Armor Steel-2	1250	1600	8	480-540

UHSSs are widely and commonly used in order to satisfy the desired mechanical properties in such applications where high strength, remarkable toughness and moderate ductility become a necessity. FNSS usually prefers to use these two armor sheets of steel in the design of hull protection. Optical micrography images of these two UHSS sheets of steel are given in Figure 2.2.
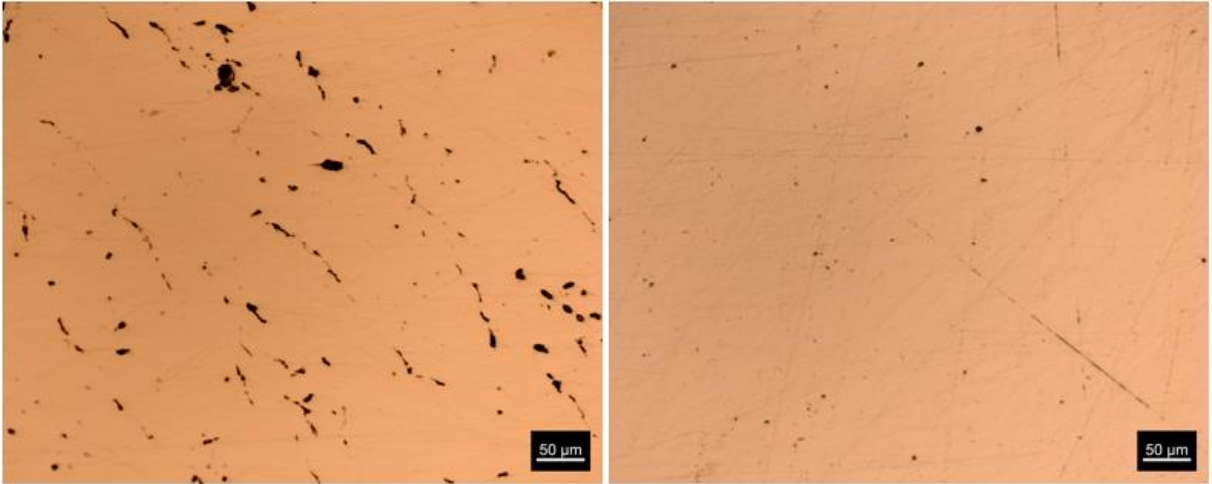
Figure 2.2 Optical microscopy images of Armor Steel-1 (on the left) and Armor Steel-2 (on the right)

Chapter 3

3. Hydrogen Embrittlement (HE) Phenomena and Its Adverse Effects on UHSSs

3.1 Introduction and Literature Review On HE

It is a well-known fact that hydrogen, own one of the smallest atomic radii in the periodic table with 0.53 Å, causes mechanical degradation of a certain type of metals and alloy systems which results in loss of ductility and reduction of load-bearing capacity [36,37]. The presence of hydrogen atoms (environmental or internal) in high-strength steels typically leads to fracture or catastrophic brittle failures of structural components while working in service environments. The fracture initiation in this mode, called hydrogen embrittlement, usually occurs by the synergetic action of hydrogen atoms with crystal lattice structures and highly depends on various factors such as applied stress, residual stress, temperature, the supply of hydrogen and pressure [38]. The deleterious effect of hydrogen could be in various modes and each of them is highly dependent on the type of material, microstructure, service environment. There are commonly known five different types of hydrogen-induced damage to metallic materials in the literature [39]. These are classified as follows;

- ➢ Hydrogen embrittlement
- ➢ Hydrogen attack
- ➢ Hydrogen-induced blistering
- ➢ Cracking from precipitation of internal hydrogen
- ➢ Cracking from hydride formation

Understanding the nature of the abovementioned hydrogen-induced damage types, except for hydrogen embrittlement, is relatively easy since a phase transformation does occur during the degradation process. For example, hydrogen-induced blistering occurs by the formation and collection of molecular hydrogen at internal defects [40]. Afterward, these molecular hydrogens build up high pressure due to volume expansion and lead to micro-crack formation. This type

of damage could be prevented by prohibiting the entrance of atomic hydrogen from the material surface. However, understanding the nature of the fifth-one namely hydrogen embrittlement is more complex and elusive and therefore avoiding the catastrophic damage induced by HE is rather difficult [17,18,41]. HE is a process by which the mechanical properties of metals and alloys are significantly reduced by the introduction of atomic hydrogen into the crystalline structure [42,43]. Since the size of atomic hydrogen is quite small which composed of one proton and one electron, it can easily be dissolved and diffused into a lattice structure. Continuous research studies regarding the adverse effects of hydrogen on metals and alloys were begun with Johnson towards the end of the nineteenth century [44]. He has realized some unusual changes in the fracture toughness and strain at fracture of iron that was soaked in acid for a while. This was later confirmed by Reynolds [45]. Despite massive, enormous and ongoing research efforts shown by scientists and researchers, the exact nature of this phenomenon is still controversial [46,47]. It remains popular in the world of science and academia due to its complexity and several mechanisms and theories are suggested to solve its multifaced nature.
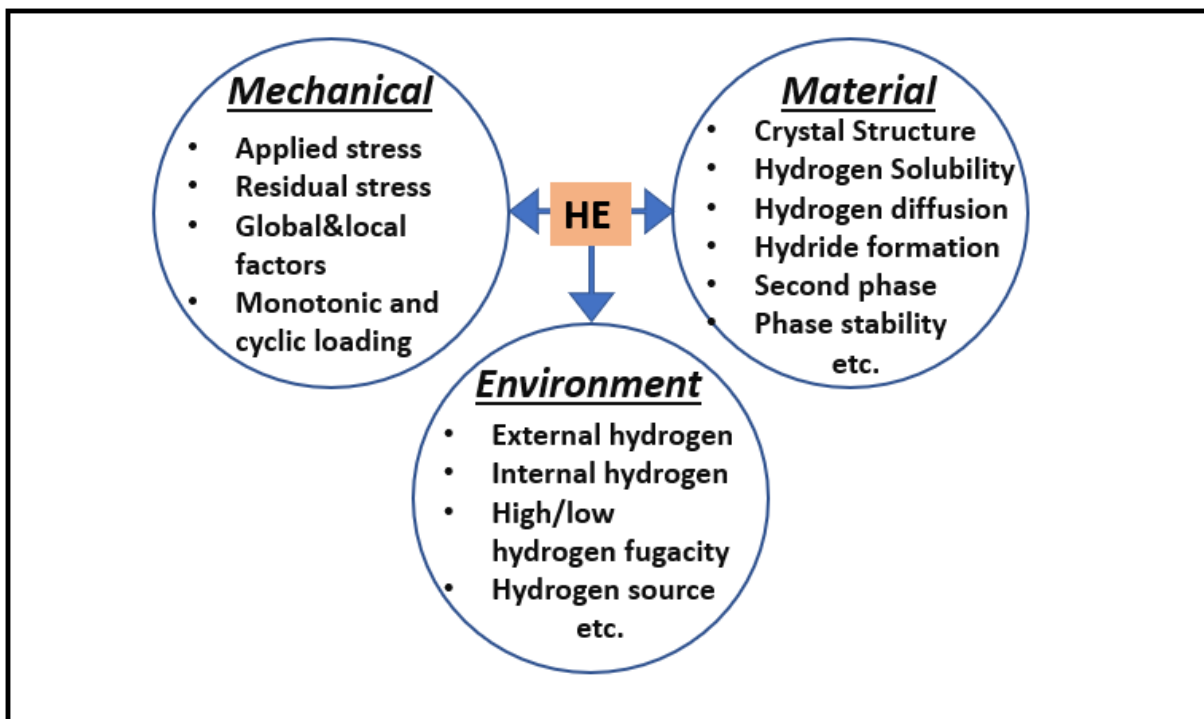
Figure 3.1 General description of hydrogen embrittlement interaction in global aspects (**recompiled from [48]**)

Three essential aspects trigger the occurrence of this phenomenon; namely: mechanical, material and environmental characteristics. HE is almost inevitable once these aspects are present in a material [49]. Figure 3.1shows some of the factors which are responsible for HE. These are specified as follows;

- ➤ UTS of the material
- ➤ Residual stress of the material
- ➤ The surface texture of the material
- ➤ Applied strain rate
- ➤ Hydrogen content & Trapped hydrogen amount
- ➤ Microstructure
- ➤ Metallic coatings
- ➤ Heat treatment procedure
- ➤ Service environment of material
- ➤ Temperature and pressure

The susceptibility to hydrogen embrittlement is directly associated with the strength of material, hardness, composition and type of microstructure. In other saying, the material condition is considered as the root source among three global aspects. The source of hydrogen and mechanical circumstances are triggering sources to hydrogen embrittlement. HE phenomena have three distinct characteristics which must be accomplished by material for the degradation of mechanical properties.

- ➤ UTS > 1000 MPa and/or surface hardness > 37 HRC
- ➤ The existence of hydrogen in the material either pre-existing or in the environment
- ➤ Applied stresses and loads when working in aggressive service environments

In general, high-strength materials are more vulnerable and susceptible to hydrogen embrittlement especially when they are exposed to a hydrogen environment. High manganese steels, AHSS, armor steels, titanium and aluminum alloy are some of the material types which are prone to this phenomenon. Several studies published in the literature have proven that the steels whose tensile strength is more than 1000 MPa and/or having a hardness higher or equal than 39 HRC are more susceptible to hydrogen embrittlement. Because high strength steels, which are subjected to higher stresses in usage, allow for larger plastic deformations and thus the driving force for hydrogen to go to high-stress concentration regions is relatively higher. Therefore, it could be deduced that the risk for the occurrence of HE is greater at high-stress concentration like a crack tip. The negative side of these high-strength steels being responsive to HE is that they are widely used in a wide variety of applications, including aerospace, marine, defense industry, armored vehicles, automotive applications, etc. Although high strength steels satisfy the expectations in terms of mechanical properties such as high strength, moderate ductility, remarkable toughness, hydrogen embrittlement has been a bottleneck problem that restrains further developments in all these application areas. Moreover, hydrogen embrittlement

20

is more pronounced at low strain rates because hydrogen atoms can find enough time to interact with dislocations and hinder the movement of them which results in the catastrophically premature failure of materials below their satisfying mechanical strength.
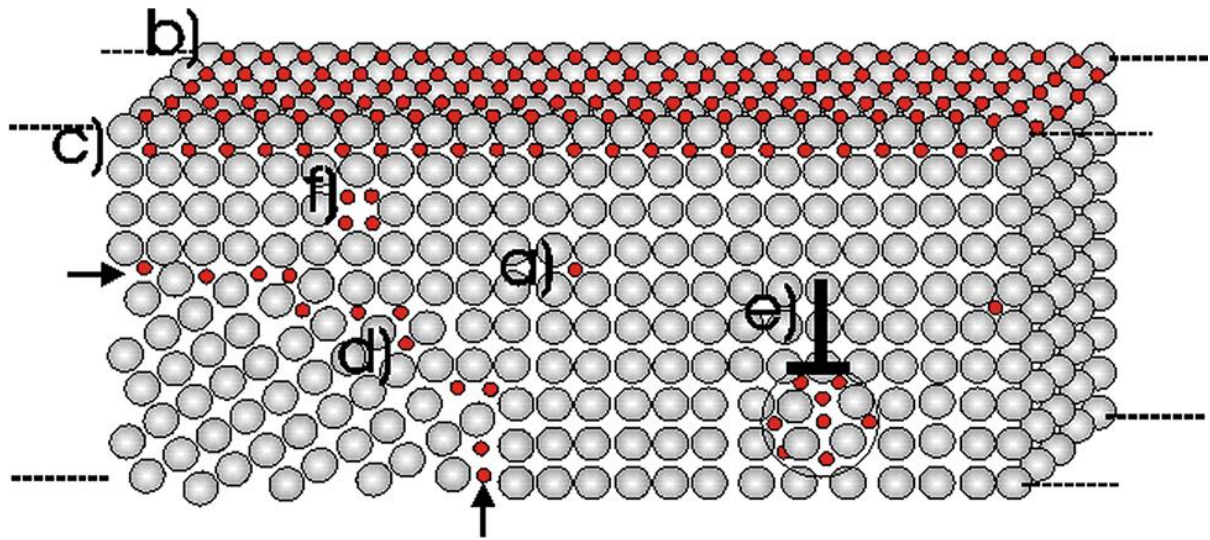
Figure 3.2 The schematic representation of hydrogen-metal interaction at lattice defects a) interstitial sites; b) surface traps; c) subsurface traps; d) grain boundary traps; e) dislocation traps; f) vacancy traps. (Adopted from [50])

Figure 3.2 shows the interaction of atomic hydrogen with metal lattices and possible trap locations. Hydrogen is abundantly found in the molecular form on earth which constitutes almost 75% of all universe. Therefore, hydrogen could either be in the molecular or atomic form on the surface of the material at the beginning. The dissociation of molecular hydrogen into atoms occurs in the progress of time using temperature and pressure. Once hydrogen atoms adsorb to the metallic surface of components, they begin to settle beneath of surface. Thereafter, hydrogen atoms diffuse through the lattice and interact with crystal defects such as vacancies, dislocations, grain boundaries as shown in Figure 3.2. The time for migration of hydrogen atoms into metal lattices highly depends on some factors such as temperature, pressure, exposure to gaseous hydrogen, type of microstructure, etc. It is important to note that hydrogen could be available before service life. When metallic materials are in a liquid state during manufacturing processes, the concentration of hydrogen content increases within the microstructure because the solubility of hydrogen is substantially higher at elevated temperatures. The amount of hydrogen atoms then decreases as the materials turn into a solid form. However, nascent hydrogen atoms are trapped in crystal defects such as vacancies, dislocations, grain boundaries, etc. For that reason, it is vital to detect the amount of hydrogen present in the microstructure of materials and applying some methods to diffuse out the trapped hydrogen atoms.

3.2 He Sources, Entry and Transport in Steels

3.2.1 HE Sources

HE is a global problem that affects the characteristic features of the most important alloy and steels used in various applications such as aerospace, marine, space and automotive [1,51]. A vast number of studies addressing possible solutions to overcome this global challenge have been performed so far by different scientists, researchers and institutions [52,53]. However, it is clearly understood that HE is a rather complex phenomenon since hydrogen is very hard to detect within microstructure and it also involves a variety of possible mechanisms such as location region of hydrogen, atomic or recombined molecular form, diffusion coefficient rate of hydrogen, etc. It is therefore essential to investigate;

- ➢ Source of hydrogen
- ➢ Evaluation of hydrogen at the material surface
- ➢ Adsorption, absorption and transportation of hydrogen in metals

The embrittlement of metals due to hydrogen could be mainly classified into two groups: internal hydrogen embrittlement (IHE) and hydrogen environmental embrittlement (HEE) [54]. The source of hydrogen is the main reason for this phenomenon to be studied separately. Hydrogen atoms can be introduced into steel during manufacturing and/or service environments. For the case of IHE, atomic or molecular hydrogen is diffused into steel throughout the manufacturing processes such as electroplating, cleaning with chemicals, welding, etc. Especially, the solubility of hydrogen increases as temperature increases and reaches a maximum point when steel is in molten form as shown in Figure 3.2.1. For that reason, hydrogen atoms can easily enter the metal matrix in the liquid phase. During the process of solidification, the solubility of hydrogen in steels decreases significantly and diffused hydrogen atoms drive out of microstructure. However, sometimes hydrogen atoms or molecules could be trapped in lattice defects such as voids, dislocations, grain boundaries, impurities, etc. [55,56]. Trapped hydrogen is therefore unable to escape metal matrix and leads to premature failure of structural components even before service life. Because susceptible metallic materials are adversely affected by micro-cracks and brittle type of fractures at applied stresses and loads well below their yield strength. To sum up, hydrogen that enters the metal lattice during manufacturing and fabrication processes is called IHE.
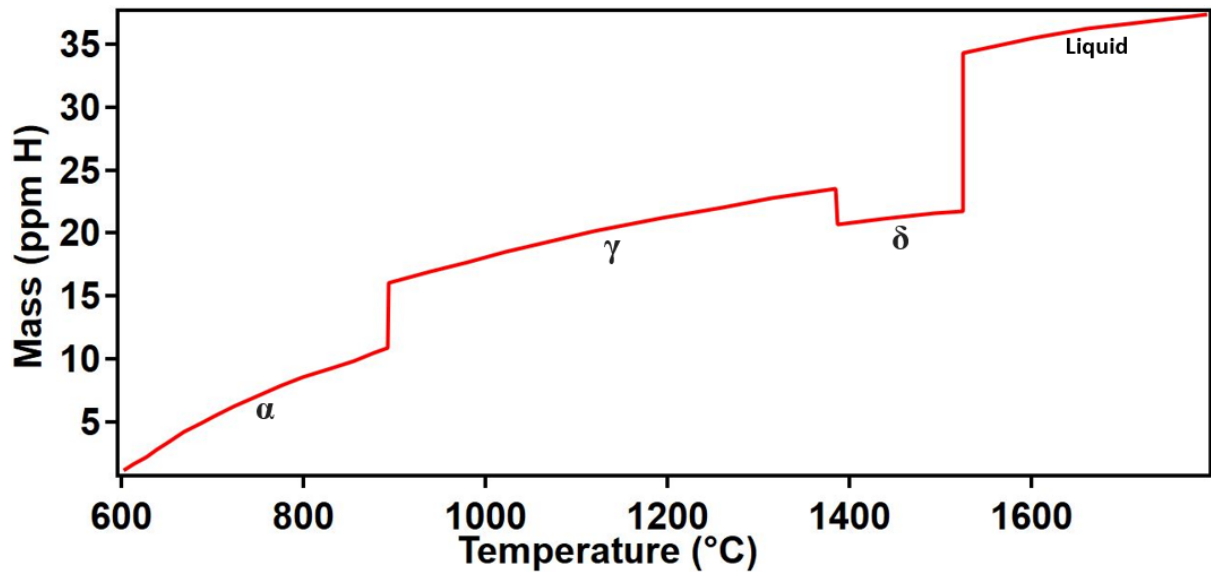
Figure 3.3 Hydrogen solubility of pure iron at 1 atm pressure of H2 (Recompiled from [57])

On the other hand, hydrogen can also be ingress into components in service when exposed to hydrogen-rich environments. This type of embrittlement is called HEE. In this case, hydrogen could be pickled by different external sources such as;

➢ In some manufacturing processes such as casting, electroplating, carbonizing, welding, electrochemical machining, phosphating, pickling roll forming, cathodic protection, etc.

➢ As a result of corrosion reactions that occur on the surface of metallic components.

➢ The usage of cathodic protection in order to prevent corrosion of structural components. In case of using not properly, the protection process leads to embrittlement.

Hydrogen atoms are firstly produced at the surface of metals. Later on, the adsorption of hydrogen atoms takes place and moves through the crystal lattices to reach the hydrostatic stress zone (usually the tip of a crack). When hydrogen concentration reaches a critical level (sometimes only a few ppm), they distort the crystal lattices and thus enhances the local stresses. Increased stress level leads to micro and nano-sized cracks and further these cracks propagate through grain boundaries. In the end, intergranular brittle fracture occurs below its permissible stress values. The schematic representation of hydrogen sources for two different forms of HE is given in Figure 3.2.2.
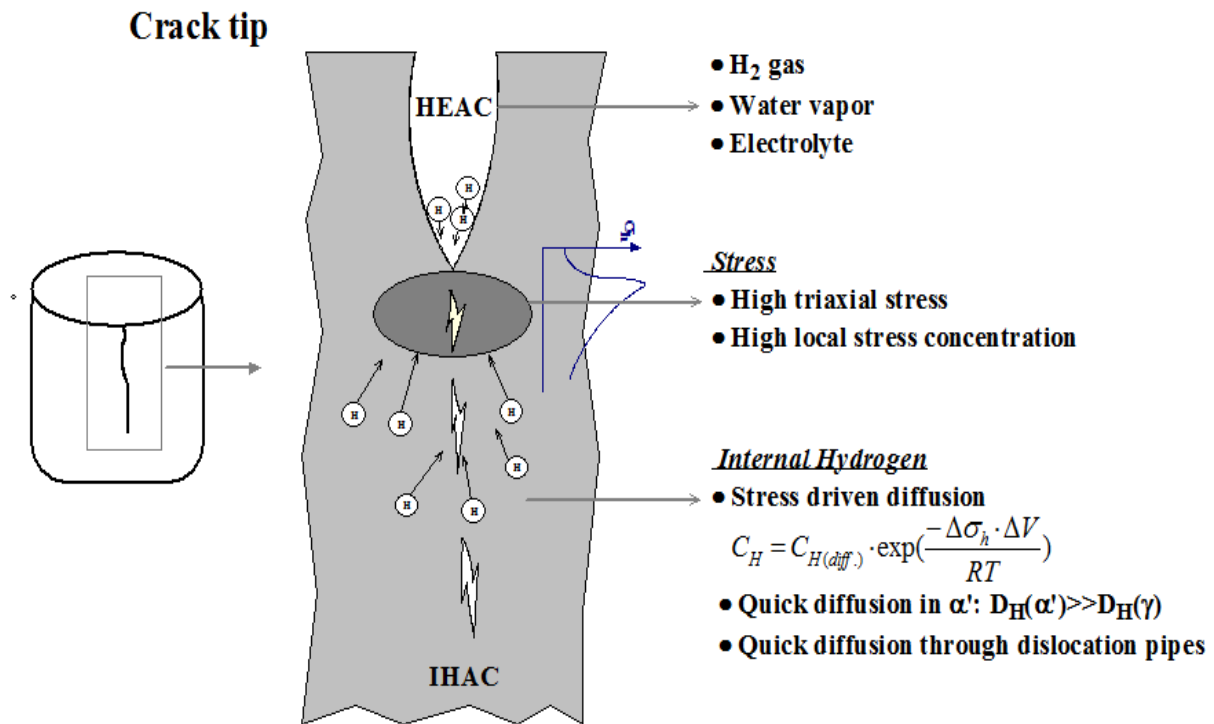
Figure 3.4 Two different sources of hydrogen that cause HE

3.2.2 HE Entry

The ingress of hydrogen into metallic materials in service occurs by two sources, which are known as hydrogen gas and corrosion reaction [58]. When metallic components are located in a gaseous hydrogen environment, the synergetic action and interplay of hydrogen with some metals, steels, and alloys involves a couple of stages including adsorption, chemisorption (chemical adsorption) and physisorption (physical adsorption). Physisorption is described as the adsorption of a molecule to the surface of absorbent material is occurred by weak van der Waals forces. It is considered reversible and very often occurs quickly due to adsorbate molecules are held by weak forces. Since the adsorption energy of physisorption (approximately 20 kJ mol^{-1}) is fairly low compared to chemisorption, reaching the equilibrium is much easier. Speaking of chemisorption, unlike physisorption, the adsorption of a molecule to the surface of an absorbent takes place by chemical bonds. Therefore, hydrogen uptake is mainly dominated by chemisorption at elevated temperatures. The adsorption energy is highly dependent on M-H and H-H bond energies. Pasco et al. calculated Fe-H bond energy as 282 kJ mol^{-1} [59] which is much higher than physical adsorption. Lastly, chemical adsorption could either be slowly reversible or irreversible. The final stage of hydrogen-solid interaction is adsorption. It involves the ingress of chemical adsorption products into the crystal lattice

structure. Hydrogen pressure and temperature play a key role in the amount of hydrogen absorbed by metal [58].

Another main hydrogen source is known as corrosion or cathodic polarization. Evaluation reactions of hydrogen can take place at acidic, neutral and alkaline conditions [60] which are given as follows;

> $H_3O^+ + M + e \rightarrow M \cdot H_{ads} + H_2O$ (Volmer-acidic solution)   **(3.1)**

> $H_2O + M + e \rightarrow M \cdot H_{ads} + OH^-$ (Volmer-neutral and alkaline solutions)   **(3.2)**

> $MH_{ads} + H_3O^+ + e \rightarrow H_2 + H_2O + M$ (Heyrovsky-acidic solution)   **(3.3)**

> $MH_{ads} + H_2O + e \rightarrow H_2 + OH^- + M$ (Heyrovsky alkaline solutions)   **(3.4)**

> $2MH_{ads} \rightarrow H_2 + 2M$ (chemical desorption)   **(3.5)**

> $MH_{ads} \rightarrow MH_{abs}$ **(3.6)**
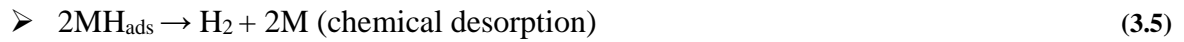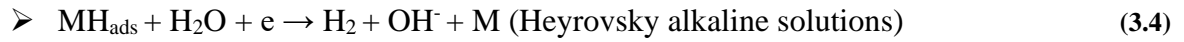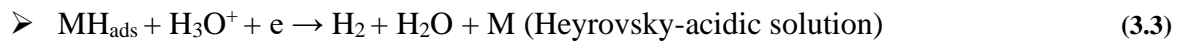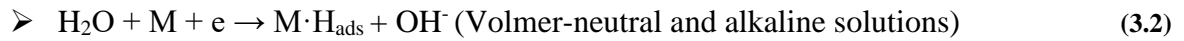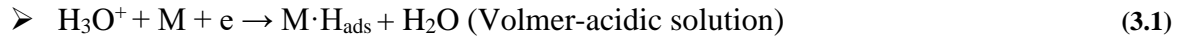
where M represents the surface of the metal, MH_{ads} and MH_{abs} represent the adsorbed and absorbed hydrogen on the metal surface. In the reactions of (3.1) and (3.2), atomic hydrogen is adsorbed on the surface of the metal. The desorption of adsorbed atomic hydrogen could be via electrochemical (given in reactions (3.3) and (3.4)) or chemical (given in reaction (3.5)) desorption reaction in order to create molecular hydrogen. Lastly, some of the hydrogen atoms on the surface enter the crystal lattice by absorption reaction. It should also be pointed out that Sievert's law depicts the dissolved hydrogen concentration (C_H) for high-pressure hydrogen gas [61] as follows;

$$C_H = S\sqrt{P_{H_2}}$$ **(3.7)**

where S represents the solubility constant which differs by the type of alloys and temperature [62] and P_{H_2} represents the hydrogen partial pressure.

3.2.3 Hydrogen Diffusion and Trapping in UHSS

The development and production of UHSS have dramatically increased in the last decades due to the profound desire of different industries including automotive, defense and aerospace

25

[63]. The reason for the growing demand for these steels is because their high strength combined with moderate ductility, exceptional toughness, outstanding formability and reasonable prices compared to other steel grades makes them excellent potential candidates in the present and upcoming future [64]. However, one of the drawbacks of using UHSS in the service environment is to possess high susceptibility and vulnerability to HE. The underlying reason for UHSS being susceptible to hydrogen-induced component failure is to have a complex microstructure. Having complex microstructures significantly enhances the possibility of binding hydrogen in the crystal lattice defects. Thus, the absorbed hydrogen (during production stages or in-service environments) could be trapped in the lattice defects or known as so-called hydrogen traps [65]. These hydrogen traps include grain boundaries, impurities, dislocation regions, inhomogeneities, inclusions, etc. Numerous studies have been performed to analyze the diffusivity and the solubility of hydrogen atoms in UHSS [65,66]. In general, the results showed that diffusion and solubility of hydrogen depend on various parameters at different materials. The diffusion and trapping of hydrogen in microstructure occur after adsorption and absorption processes. Fick's first law expresses the diffusion flux of hydrogen as;

$$J = -D \frac{\partial C}{\partial x} \tag{3.8}$$

where J is the diffusion flux (mol m^{-2} s^{-1}), D is the diffusion coefficient (m^2 s^{-1}) and $\partial C/\partial x$ is the concentration gradient. It is important to bear in mind that the diffusion coefficient is significantly affected by the system and temperature. Arrhenius equation depicts this relation as;

$$D = D_0 \exp\left(-\frac{Q}{RT}\right) \tag{3.9}$$

where D_0 is the temperature-independent constant (m^2 s^{-1}), Q is the energy for activation of diffusion (J mol^{-1}), R is the gas constant (8.314 J mol−1 K−1) and lastly, T (K) is the absolute temperature. Only experimental methods are valid to determine the hydrogen diffusion coefficient. Thermal desorption spectroscopy (TDS) and electrochemical permeation methods are the most commonly used techniques in the literature. The electrochemical permeation technique (EPT) is widely used for hydrogen diffusion through metals. This technique was developed by Devanathan and Stachurski in 1962 [67]. The schematic representation of the EPT technique is given in Figure 3.5, which was recompiled from [68]. Figure 3.5 shows two different electrochemical cells separated by a metal sample which acts as a working electrode (WE) for both cells. Moreover, electrochemical cells also possess Platinum wires that work as a counter
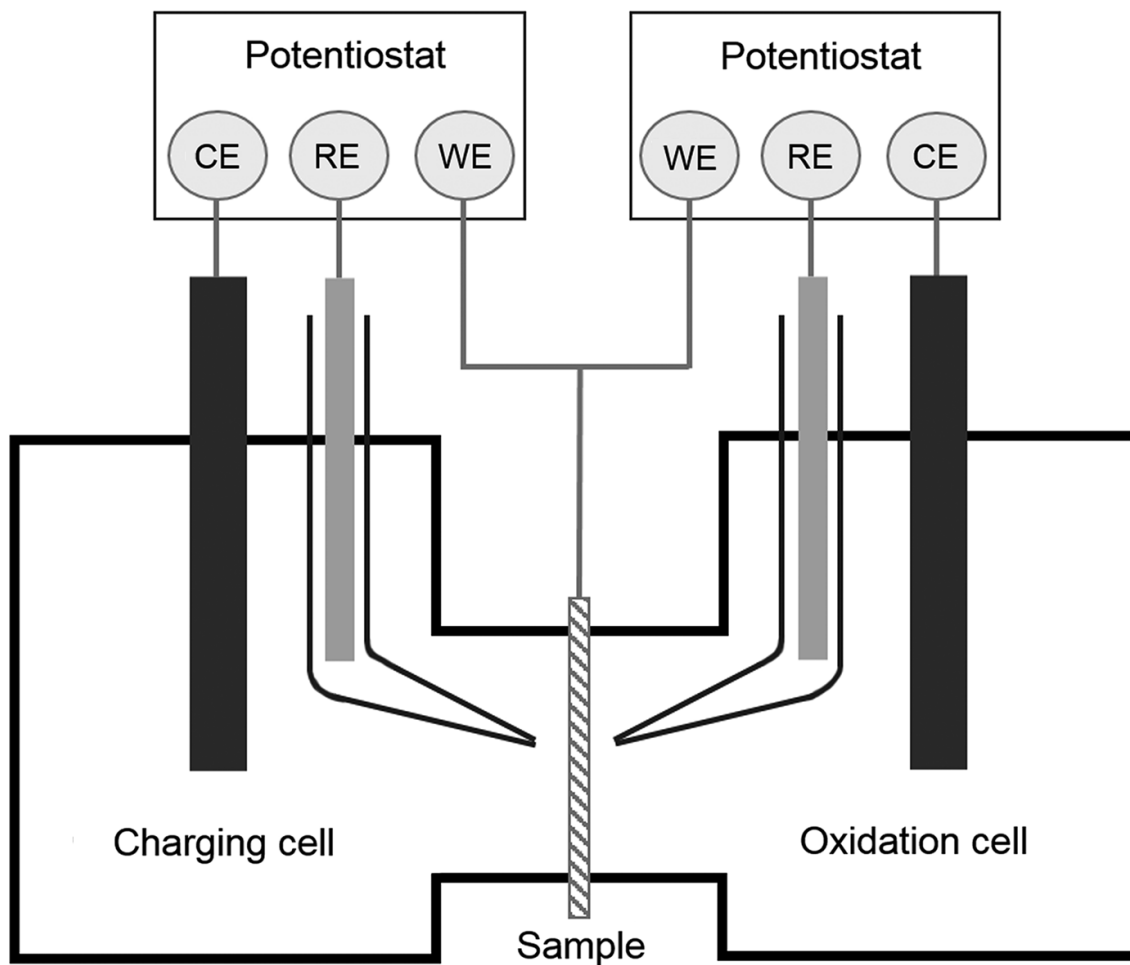
Figure 3.5 Schematic representation of EPT cell (Adapted from [68])

electrode (CE) and Luggin capillary act as a reference electrode (RE). In order to avoid the oxidation and formation of the passive layer in the anodic side of the specimen, it is mostly covered with a palladium coating to ensure hydrogen permeation consistency. EPT technique not only provides the measurement of hydrogen diffusion coefficient but also provides an opportunity to detect hydrogen concentration at the sub-surface of metals and steady-state permeation rate. The success of the EPT technique is confirmed in various studies published in the literature [69,70]. Furthermore, the TDS technique is widely used to detect hydrogen traps in metals. It involves a continuous heating rate to initiate the gas flow that drives out of the material. This gas flow is being recorded by a mass spectrometer throughout the heating process [71]. To quantify the hydrogen released from the material, Gas chromatography and mass spectroscopy is used. This method is very useful since it gives information about the binding energy of trap sites and also the density of the traps located in the material. Hydrogen traps are classified as reversible and irreversible traps in materials. Irreversible traps in the microstructural features are known as carbide interfaces, incoherent precipitates and high angle grain boundaries. Since they are trapped by high activation energy trapping sites in these lattice

defects, they become non-diffusible which results in an increase in hydrogen solubility and a decrease in hydrogen diffusion. On the other hand, reversible traps have relatively lower hydrogen trapping activation energy and are thus considered as diffusible hydrogen. Dislocations, low angle grain boundaries, coherent precipitates and voids are the example for reversible traps. This reversibility and irreversibility of hydrogen atoms significantly affect the HE behavior of steels [72]. Two parameters can be used to characterize hydrogen trapping: hydrogen-trap binding energy (E_b) and the density of trap sites (N_t). In order to calculate the hydrogen trap sites (N_t) for per unit volume, a formula is used in the literature published by Dong et al. [73]:

$$\ln\left(\frac{D_L}{D_{eff}}\right) - 1 = ln\frac{N_t}{N_L} + \frac{E_b}{RT} \tag{3.10}$$

where D_L represents the lattice diffusion coefficient of hydrogen ($cm^2\ s^{-1}$), D_{eff} is the effective diffusion coefficient of hydrogen in the presence of traps ($cm^2\ s^{-1}$), N_L is the density of the interstitial sites in the steel (sites cm^{-3}) and finally E_b is the hydrogen trap binding energy (kJ mol^{-1}). EPT technique is also determining hydrogen trap density.

3.3 HE Mechanisms

Numerous research studies have been devoted to comprehending the failure mechanisms arising from the ingress of hydrogen atoms or molecules through the metals, which results in the abrupt mechanical failures of structural components used in various industries. It should be pointed out that the effect of hydrogen on mechanical properties extraordinarily varies with the type of materials. The primary reason for this variation is directly associated with having complex microstructures which provide various possibilities for hydrogen binding. There are various hydrogen embrittlement mechanisms published in the literature, all of which partly elucidate the nature of HE for different material features. However, there is no fundamental mechanism of HE that completely explains the exact nature of this type of failure and contradictory opinions among researchers currently exist in the publications dedicated to solving this phenomenon. Most-known hydrogen embrittlement mechanisms are hydride-induced embrittlement (HIE), hydrogen-induced decohesion (HEDE), hydrogen-enhanced localized plasticity (HELP) and adsorption-induced dislocation emission (AIDE). Henceforth, these well-

known mechanisms will be explained in detail throughout this sub-chapter to shed light on the origins of HE.

3.3.1 Hydride-induced Embrittlement (HIE)

HIE mechanism relies on the formation and subsequent fracture of hydrides at the crack tip. It was first proposed in 1969 by Westlake [74] and there being no conflict by researchers regarding this mechanism since only since certain hydride forming materials involving vanadium, zirconium, niobium, tantalum and titanium encounter cracking and failure when the concentration of hydrogen (usually at the tip of a crack) surpass the solubility limit [17,75]. It involves various steps as follows;

- ➢ Diffusion of hydrogen to the regions of hydrostatic stress zones at the crack tip
- ➢ Formation and growth of brittle hydrides
- ➢ The occurrence of crack initiations at hydrides since their size reach a critical point
- ➢ Crack propagation and crack-arrest at hydride phases

Furthermore, temperature and strain-rate regimes play an important role in the occurrence of this mechanism. Because the diffusion of hydrogen atoms from a metal's surface to ahead of a crack tip needs for a length of time and the stability of hydride phase takes place at certain temperatures. Contrary to what has been learned so far, materials experience a significant amount of plastic deformation without fracturing and embrittlement has not occurred although there exists hydrogen in crystal lattices. This is because hydrogen atoms exist as solutes and the nucleation of hydrides would not happen before fracture. A schematic representation of the HIE mechanism is given in Figure 3.3.1.1. As supporting evidence, microstructural observations via scanning electron microscopy (SEM) and transmission electron microscopy (TEM) were performed for brightening the unknowns behind this mechanism [76,77]. It is observed that a strong thermomechanical driving force is necessary for hydrogen formation. Also, crack arrest markings and cleavage-like fractures were observed on fracture surfaces of corresponding materials.
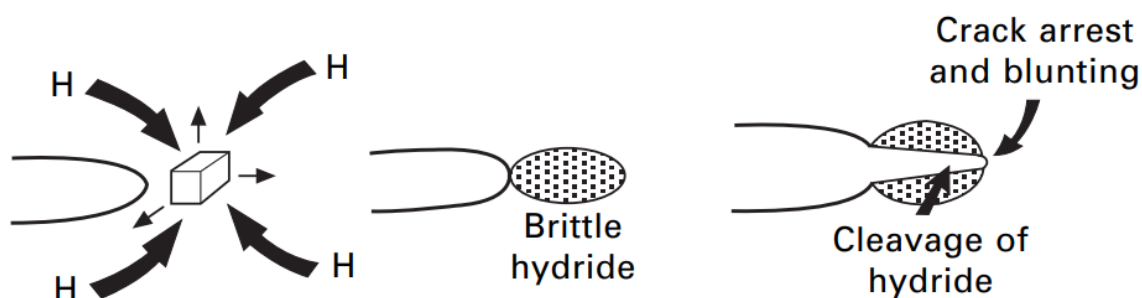
Figure 3.6 Schematic representation of HIE mechanism (Adapted from [78])

29

3.3.2 Hydrogen-enhanced Decohesion (HEDE)

HEDE mechanism is a simple mechanism and widely accepted by researchers. It was first proposed by Pfeil in 1926 [79], saying that the cohesive energy across cubic cleavage planes is lowered by hydrogen atoms. This theory is based on the fact that the interatomic bond energy is weakened in the presence of hydrogen atoms, which results in the increased risk factor of decohesion. In other words, diffused hydrogen atoms decrease the cohesive energy between atoms and cause the reduction of interatomic bond strength, which is followed by crack initiation, propagation and finally failure of materials.
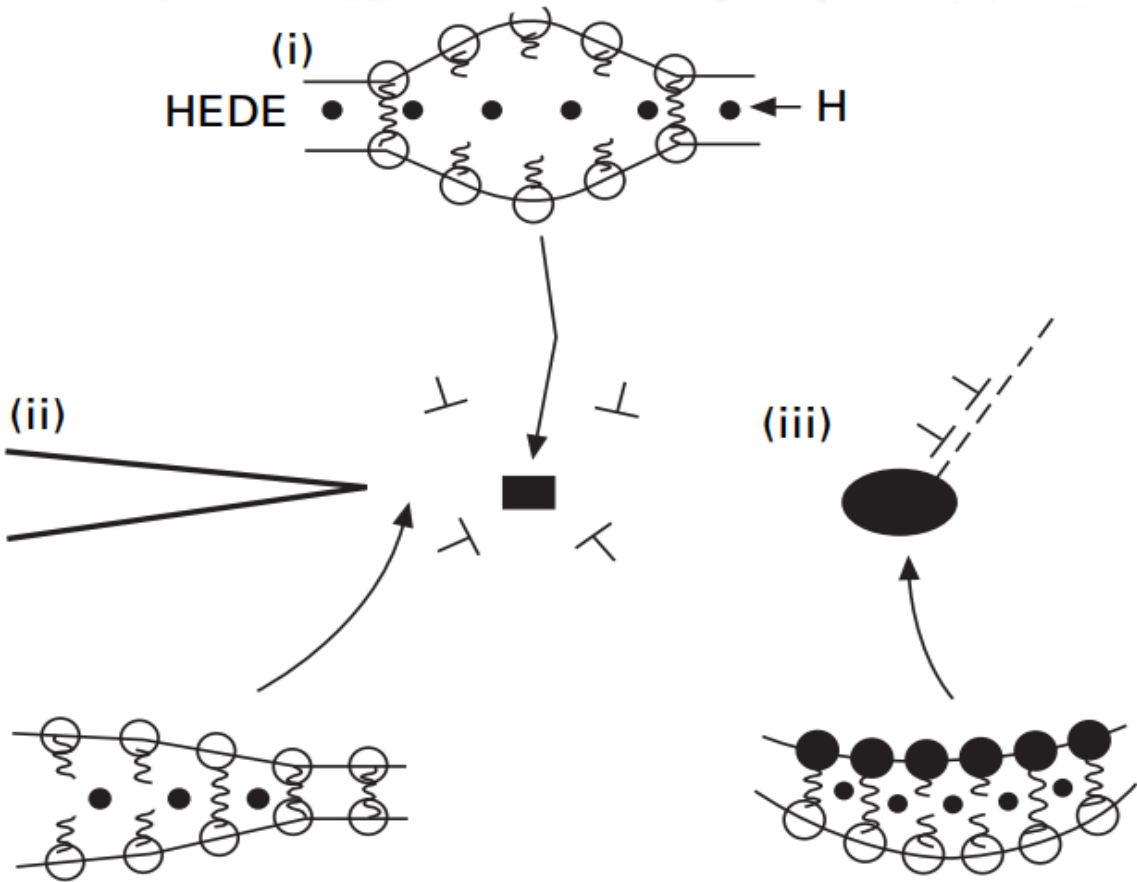
Figure 3.7 Schematic representation of HEDE mechanism with different diagrams (Adapted from [78])

Figure 3.7 represents several schematic diagrams that explain how this mechanism has occurred. For example, separation of atomic bonds due to the presence of hydrogen atoms in the lattice (i), at the crack tip (ii) and the particle-matrix interfaces are shown. It is because when the specimen is subjected to a hydrogen-rich environment and the concentration of hydrogen is in large quantities in the metal matrix, hydrogen donates its 1s electron to iron's unfilled 3d shell. For that reason, cracks initiate and following fractures occur by applied tensile stress well below its working stress and loads [80,81]. With the continuous research efforts, this

hypothesis was first qualitatively developed and explained by Oriani [82] and other researchers [80,83]. Decohesion usually occurs when the cohesive strength of atoms is lower than maximum acting tensile stress and when critical crack-tip-opening displacement (CTOD), nearly half of the distance between atoms, is achieved by the material due to tensile separation. It is essential to know that it generally takes place at the tip of a crack atmosphere because of the maximum hydrostatic stress zone generated by absorbed hydrogen. HEDE mechanism has widely been used to define intergranular brittle fracture surfaces of high strength steels because hydrogen atoms are accumulated and trapped at grain boundary interfaces and then causes a local weakening of interatomic cohesive energies of metal atoms. It is important to emphasize that this mechanism has not yet been proven by any experimental method. Several atomistic simulation studies have also helped to explain the hypotheses of decohesion of metal atoms in the presence of hydrogen [84,85].

3.3.3 Hydrogen-enhanced Localized Plasticity (HELP)

HELP theory [86] claims that HE occurs due to the increase in the mobility of dislocations in the existence of hydrogen atoms. It was proposed and introduced by Beachem in 1972, which suggests that the dislocation activities at the crack tip, where hydrogen atoms are diffused or segregated these areas due to hydrostatic stresses, are facilitated by localized hydrogen atoms around the crack tips. In other words, the resistance to motion of dislocations is decreased due to localized hydrogen atoms at the crack tip because it was proposed that hydrogen has a shielding effect which results in the increase in dislocation mobility and localized slip. Therefore, a local movement of dislocations is possible due to the drop in yield stress caused by hydrogen atoms and the fractured surface of embrittled material would reveal slip bands at the tip of cracks and locally plastic deformation [81,87,88]. A schematic illustration of this theory is given in Figure 3.8.
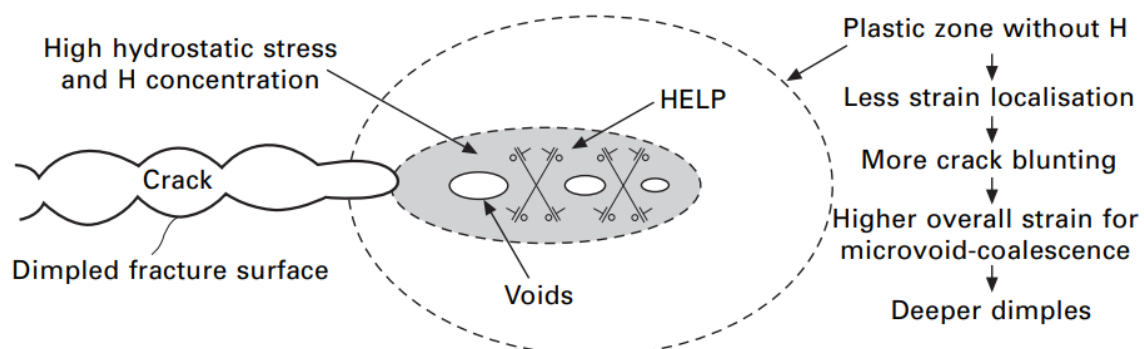
Figure 3.8 Schematic representation of HELP mechanism (Adapted from [78])

It includes the nucleation of micro and nano-scale voids, their growth process and finally coalescence of formed voids by synergetic action of dislocation motion near the crack tips where hydrogen amount is abundant. Unlike the HEDE mechanism, miscellaneous fracture modes including transgranular, quasi-cleavage and intergranular were observed in the fractographic analysis of different steels and alloy systems. The diversity of various fracture modes is directly associated with the region of hydrogen concentration zones, which would either be grain interiors or adjacent to grains. It is fair to state that hydrogen-induced failures of most important metallic materials having FCC, BCC and HCP type microstructures could be explained by HELP theory [78]. For example, a vast amount of evidence is available for FCC metals that gives a reasonable answer for failures resulted from the HELP mechanism. It is believed that a decrease in the stacking fault energy (STE) of FCC metals has occurred in the existence of hydrogen atoms, which has been proven by experimental studies [89] and also through ab-initio modeling [90]. Following the decrease of STF causes an increase in dislocation activities due to the accumulation of hydrogen atoms near high-stress concentration points such as crack tips. Even though the hydrogen-induced local decrease in SFE is not considered within the context of the HELP mechanism, the rise in the cross slip of partial dislocations (due to a decrease in SFE) can contribute to the localized plasticity. Among other hydrogen embrittlement mechanisms, the HELP theory is well accepted since significant amount of proofs for hydrogen-related failures by localized plasticity has been unveiled by fractographic analysis, TEM studies, dislocation motion measurements and flow stress data by macroscopic analysis [91–94]. Tensile test results also revealed sometimes a decrease in the flow stress of hydrogen-charged specimen was observed in comparison with as-received specimens, indicating that hydrogen had an impact on yield stress. However, the flow stress of a material highly depends on the type of material, temperature, strain rate, etc.

3.3.4 Adsorption-induced Dislocation Emission (AIDE)

The AIDE theory was introduced by Lynch in 1976 and then further improved by other researchers [1,95,96]. He suggested that hydrogen-related failures of structural components are a result of the adsorption of hydrogen atoms at the crack tip. This theory is also considered as the combination of well-accepted HELP and the HEDE mechanisms in some respects and thus evolving into a more complex phenomenon that requires a detailed and further explanation. In this mechanism, the term "adsorption-induced" stands for adsorbed hydrogen atoms from the crack tip of metal's surface to the crystal lattices and cause dilation of interatomic bonds due to

the reduced cohesive strength in the presence of hydrogen (HEDE mechanism). the term "dislocation emission", on the other hand, stands for easier nucleation process and movement of dislocations by means of adsorbed and accumulated hydrogen atoms near the crack tip which facilitates the dislocation motion by its shielding effect (HELP mechanism). Figure 3.9 represents the evaluation of AIDE mechanisms.
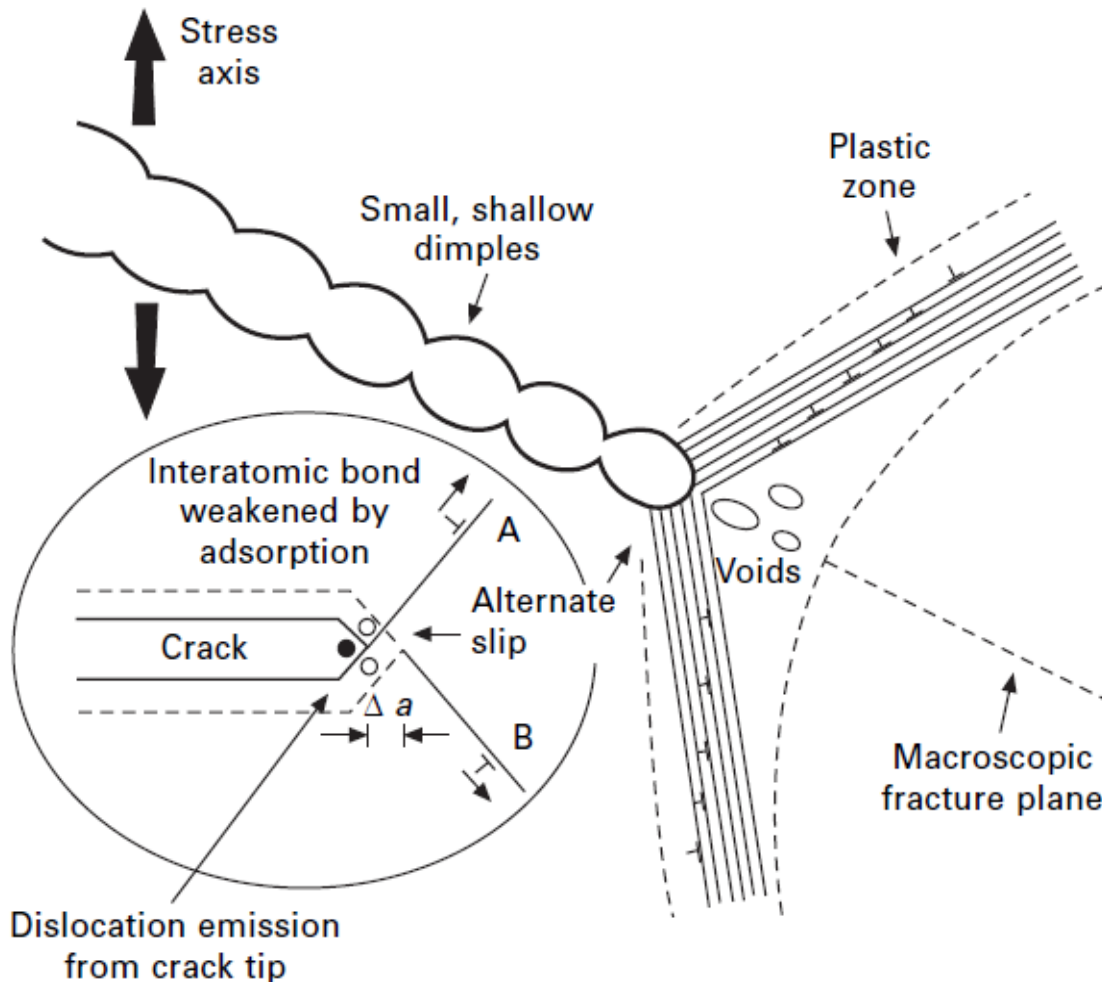
Figure 3.9 Schematic representation of AIDE mechanism (Adapted from [78])

To sum up, crack initiation and its growth start with the synergetic action of decohesion and dislocation emission and result in the fracture at the tip of the cracks by dislocation slip and micro-void coalescence (MVC). A high amount of absorbed hydrogen atoms were detected in such materials as austenitic stainless steels, nickel-based alloys and titanium alloys in order to validate AIDE theory [97–99]. Fractographic analysis and metallographic studies revealed that the most important metallic materials-including aluminum alloys, titanium alloys and high strength steels-are embrittled in hydrogen-rich environments (in aqueous or gaseous hydrogen), which is also called environmental assisted cracking (EAC). Studies revealed that EAC occurs due to the localized plastic flow with applied stress and leads to the evaluation of microvoids. Lynch finally concluded that the adsorption of hydrogen atoms near the crack tip facilitates the

dislocation emission process and therefore causes the coalescence of voids that creates bigger cracks. In addition to this, this process is responsible for the dimpled fracture surface of hydrogen-charged specimens.

Chapter 4

4. Experimental Methods and Results

4.1 Hydrogen Charging System

To study the hydrogen embrittlement behavior of armor steels used by FNSS in the production of armored combat vehicles, one of the most important tasks in this thesis was to establish a hydrogen-charging system before experimental observations. Several different hydrogen charging methods have been developed and well-studied in the literature [100–102]. Among various methods, a cathodic hydrogen-charging system which includes a power supply, a water bath, air pump and a chemical solution was selected and used to perform the hydrogenation process of as-received specimens. Figure 4.1 shows the supplied fixtures for the charging operation.
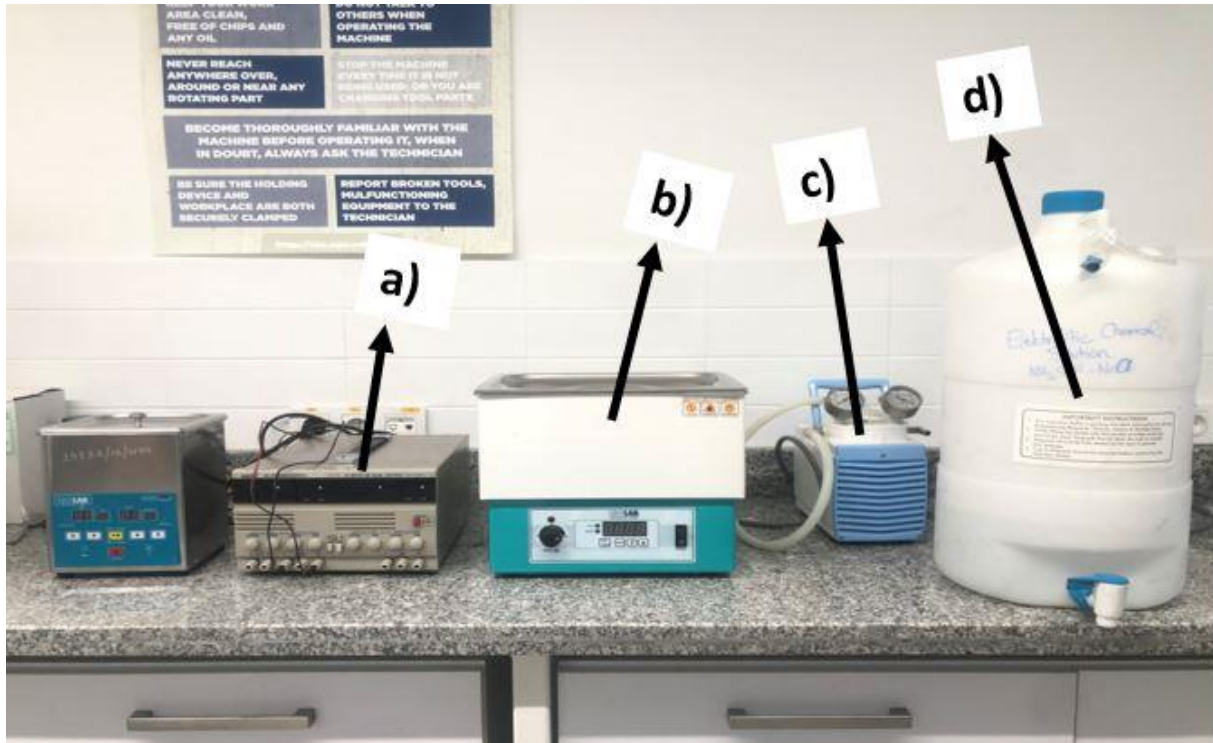
Figure 4.1 The fixtures for the hydrogen-charging operation a) power supply, b) water-bath, c) air pump, d) electrolytic chemical solution.

The electrolytic solution was prepared using ammonium thiocyanate (NH$_4$SCN), sodium chloride (NaCl) and purified water with definite proportions. The preparation of electrolytic solution was performed by the following procedure;

➢ A definite mass of purified water (e.g., 1000 gr or 1000 mL)

➢ 3% NaCl (wt.%) according to the pure water's mass

➢ 3g/lt NH$_4$SCN (volume percentage) according to the solution's total volume

Once they were shaken in the drum, the preparation of the chemical solution was completed. All the specimens used in the experiments throughout the thesis were electrochemically charged with hydrogen at a fixed current density of 100 A/m^2. Platinum rod was used as the counter electrode (anode) and the specimen was placed within the chemical solution which acted as the working electrode (cathode). In order to accelerate the diffusion of hydrogen atoms through the specimens, the temperature of the water in the water bath was arranged as 353K for all hydrogen-charging operations. Before the charging process, mechanical grinding and polishing were utilized to obtain a clean and shiny surface which would make the adsorption of hydrogen atoms on the metal's surface easier. The power supply is an essential device required for the cathodic hydrogen charging process because controlling the current in this operation plays an important role to conduct the experiments properly. Higher current densities increase the chance of the diffusion of hydrogen atoms into metallic materials. In order to calculate the constant current through the hydrogen charging operation of the armor steels, the following formula was used;

$$\frac{\text{Constant Current (A)}}{\text{Surface area (m}^2)} = \text{Current Density} \left(\frac{\text{A}}{\text{m}^2}\right) \qquad \textbf{(4.1)}$$

The only unknown in this equation is the constant current. Precise surface area calculation was performed using the Solidworks drawing program. The current density was determined as 100 A/m^{-2} in order to enhance the possibility of hydrogen diffusion through metals. The schematic representation of the cathodic hydrogen charging system is given in Figure 4.2.
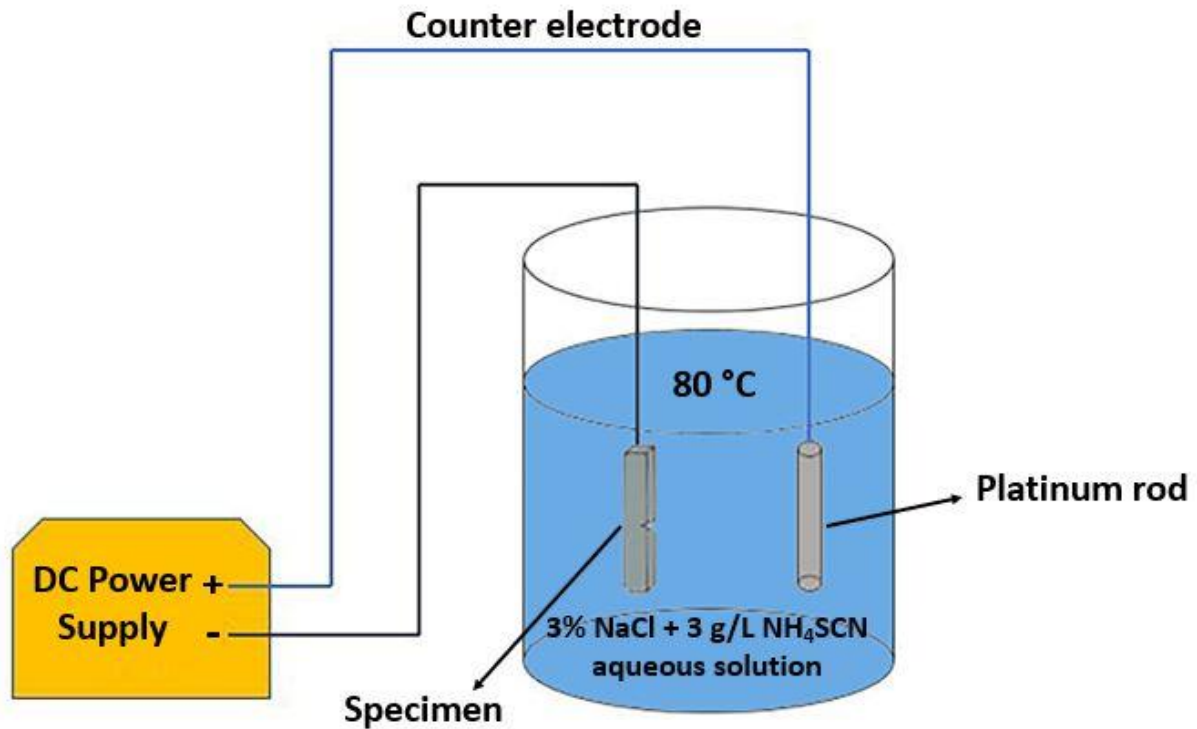
Figure 4.2 Cathodic hydrogen charging set-up [103]

4.2 Mechanical Tests

The selection of a material in the defense industry sector is of utmost importance since produced armored vehicles carry out their duties in extremely harsh conditions. Therefore, knowing the material used in the manufacturing of armored vehicles with all its aspects provides an essential advantage to the companies and also helps them to achieve their goals. The behavior of materials under mechanical loads is called mechanical properties. It is quite important to know the capability of an engineering structure whether the material is strong enough to withstand the loads to which it will be subjected in service. In order to get familiar with the mechanical properties of the material, various mechanical test methods are used such as tensile/compression tests, hardness, the Charpy impact test, high strain rate test, etc. Mechanical tests play an important role in evaluating the basic properties of materials, in their development, in quality control and in the selection of materials for a designed product. The mechanical behavior of materials is highly dependent on the strengths of interatomic bonds but microstructural activities also play an important role in the development of mechanical characteristics. Since armored combat vehicles operate in extremely difficult working conditions, realizing the strengths and weaknesses of used materials before producing the armored vehicles will save time and money for the companies. As said before, FNSS uses

Armor Steel-1 and Armor Steel-2 in the production of armored combat and wheeled vehicles to confer the desired mechanical properties of the Turkish Armed Forces and other suppliers. One of the drawbacks of using such materials which possess tempered martensitic microstructure is to be highly susceptible to embrittlement due to diffused hydrogen atoms from the service environment. This thesis aims to identify the hydrogen embrittlement behavior of these materials because fractures and cracks occur when they are subjected to some manufacturing processes such as bending, welding and laser cutting. Therefore, starting with the tensile tests, various mechanical tests methods including compression tests, micro and macro hardness tests, high strain rate (gleeble) tests and Charpy V-notched impact tests are utilized to shed light on the mechanical behavior of used materials with and without hydrogen presence. Most of the experiments and hydrogen charging operations were conducted at AGU laboratories. Only tensile tests with notched specimens and high strain rate tests are performed at TAUM Erciyes Center and Atılım University Metal Forming Center of Excellence, respectively. Additionally, hydrogen bake-out operation and SEM analysis were also performed at AGU laboratories. Finally, ballistic tests with as-received and hydrogen-charged specimens were carried out at FNSS Laboratory.

4.2.1 Tensile Tests

Tensile testing stands out as one of the most common mechanical test methods used to determine the mechanical properties of materials. It is a basic materials science test method in which a sample is subjected to uniaxial tensile forces until it breaks. The results from the test are used for material selection, quality control and predicting how the material will behave under other forces for any application. Within this scope, tension tests with standard tensile specimens and notched specimens were carried out with as-received and hydrogen-charged specimens to figure out the effect of hydrogen on the mechanical response of armored steels. Both ends of the tensile specimens should be long enough to ensure that there is an extra area for gripping so that the specimen will not be able to slip from grips and affect the test results (Figure 4.2.3).
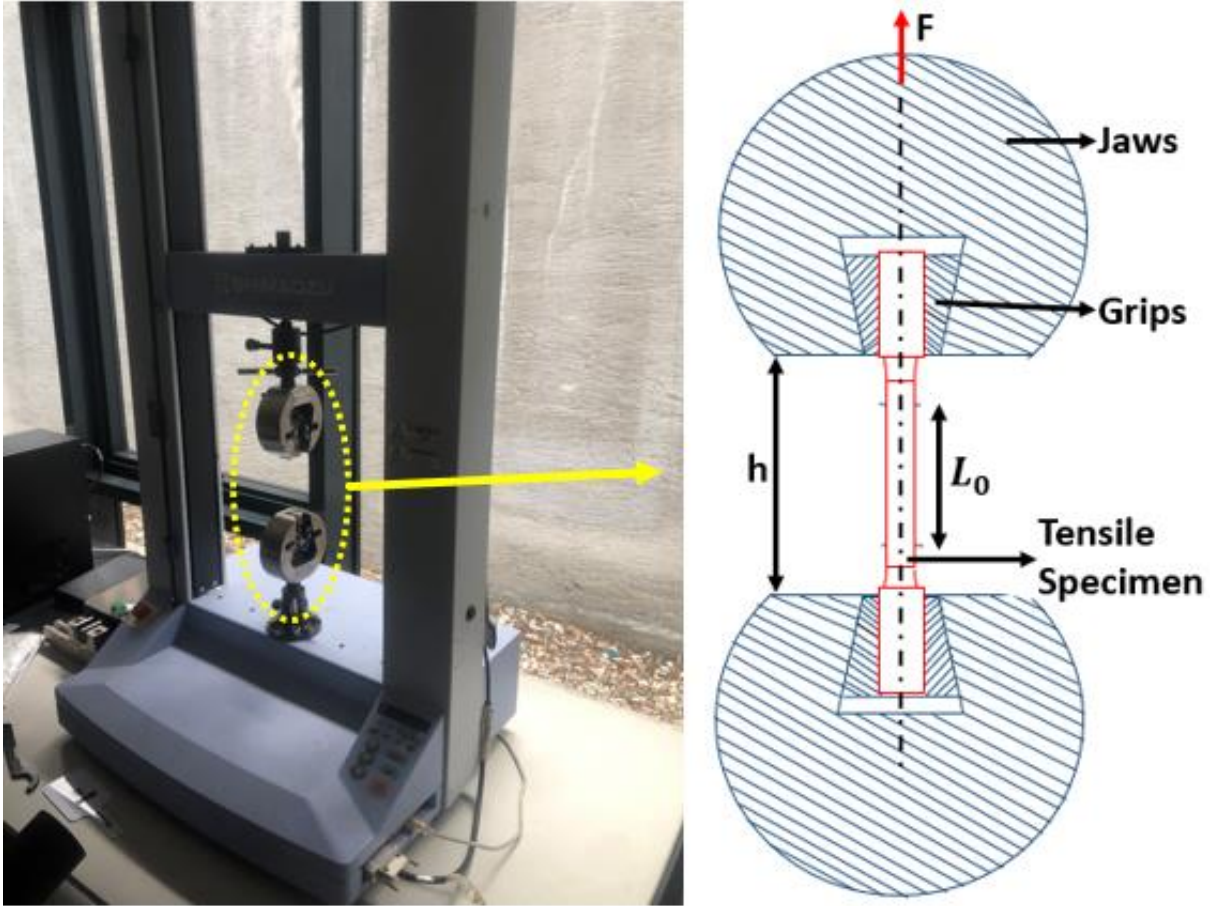
Figure 4.3 10 kN universal Shimadzu AGS-X and schematic representation of universal tensile testing machine (on the right)

Deforming the specimen at a constant cross-head displacement speed or strain rate is the standard approach to conduct the tensile tests. Therefore, the distance h, in the figure above, varies by the time so that the load must be applied to ensure the displacement rate as the test continues.

$$\frac{dh}{dt} = \dot{h} = constant \tag{4.2}$$

The tensile testing device only provided the force and displacement data throughout the experiments. To obtain the engineering stress data of the tested specimens, the following formula was used;

$$\sigma_{eng} = \frac{F}{A_0} \tag{4.3}$$

where F is the applied load and A_0 is the initial cross-sectional area. Displacements on the gauge length L_0 were recorded for the calculation of engineering strain by the following formula;

$$\varepsilon_{eng} = \frac{\Delta L}{L_0} \tag{4.4}$$

where ΔL is the change in the gauge length during test and L_0 represents the gauge length. To find the true strain and true stress data, a conventional conversion method from engineering to true was used. The test speeds were determined as 0.25 mm/min and 0.50 mm/min cross-head speeds to conduct the tensile test. Relatively slow displacement speeds were selected in order to observe the effect of hydrogen in the results because when hydrogen-charged specimens are subjected to a high rate of loadings or high strain rates, the effect of hydrogen on the total elongation of specimens is not often observed since dislocations could not able to find enough time to interact with the diffused or trapped hydrogen atoms. For that reason, two slow cross-head displacement speeds were chosen for easily tracking the hydrogen embrittlement phenomenon on stress-strain curves. As aforementioned earlier, tensile tests were performed with standard tensile test specimens and notched tensile test specimens. Figure 4.4 shows the dimensions of the standard tensile test specimen.
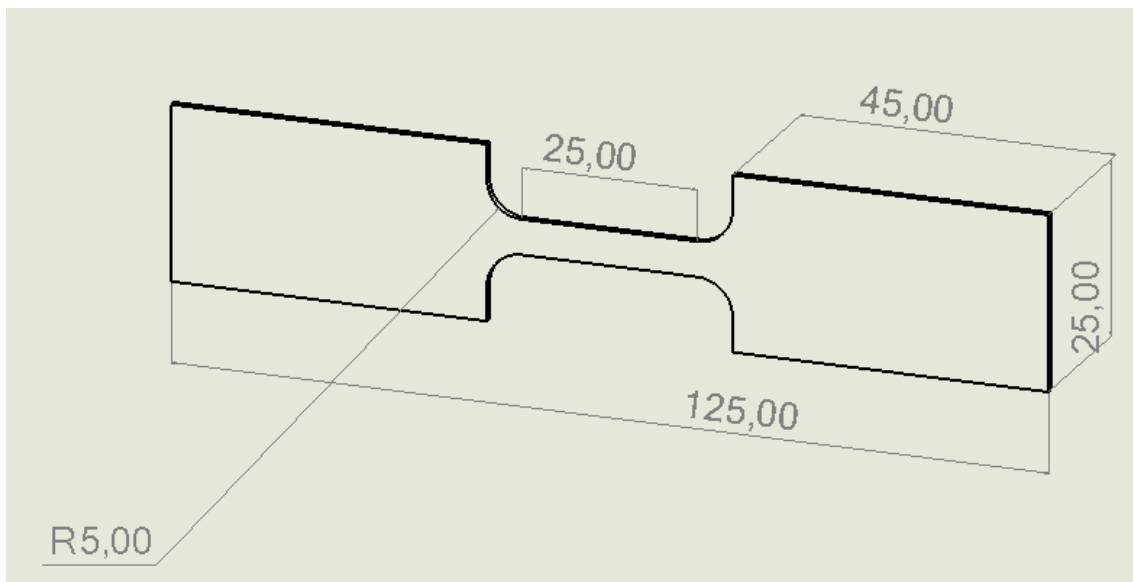
Figure 4.4 Standard tensile test specimen dimensions for Armor Steel-1 and Armor Steel-2

All tensile tests were carried out using a servo-hydraulic 10 kN universal tensile testing machine Shimadzu AGS-X and were repeated two times with and without hydrogen-charged specimens at each cross-head displacement speed to ensure the consistency of the results. Figure 4.5 demonstrates the true stress-true strain curves of armor steel-1 and armor steel-2 with and without hydrogen-charged specimens. To understand the detrimental effect of hydrogen on the mechanical behavior, specimens were subjected to 72 hours cathodic hydrogen-charging operation as defined in sub-section 4.1. Armor steel-1 exhibited a tensile elongation at break (fracture strain) as 0.103 and UTS of 1565 MPa. However, when exposed to hydrogen-rich environment, the mechanical properties of armor steel-1 were diminished as the fracture strain

and UTS of armor steel-1 were reduced to 0.076 and 1370 MPa, respectively. Armor steel-2, on the other hand, exhibited similar mechanical responses in line with armor steel-1 in the presence of hydrogen since they are both vulnerable to hydrogen embrittlement due to microstructural features. While as-received armor steel-2 had a total tensile elongation of 0.111 and UTS of 1875 MPa, the mechanical features of hydrogen-charged specimen remarkably reduced to 0.093 and 1772 MPa, respectively.
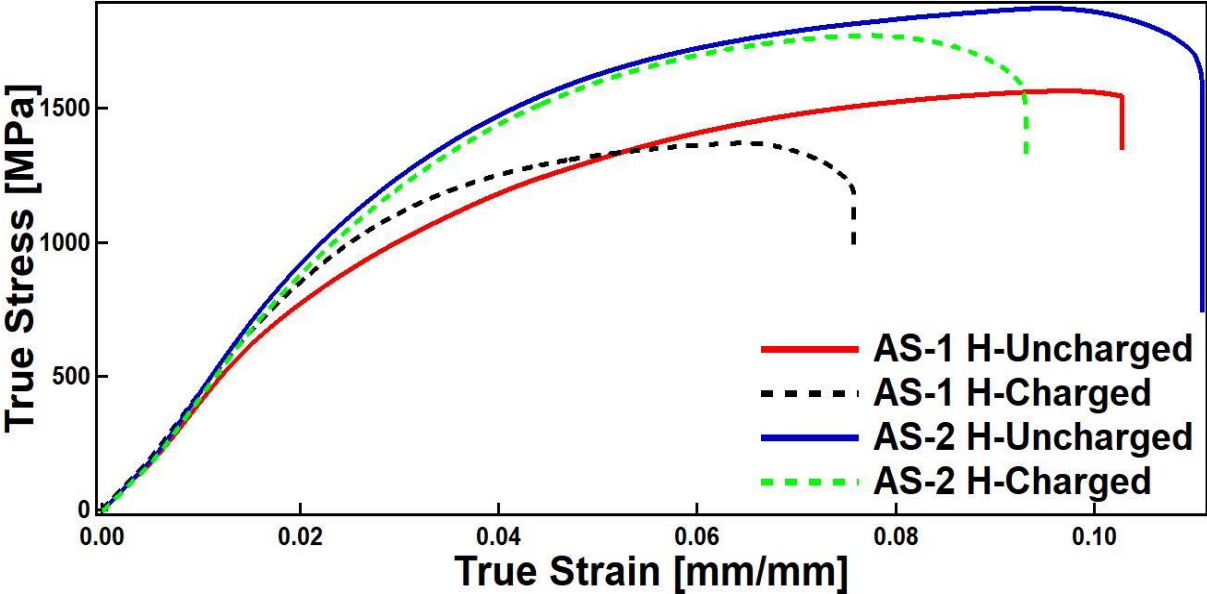
Figure 4.5 The true stress-true strain graph of as-received and hydrogen-charged Armor Steel-1 and Armor-Steel 2 specimens at 0.25 mm/min cross-head displacement speed

Furthermore, Figure 4.6 shows the true stress-true strain curves of as-received and hydrogen charged two different armor steels conducted at 0.5 mm/min cross-head displacement speed. Similar to the conducted tests at 0.25 mm/min, charging the specimens with hydrogen significantly reduced the fracture resistance, toughness and ductility of armor steel-1 and armor steel-2. For the case of armor steel-1, maximum tensile strength and yield strength slightly increased and fracture strain was reduced from 0.094 to 0.089 which was around 5.3% decrease in the ductility. On the other hand, the reduction in the total elongation of armor steel-2 was nearly 9.5%. In general, the ductility of armor steel-2 is relatively higher than that of armor steel-1 because the vulnerability of materials to the hydrogen embrittlement increases at higher UTS values in most cases.
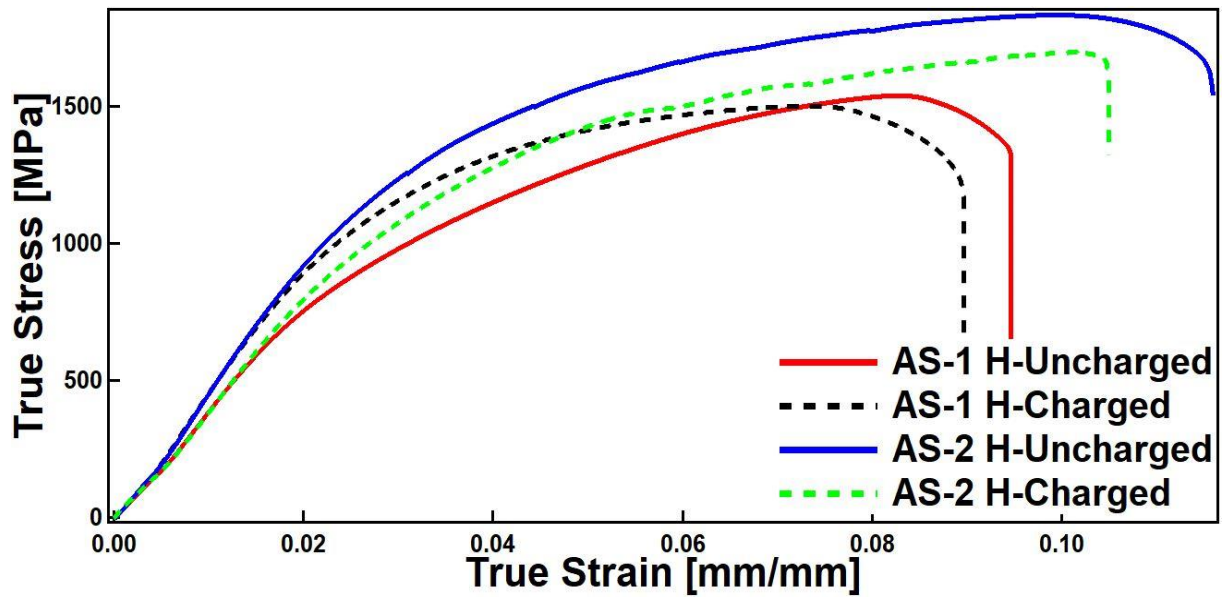
Figure 4.6 The true stress- true strain graph of as-received and hydrogen-charged Armor Steel-1 and Armor-Steel 2 specimens at 0.5 mm/min cross-head displacement speed

The influences of hydrogen on the mechanical behavior of armor steels, which possess nearly %100 martensitic microstructure and a small amount of retained austenite, were significantly observed because these steels are highly susceptible to hydrogen embrittlement due to their microstructures. As pointed out earlier in the thesis, armor steel-1 and armor steel-2 possess tempered martensitic microstructures and a vast number of review articles have been published on the HE behavior of martensitic steels and available in the literature. These review articles are mostly focused on the effect of HE on mechanical properties [104], microstructural activities [105], crack growth [106], type of material on hydrogen embrittlement threshold and most importantly HE mechanisms [107]. The diffusivity and solubility of hydrogen atoms in martensitic steels are considerably changed with the carbon content and also lattice defects such as dislocations, vacancies, subgrain boundaries occurred during the martensitic transformation, etc. [108]. Moreover, the amount of cementite/ferrite interfaces increases as a result of the tempering operation and they behave as newly occurred hydrogen trapping sites in the microstructure. Diffused hydrogen atoms are trapped in reversible and irreversible trapping sites and substantially affect the mechanical behavior of steels. The current literature on hydrogen embrittlement behavior of a different group of metals, steels and alloys remarks that the effect of hydrogen on the tensile properties of advanced high strength steels can be summarized in three subgroups;

➢ Diffused hydrogen atoms can harden the steel, as illustrated in the figure by the increase in the yield strength and maximum load.

➢ Diffused hydrogen atoms can soften the steel, as illustrated in the figure by the decrease in the yield strength and maximum load.

➢ Diffused hydrogen atoms usually can cause a reduction in ductility.

The experimental results obtained from tensile tests showed all possible scenarios that a reduction in ductility, a slight increase in the yield stress/UTS and lastly a decrease in the yield stress/UTS of armor steel-1 and armor steel-2 were observed. Moreover, these results also exhibit the success of cathodic hydrogen charging operation since similar influences of hydrogen on the mechanical behavior of martensitic steels are published in the literature.

4.2.2 Compression Tests

The uniaxial compression tests were carried out at 10^{-2} and 10^{-3} strain rates using a 100 kN Servohydraulic Instron 8801 testing machine. Figure 4.7 shows the as-received round specimens used in the experiments, the final shapes of specimens after the test and the Instron 8801 machine. While a round specimen with 8 mm diameter and 12 mm height was used to employ the experiments for the armor steel-1, the specimen with 6 mm diameter and 9 mm height was used for the armor steel-2. The tests for each condition (as-received, hydrogen charged and different strain rates) were repeated at least three times to ensure the accuracy of the results. Prior to compression tests, the upper and the lower surfaces of the specimens were oiled in order to reduce the friction.
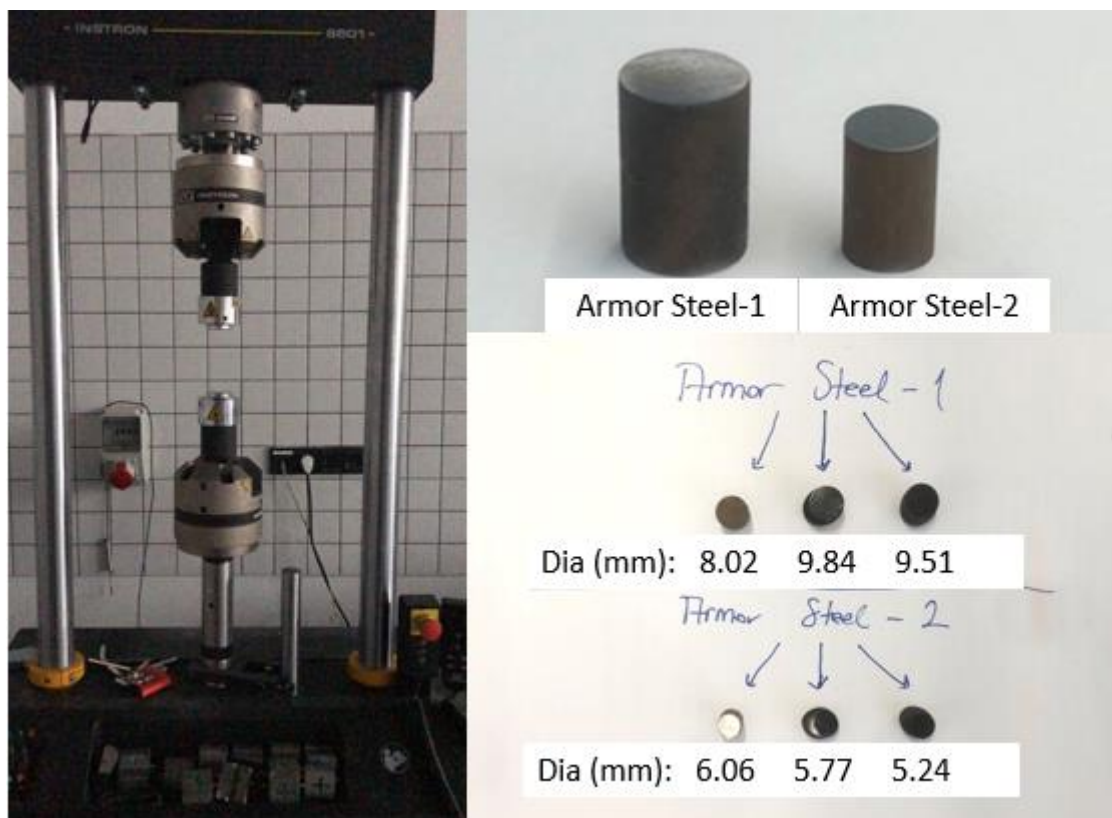
Figure 4.7 Instron 8801 hydraulic testing machine (on the left), compression test specimens and the diameter of as-received, hydrogen-charged and hydrogen-uncharged specimens after compression tests at 10⁻³ strain rate

Specimens were electrochemically charged with hydrogen as described in the sub-section 4.1. It is important to emphasize that applying the compression test to observe the hydrogen embrittlement behavior is not as common as tensile tests according to the total published articles in the literature. However, the results of the compression tests give some insightful data to extend the context of the thesis study. Figure 4.8 shows the true stress-true strain data of armor steel-1 conducted at 10^{-2} and 10^{-3} strain rates with two repetitions. At the beginning, the load and displacement data were obtained as the raw data and converted to engineering stress and engineering strain by applying the Eqs. (4.3) and (4.4). Later on, true stress and strain data were obtained using conventional conversion equations from engineering data to true. The results at different strain rates show that when the specimens are exposed to a hydrogen environment, the mechanical characteristic of armor steel-1 under compressive loading explicitly changed. The deleterious effect of hydrogen was more pronounced at a low strain rate (10^{-3} s⁻¹) because even though as-received specimens at 10^{-2} and 10^{-3} strain rates had similar reduction in total length value and stress values right before it breaks, testing the hydrogen charged specimen at 10^{-3} strain rate possessed a noteworthy effect since the total length was significantly reduced from 0.38 to 0.35. Moreover, hydrogen diffusion into microstructure slightly increased the UTS value

for the experiments conducted at a 10^{-2} strain rate because hydrogen leads to an increase in the microstructural activities and makes a contribution to the strain hardening of AHSSs. It is a very well-known fact that this phenomenon is more effective at a lower strain rate. The reason is that the interaction of hydrogen with moving dislocations is more distinct because of the sufficient time period.
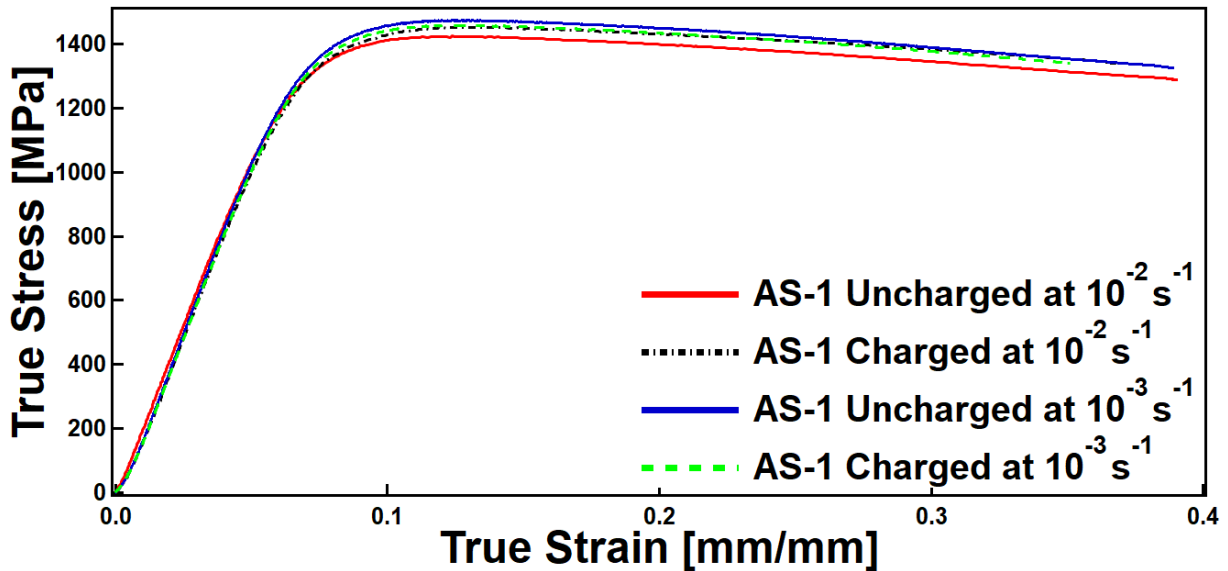
Figure 4.8 True stress vs. true strain graph of armor steel-1 at 10^{-2} and 10^{-3} strain rates with and without hydrogen charged specimens

Moreover, Figure 4.9 represents the stress-strain curves of as-received and hydrogen-charged armor steel-2 specimens conducted at 10^{-2} and 10^{-3} strain rates. Similar to the armor steel-1, the effect of hydrogen on the mechanical response of armor steel-2 was more apparent since a reduction in the total length and UTS has occurred. In addition to that, the effect of hydrogen was more pronounced at lower strain rates because the interaction of hydrogen with moving dislocations is not able to find sufficient time to cause the early fracture. These analyses were performed to figure out the fracture behavior and mechanical response by comparing the results of as-received specimens with hydrogen pre-charged specimens. Pre-charging the specimens with hydrogen undoubtedly increases the hydrogen concentration in the microstructure. It was also proven in our hydrogen measurement studies which will be mentioned in the upcoming sections. When the hydrogen content reaches a critical level, they could recombine to form hydrogen molecules and increases the internal pressure or they could form hydrides which lead to brittle fracture of structural components.
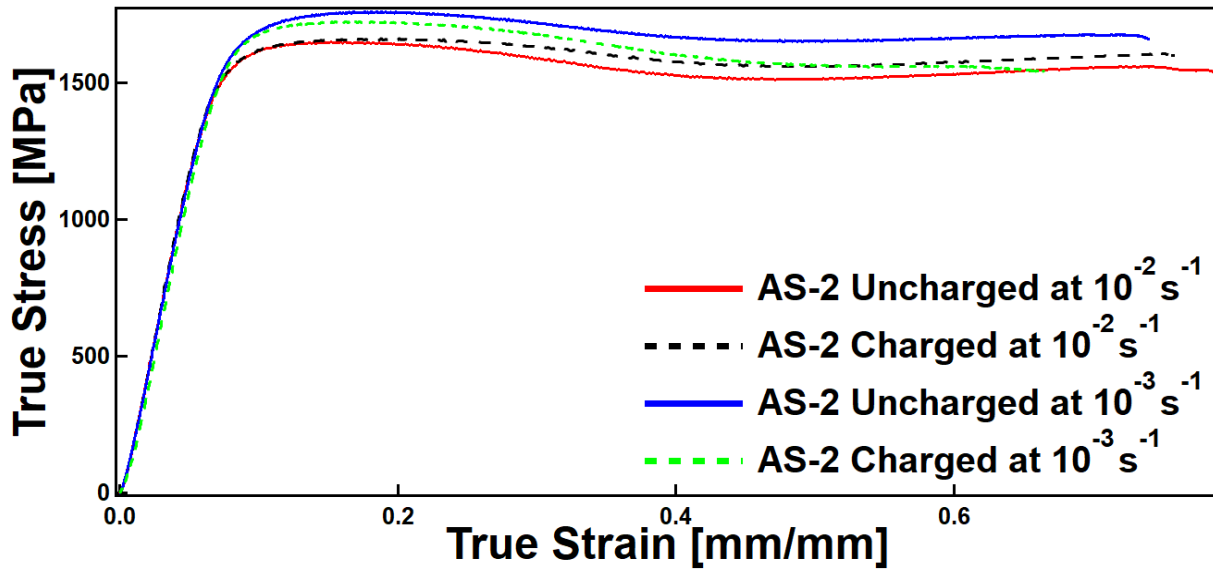
Figure 4.9 True stress vs. true strain graph of armor steel-2 at 10^{-2} and 10^{-3} strain rates with and without hydrogen charged specimens

4.2.3 Micro and Macro Hardness Tests

For further investigation of hydrogen embrittlement behavior of armor steels used in the hull protection of wheeled and combat vehicles of FNSS, micro and macro hardness tests were performed in the laboratory located at AGU. One of the most common mechanical tests performed on the material is the hardness test because it is simple in terms of applicability and does not damage the material compared to other test methods. In addition to that, when the hardness of a material is known, a connection can be made with other mechanical properties and thus some other properties can be obtained. For instance, the tensile strength of the steel is directly proportional to the hardness value. A simple hardness test, therefore, could shed light on some mechanical properties of materials. In order to determine the variation and the change in hardness value of as-received and hydrogen charged specimens, micro and macro hardness experiments were conducted at the AGU laboratory. Figure 4.10 shows the micro and macro hardness test devices. While microhardness tests were performed using a MICROBUL 1000D testing device, macro hardness tests were conducted with DIGIROCK Hardness Tester device. Both hardness measurements were repeated at least three times with as-received and hydrogen-charged specimens to obtain the data consistency and variation in the results. Figure 4.11 shows the dimensions of the specimen used in both hardness measurements. Measurements were taken near the notched area of specimens.

Figure 4.10 Microhardness (on the left) and macro hardness (on the right) test devices
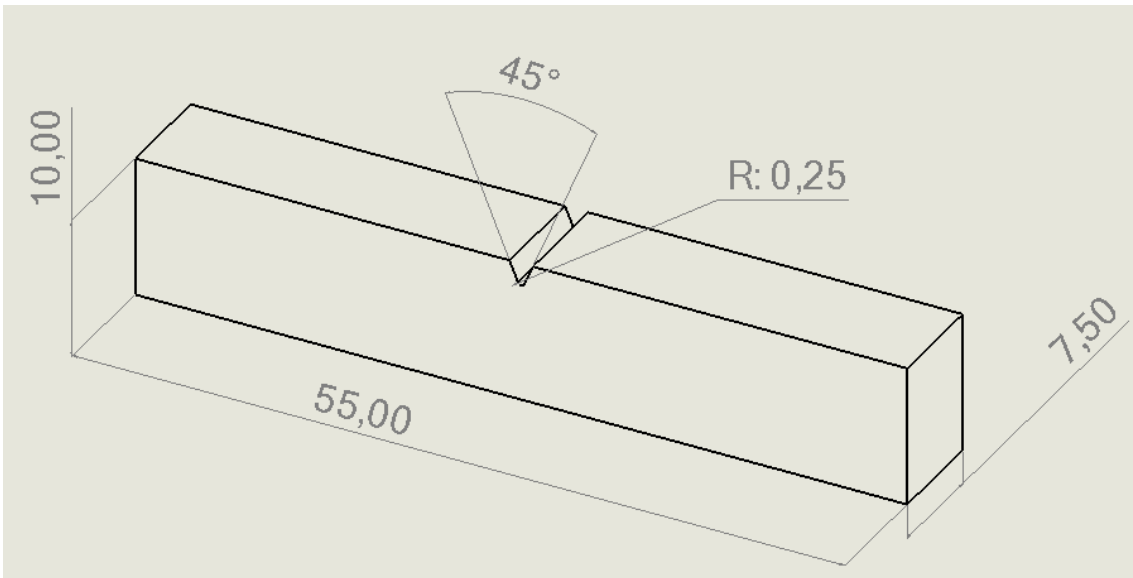
Figure 4.11 The specimen dimensions (in mm) used in hardness measurements

As the cathodic hydrogen charging process considerably affected the tensile and compression properties of the material, hardness property was also exhibited remarkable changes in the results. The previous studies published in the literature [109,110] also reveal that charging the specimen with hydrogen caused the hardening on the surface. Therefore, the

hardness measurements of hydrogen-charged specimens demonstrated a slight increase in both micro and macro hardness test results.

Table 4.1 Micro-hardness test results of armor steel-1 and armor steel-2

	Armor Steel-1		Armor Steel-2	
	As-received	**H-charged**	**As-received**	**H-charged**
TRIAL 1	465.8 HV1	481.8 HV1	510.3 HV1	527.3 HV1
TRIAL 2	462.8 HV1	470.8 HV1	509.2 HV1	523.2 HV1
TRIAL 3	457.6 HV1	473.6 HV1	501.8 HV1	518.8 HV1

Table 4.2 Macro-hardness test results of armor steel-1 and armor steel-2

	Armor Steel-1		Armor Steel-2	
	As-received	**H-charged**	**As-received**	**H-charged**
TRIAL 1	111.2 HRB	113.7 HRB	113.3 HRB	116.6 HRB
TRIAL 2	111.4 HRB	114.5 HRB	113.8 HRB	118.9 HRB
TRIAL 3	111.7 HRB	113.1 HRB	114.5 HRB	114.9 HRB

The average microhardness test results of as-received specimens of armor steel-1 and armor steel-2 were 462 and 507.1, respectively. However, when the specimens were subjected to electrochemical hydrogen charging for 72 hours at 100 A/m^{-2} current density, a remarkable increase in the hardness test results of hydrogen-charged specimens of armor steel-1 and armor steel-2 was obtained as 475.4 and 524.1, respectively. The current density and duration of charging time also affect the hardness test results. This increase may be attributed to the fact that diffused hydrogen atoms are pinning the dislocations in the microstructure and thus causes the hardening at the surface region. It is also a well-known fact that hydrogen atoms inhibit the movements of dislocations and contribute to the strain hardening of steels. When it comes to

the macro hardness test results, similar mechanical responses as in microhardness tests were observed. In the case of armor steel-1, charging the specimens with hydrogen led to a 2.2% average increase. On the other hand, the average test results of as-received and hydrogen-charged specimens were 111.4 and 116.6, respectively, which showed an average increase of 2.2% again. Thus, higher current density and long charging times allowed the specimens to be saturated enough with hydrogen and resulted in the increase in the hardness values due to the enhanced surface tension by pinning the dislocations in the microstructure.

4.2.4 High Strain Rate Tests

As it should be, armored combat and wheeled vehicles of FNSS must be conferred the safety-design regulations of suppliers in order to prove the reliability of the products. Particular attention has been given to the mechanical response of armored components at high strain rates and the earlier studies revealed that mechanical characteristics of metallic materials are strongly influenced by the rate of loadings [111]. Considering the working conditions of armored vehicles, at any time, they should provide enhanced protection against external threats such as mine explosions. Therefore, understanding the mechanical response of armored vehicles at high strain rates is of having importance and it is also vital to figure out the embrittlement behavior of material responses at high strain rate conditions. In addition to that, as in other experiments, high-speed deformation tests were performed with as-received and hydrogen-charged specimens to unveils the influence of hydrogen exposure on the mechanical response of armor steel-1 and armor steel-2 under high strain rates. The experiments with and without hydrogen charged specimens were carried out in the Gleeble 3500 thermo-physical simulator device in three repetitions. Figure 4.12 shows the Gleeble 3500 high strain testing device located at Metal Forming Center of Excellence in Atılım University and Figure 4.13 represents the dimensions of the specimen used in the high strain rate experiments. As in other experiments, the tests were conducted at least three times to ensure the consistency of the results.

Figure 4.12 Gleeble 3500 mechanical testing system
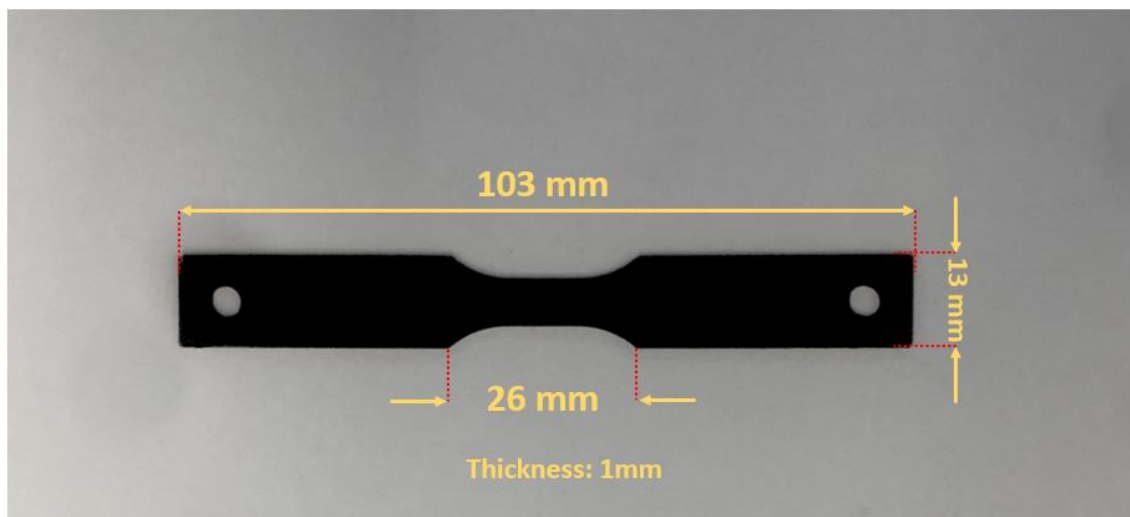
Figure 4.13 The dimensions of specimen used in high strain rate tests.

The mechanical behavior of armor steel-1 and armor steel-2 was investigated with and without hydrogen-charged specimens at 100 s^{-1}. Specimens were charged with hydrogen for 72 hours in an aqueous electrolyte solution at a current density of 100 A/m^2 to make sure that the specimen is enough saturated with hydrogen. Figure 4.14 shows the true stress-true strain behavior of as-received and hydrogen charged armor steel-1 specimens conducted at 100 s^{-1}. The load and displacement data were converted to engineering stress-engineering strain data by using the Eqs. (4.3) and (4.4) and then to true stress and true strain. In order to avoid the complexity of the graphs, only two of the performed experiments were given on the stress-strain graph. Since the specimens were pulled at a very high rate of loadings compared to quasi-static strain tests, some distinguished fluctuations were seen on the graphs, which are possible because of the slipping that occurred during the ongoing experiments. As outlined in the graph, as-received and hydrogen-charged specimens of armor steel-1 exhibited totally different elastic and plastic mechanical responses at a high strain rate. While the average total strain at fracture of as-received specimens was 0.275, a remarkable decrease in the average total strain of hydrogen-charged specimens was observed by 0.1729. This decrement was calculated to be approximately 37% for the hydrogen-charged specimens in comparison with the uncharged samples. This is a considerable and undesirable reduction not only for the defense industry but for all applications. Additionally, pre-charging the specimens with hydrogen caused a considerable increase in the yield strengths and a decrease in the UTS values when compared to uncharged specimens. These extraordinary alterations in the mechanical properties of armor steel-1 due to the pre-charging conditions could be attributed to the fact that atomic hydrogen notably enhances the microstructural activities in the microstructure. In the simplest terms, no

material is perfect in terms of atomic arrangement. In other words, there are some imperfections in the microstructure of the material. Voids, grain boundaries, dislocations, inclusions, etc. are some examples of these defects and are the best known. These imperfections are ideal places for the accumulation of hydrogen atoms, and whenever possible, these hydrogen atoms are diffused through the metals, they are accumulated to the interstitial sites and/or extraordinary sites. Later, these hydrogen atoms may be recombined in the lattice structure and increase the internal pressure which further leads to crack propagation in micro and nanoscales. Moreover, these diffused hydrogen atoms could also act as barriers against dislocations and restrict the movement of them. As the motion of dislocations is inhibited, the material gets more and more hardened which increases the yield strength. Yet, the failure occurs at the earlier stages as a result of the decrease in the mobility of dislocations [112].
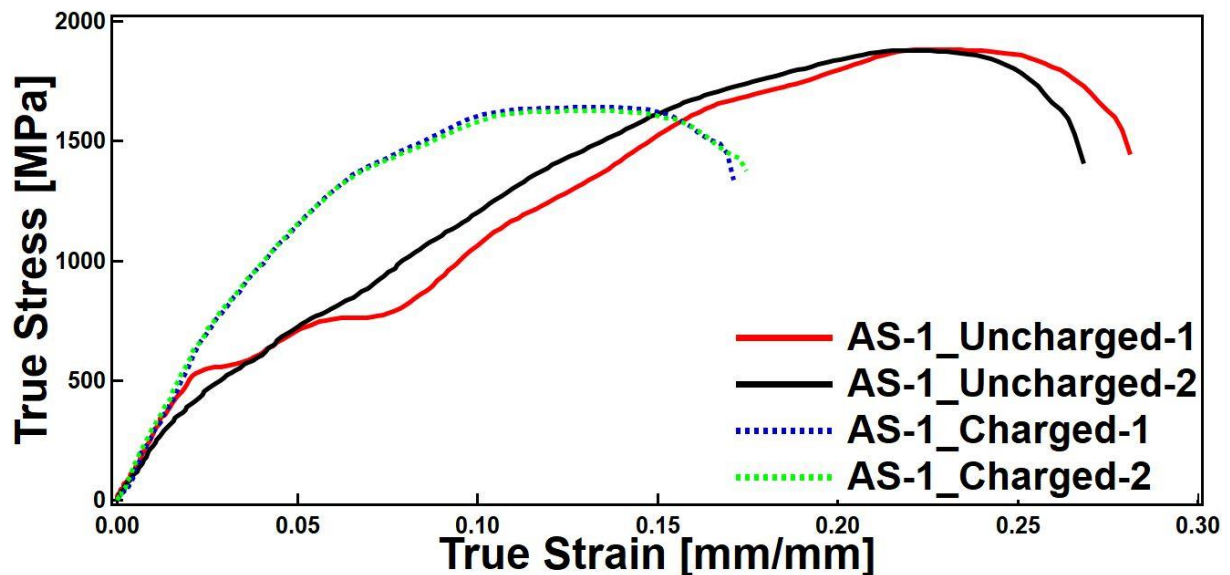
Figure 4.14 The true stress- true strain behavior of armor steel-1 with and without hydrogen conditions conducted at 100 s^{-1} strain rate.

Figure 4.15 shows the mechanical response of armor steel-2 with and without hydrogen presence under a high strain rate of 100 s^{-1}. Similar to the armor steel-1, pre-charging the armor steel-2 specimens with hydrogen caused noteworthy changes in the elastic and plastic properties. The most obvious change in the stress-strain response was in the ductility as always. The average fracture strain of armor steel-2 under a high strain rate reduced around 22% in the presence of hydrogen. However, no significant change in the yield strength and UTS was detected when compared to armor steel-1. To conclude the results obtained from experiments with armor steel-1 and armor steel-2 at 100 s^{-1}, the mechanical properties of armor steels in the presence of hydrogen remarkably decreased because of the detrimental effect of hydrogen

atoms in microstructure. It is obvious that the nature of hydrogen pre-charged armor steels changed from ductile behavior to brittle.
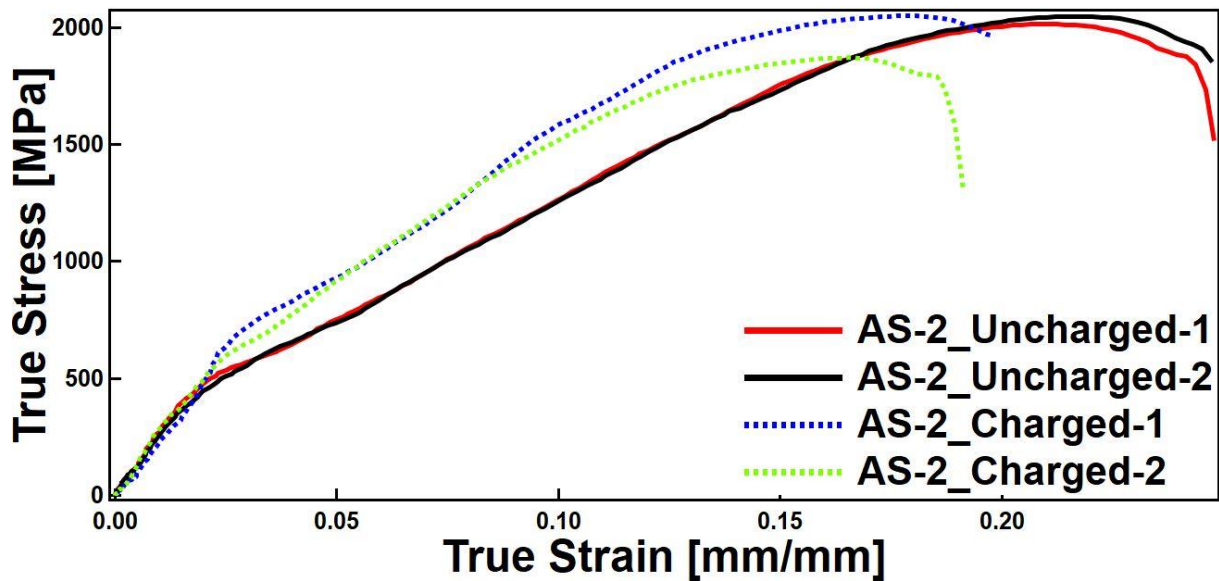
Figure 4.15 The stress-strain behavior of armor steel-2 with and without hydrogen conditions obtained at 100 s⁻¹ strain rate.

4.2.5 Charpy V-notched Impact Tests and Hydrogen Back-Diffusion

An impact test is performed to determine the amount of energy absorbed by material for breaking metallic and non-metallic materials under dynamic forces. It is carried out in order to obtain an idea about the mechanical properties of metallic materials such as toughness and ductile to brittle transition temperature. In other words, it is a widely used mechanical test technique to figure out whether the material is ductile or brittle. For the hydrogen embrittlement studies, applying the impact tests is very common to unveil the effect of hydrogen pre-charging on the mechanical properties of metallic materials [37,113,114]. Because charging the metallic materials with hydrogen significantly changes the mechanical responses as previously reported in this thesis studies and other studies published in the literature. Charpy V-notched (CVN) impact specimens were used in the experiments. The main purpose of the notch in the impact tests is to create a stress concentration (stress intensity) that will possibly exist within the material of the material at the bottom of the notch during impact and to determine the resistance of the material to dynamic forces in this case. When the impact force is applied to a notched sample, it creates a tension that is perpendicular to the bottom of the notch. As a result, fracture occurs with the effect of this tension force. To break the specimen, this vertical (normal) stress must be greater than the cohesive strength that holds the crystalline structure together or resists shifting of the crystals. If this happens before the sample has a chance for the occurrence of

plastic deformation, it is called brittle fracture in general terms. The CVN impact tests in this thesis were performed using armor steel-1 and armor steel-2 specimens with and without hydrogen-charged conditions. Specimens were continuously charged with hydrogen for 72 hours in the electrolyte solution at 353K. Figure 4.16 shows the impact test specimen used in the experiments. The reason of using these specific dimensions is to conform the MIL-DTL-12560 and MIL-DTL-46100 standards. In addition to that, all the experiments were performed at -40 ºC in accordance with abovementioned specific military standards.
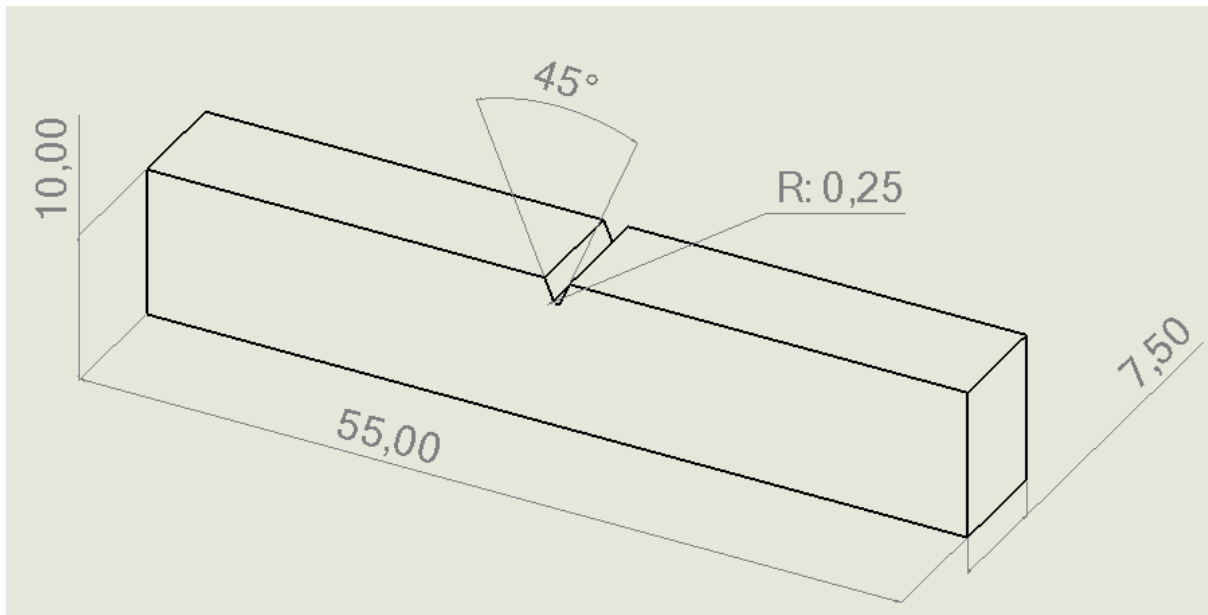
Figure 4.16 The dimensions of armor steel-1 and armor steel-2 impact test specimens in mm.

The experiments were carried out three times for each condition to measure the average results as well as data consistency. On the other hand, the hydrogen back-out operation was utilized to remove the diffused hydrogen atoms out of the microstructure. As reported in the introduction section, hydrogen embrittlement is a reversible process if the hydrogen atoms are driven out of the microstructure. Baking out the specimen is a common method that relies on heating the material at a certain temperature for a certain time. ASTM B850 – 98 is a standard that guides to reduce the risk of hydrogen embrittlement. This method suggests the necessary temperature and duration to completely remove the hydrogen from the crystal lattice based on the tensile strength of the material. However, these temperature and duration parameters need to be optimized for each material since the solubility and diffusion of hydrogen considerably changes by the type of material, microstructural features and specific conditions. Considering this situation, hydrogen bake-out process trials in armor steels used by FNSS were carried out at different temperature and duration parameters starting with the suggested ones in the ASTM B850 – 98. In the beginning, impact tests with CVN specimens were carried out with as-

received and hydrogen-charged specimens with three trials for each condition. The fracture resistance of specimens was performed with an AIT-300 EN test machine and Protherm PC442T is used for the baking of the hydrogen-charged specimens.

Figure 4.17 The AIT-300 EN impact test machine and Protherm PC442T baking device.

The average impact test results of armor steel-1 and armor steel-2 with and without hydrogen-charged specimens were obtained to determine the upper and the lower test values before the hydrogen bake-out process. While impacts tests with as-received and hydrogen-charged specimens of armor steel-1 were revealed the results as 41 J and 30 J respectively, the results were found as 27 J and 19.5 J. The obtained results from impact test experiments exhibited that pre-charging the specimens with hydrogen remarkably reduced the fracture resistance or toughness of armor steel-1 and armor steel-2. The average reduction percentage of two armor sheets of steel was more than 25%. As outlined in the HEDE mechanism, diffused hydrogen atoms dramatically lower the cohesive strength between atoms and lead to the premature fracture well below its permissible strength. Moreover, hydrogen atoms recombine in the metal lattices to form hydrogen molecules which increases the pressure effect on the grain walls. Micro and nano-sized cracks occur and decrease the fracture resistance. Table 4.3 shows all the experimental results of armor steel-1 and Figure 4.18 represents the corresponding fracture surfaces for each condition. In addition to the CVN impact values in the table, optimization parameters used in the experiments for the hydrogen bake-out process were also

provided. To begin with, the experimental results carried out with as-received and hydrogen-charged specimens gave an idea about the influence of hydrogen on the impact resistance. It has been observed that hydrogen-charged specimens were easily separated into two pieces compared to as-received specimens because of the lowered absorbed energy due to hydrogen. Also, the impact test results of as-received specimens were well consistent with the MIL-DTL-12560 military standard.

Table 4.3 CVN experimental results and corresponding bake-out parameters for Armor steel-1

	Trials	Baking Temperature	Baking Hours	Charpy Test Result
	As-received	-	-	41 J
	Charged	-	-	30 J
Armor Steel-1	#1	190 ºC	16	32 J
	#2	210 ºC	16	33.5 J
	#3	210 ºC	20	36.5 J
	#4	210 ºC	28	40 J
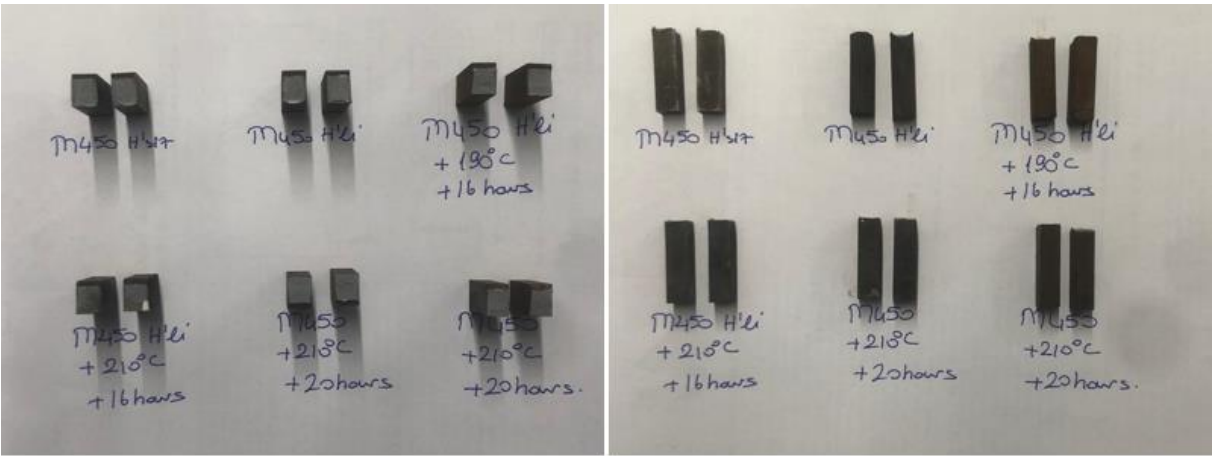
Figure 4.18 The fracture surfaces of all experiments carried out with armor steel-1

After performing the impact tests with as-received and hydrogen-charged specimens, hydrogen bake-out trials were started. Bake-out process parameters were selected from ASTM B850 – 98, which is shown in Figure 4.19. Prior to CVN impact tests, specimens were continuously charged with hydrogen under same conditions for 72 hours at 353K.

Class	Steels of Tensile Strength (R_m), MPa	Temperature, °C	Time, h
Hydrogen Embrittlement-Relief Treatment Classes for High-Strength Steels			
ER-0	not applicable		
ER-1	1701 to 1800	190–220	min 22
ER-2	1601 to 1700	190–220	min 20
ER-3	1501 to 1600	190–220	min 18
ER-4	1401 to 1500	190–220	min 16
ER-5	1301 to 1400	190–220	min 14
ER-6	1201 to 1300	190–220	min 12
ER-7[A]	1525 or greater	177–205	min 12
ER-8	1101 to 1200	190–220	min 10
ER-9	1000 to 1100	190–220	min 8
ER-10[A]	1250 to 1525	177–205	min 8
ER-11[A]	1450 to 1800	190–220	min 6
ER-12[A]	1000 to 1500	177–205	min 4
ER-13	1000 to 1800 unpeened items and for engineering chromium plated items	440–480	min 1
ER-14[A]	surface-hardened parts <1401	130–160	min 8
ER-15[A]	surface-hardened parts 1401 to 1800 plated with cadmium, tin, zinc, or their alloys	130–160	min 8
ER-16	surface-hardened parts <1401 plated with cadmium, tin, zinc, or their alloys	130–160	min 16

Figure 4.19 ASTM B850 – 98 Standard guide to reducing the risk of hydrogen embrittlement.

Following the hydrogen-charging process, the necessary parameters for the baking process were set on the device and the process was initiated. For the first set of armor steel-1 impact tests with the bake-out operation, temperature and duration were selected from ASTM standard as 190 ºC and 16 hours, respectively. Later on, baked specimens were kept in a deep-freezer at -40 ºC to confer the armor steel-1 military standard. The average CVN impact test result was found as 32 J, which showed a recovery in the impact resistance behavior of armor steel-1. However, it also exhibited that the process parameter was insufficient to remove the hydrogen out of microstructure because only 20% recovery in toughness occurred with these parameters. Therefore, these temperature and duration parameters must predictably be optimized. For the following set of impact test experiments, the temperature was increased from 190 ºC to 210 ºC to observe the single effect of temperature on the bake-out operation. For that reason, the duration has remained 16 hours. At the end of all experimental procedures which

includes hydrogen charging process, baking process and keeping the specimen at the deep-freezer to reach -40 ºC. The average CVN impact test result at the second set of baking experiments was 33.5 J, which possessed a slight improvement in the fracture resistance but not completely removed the charged hydrogen from the microstructure. For the third set of baking experiments, the duration parameter was increased from 16 hours to 20 hours to realize the effect of baking the specimen for longer hours. Therefore, the temperature has remained at 210 ºC. CVN experimental results exhibited a remarkable increase in the toughness value by 36.5 J. Hydrogen bake-out process parameters were still not completely optimized because the average impact test result of as-received specimens was 41 J. Finally, the duration parameter of the baking process was selected as 28 hours because the ASTM standard suggests the temperature between 190 ºC and 220 ºC but only minimum duration time is provided in the standard. For that reason, the duration parameter was increased instead of increasing the temperature to obey the ASTM standard. The average impact test result at the end was around 40 J, which showed almost complete removal of hydrogen atoms from microstructure and mechanical properties were regained. Hydrogen bake-out operation is a widely applied technique especially for the companies to satisfy the desired mechanical properties by suppliers. Table 4.4 shows, on the other hand, all the experimental results of armor steel-2 and Figure 4.20 demonstrates the physical appearances and corresponding fracture surfaces for each condition.

Table 4.4 CVN experimental results and corresponding bake-out parameters for Armor steel-2

	Trials	Baking Temperature	Baking Hours	Charpy Test Result
Armor Steel-2	As-received	-	-	27 J
	Charged	-	-	19.5 J
	#1	210 ºC	20	25 J
	#2	210 ºC	28	26.5 J
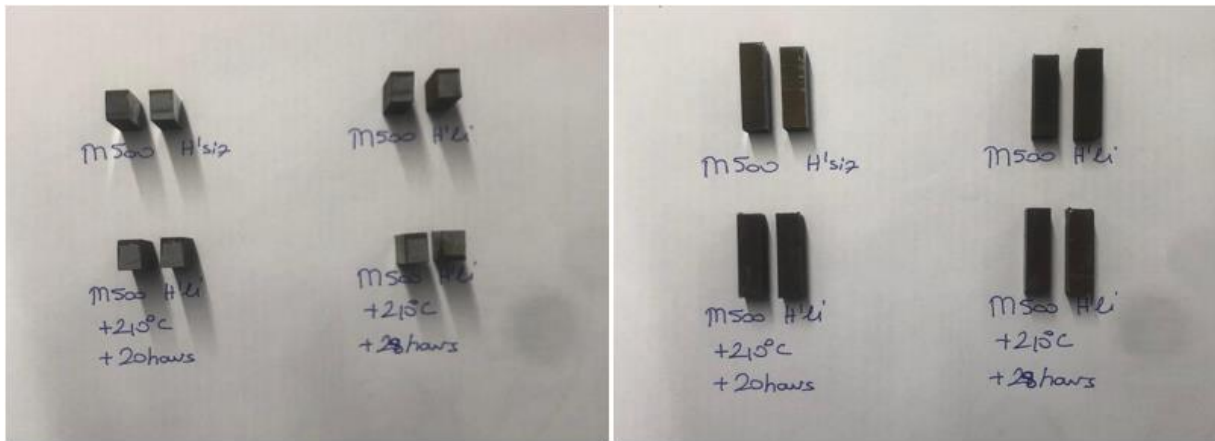
Figure 4.20 The fracture surfaces of all experiments carried out with armor steel-2

The hydrogen bake-out process and subsequent CVN impact tests provided an idea about the parameters that should be optimized for the bake-out studies. Logically, increasing the duration parameter allowed more hydrogen atoms to diffuse out of the microstructure. Heating the steel at high temperatures accelerate the mobility of hydrogen atoms in the crystal lattice but it is important to note that increasing the temperature higher than the suggested ASTM standard would cause some microstructural changes and thus lead to change in the mechanical features of materials. CVN impact test experiments of armor steel-2 with and without hydrogen-charged specimens were revealed the results as 27 J and 19.5 J respectively. The impact test results of as-received specimens were well consistent with the given MIL-DTL-46100 military standard. Since performing the bake-out operation with 190 ºC - 16 hours and 210 ºC - 16 hours for armor steel-1, experimental studies for armor steel-2 were directly started with 210 ºC and 20 hours process parameters because they do possess similar microstructural features and UTS values. The average results of CVN impact tests for the first baking operation were found as 25 J, which exhibited a remarkable recovery in the fracture toughness but not sufficient for the complete removal of hydrogen atoms from metal lattices. For that reason, the process parameters of armor steel-1 were selected to optimize the bake-out parameters for armor steel-2. The first set of CVN impact tests after baking at 210 ºC for 20 hours exhibited better results with 25 J compared to impact test experiments with hydrogen-charged specimens. However, baking the specimens for 20 hours was not enough to regain the mechanical properties as possessed without hydrogen presence. Finally, CVN impact test specimens were baked at 210 ºC for 28 hours to move the hydrogen atoms out of the microstructure and the average result of the second and last set of specimens was 26.5, which showed a total recovery in the impact resistance of armor steel-2. To sum up, it was proven that the hydrogen bake-out process was completely satisfactory based on the obtained results from CVN impact tests. To regain the

58

mechanical properties, armor steel-1 and armor steel-2 were baked at elevated temperatures for hours, starting with the process parameters suggested at ASTM B850 – 98. In the end, the process parameters were successfully optimized for two different armor sheets of steel used by FNSS.

4.3 Hydrogen Content Measurement and Hydrogen Diffusion Modeling

It is very common for hydrogen embrittlement studies to perform the content measurement of hydrogen atoms prior and after the pre-charging with hydrogen. There are several different types of hydrogen measurement techniques, such as Thermal desorption spectroscopy (TDS), inert gas fusion technique and electrochemical hydrogen permeation test, used in determining the amount of hydrogen atoms in the microstructure. Within the scope of this thesis, the content measurement of hydrogen was performed with one of the destructive measurement techniques called as inert gas fusion technique. As in other experimental studies, hydrogen charging operation was held with the cathodic hydrogen charging method for 72 hours in electrolyte hydrogen-rich solution at 353K. Using the water bath at 353K accelerated the diffusion of hydrogen atoms through the microstructure. Moreover, the electrolyte solution was changed with the fresh aqueous solution to increase the chance of higher hydrogen accumulation. Besides, the surface of specimens was ground to remove the black layer which was occurred in the period of charging. To begin with, hydrogen content measurement studies were carried out with LECO OH836 Series Elemental Analyzer, which is given in Figure 4.21.

Figure 4.21 LECO OH836 Series Elemental Analyzer

This instrument is designed for comprehensive measurement of the oxygen and hydrogen content of steel, metals and other inorganic materials. The inert gas fusion technique relies on the principle that a piece of the specimen is heated in the impulse furnace that reaches excessive temperatures up to 3000 ºC. Once the specimen is melted in the graphite crucible and the released gases are separated at the separation column and finally, the measurement of hydrogen is completed at the thermal conductivity cell. The measurement studies were conducted with 10 mm x 10 mm x 1 mm as-received and hydrogen charged specimens by two repetitions. Table 4.5 demonstrates the average measurement results of armor steel-1 and armor steel-2 specimens with and without hydrogen presence.

Table 4.5 Hydrogen content measurement results of armor steel-1 and armor steel-2

	Armor steel-1	Armor steel-2
As-received	20 ppm	13 ppm
H-charged	187 ppm	162 ppm

The hydrogen measurement results clearly show the success of the hydrogen charging operation since charging the specimens with hydrogen enhanced the average amount of hydrogen atoms approximately nine times for armor steel-1 and twelve times for armor steel-2. As outlined in the first chapter, materials become more and more susceptible as the strength and hardness increase. Armor steel-2 has higher strength and hardness values compared to armor steel-1 because they possess slightly different microstructural features due to the different

chemical compositions. Therefore, armor steel-2 has the higher capability to host hydrogen atoms.

UHSS grades are widely used as structural components in various applications but they are prone to hydrogen embrittlement due to their unique microstructures which possess higher possibilities for binding the hydrogen atoms. In summary, the diffusion of hydrogen atoms through microstructure would occur by some production and processing steps. Since hydrogen is very small element, it can be settled and accumulated in interstitial lattice sites and extraordinary hydrogen trap sites. Up to now, numerous studies have been performed to unveil the solubility and diffusivity behavior of hydrogen in UHSS [115–117]. The diffusion of hydrogen in metallic materials is greatly influenced by various factors such as alloying elements, type of microstructure, number of reversable /irreversible trap sites, plastic deformation, temperature and etc. For example, hydrogen diffusivity is significantly reduced as a result of enhancing the plastic deformation because newly generated dislocations, microcracks and distorted lattice act as a barrier for the transport of hydrogen. There are numerous methods available in the literature to measure the hydrogen diffusivity such as electrochemical hydrogen permeation measurement and TDS. In addition to that, researchers added several theoretical diffusion models to obtain a hydrogen diffusivity coefficient and they gave particular attention to the type of material, their microstructures and characteristics. The transport of hydrogen between adjacent interstitial sites occurs by the discreate jumps. As mentioned previously, water-bath was arranged to 353K during cathodic hydrogen charging to accelerate the hydrogen diffusion process and these discrete jumps. Thus, temperature is a key factor that strongly influences the hydrogen diffusion. In this thesis study, hydrogen diffusion coefficient (assumed to be constant at a given temperature) was found using Fick's second law (transitory regime) by given hydrogen charging time used in cathodic charging method. Moreover, this formula was also used to calculate the minimum required charging time for hydrogen diffusion to reach up to the center of the specimen (0.5 mm). Eq. (4.5) shows the abovementioned formula to calculate the hydrogen diffusion coefficient of armor steel-1 and armor steel-2 as follows;

$$\frac{C_{(x)} - C_0}{C_s - C_0} = 1 - \mathrm{erf}\left(\frac{x}{2\sqrt{Dt}}\right) \tag{4.5}$$

where D is the hydrogen diffusion constant, x is the depth of hydrogen in microstructure, C(x) is the hydrogen concentration at depth x, C_0 is the initial hydrogen concentration (t=0, C_0=0) and C_s is the surface hydrogen concentration (t=0, C_s=1). To obtain the hydrogen concentration at depth x at Fick's second law, SEM analysis were carried out with armor steel-1 and armor

steel-2 at high magnifications and high-resolution images were taken from fracture surface edges of notched tensile test specimens. Armor steel-1 and armor steel-2 possess unique microstructures (almost fully martensite and small island of retained austenite) but their chemical compositions slightly differ from each other. Therefore, similar hydrogen diffusion characteristics were observed for both armor steels.
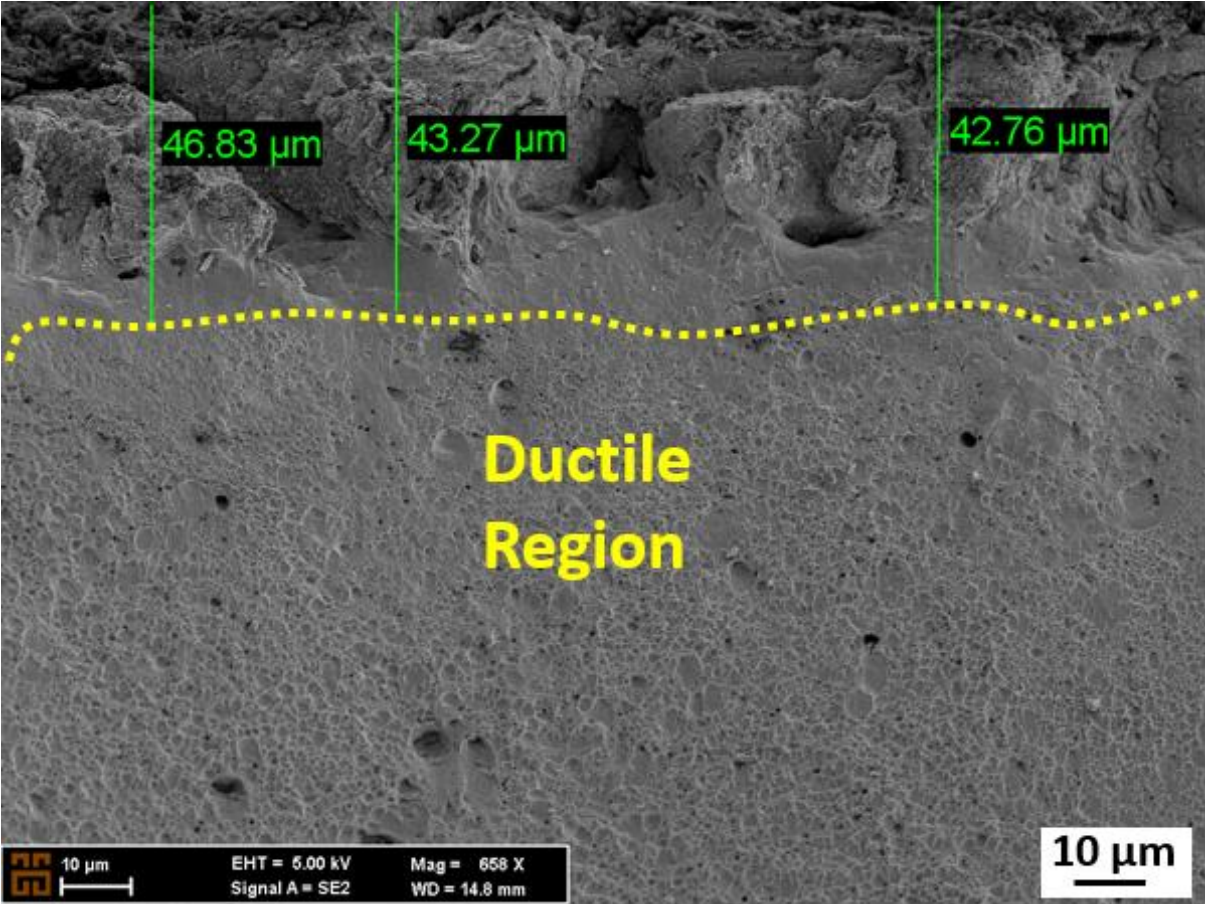
Figure 4.22 Overview of fracture surface of armor steel-1 and the depth of hydrogen-affected zone

Figure 4.22 clearly exhibits the hydrogen affected zone of armor steel-1 as a result of continuous hydrogen charging operation for 72 hours. Hydrogen was only diffused up to around 44.29 µm in average. While through the central region of armor steel-1 demonstrated a fully dimpled ductile fracture characteristic, the existence of hydrogen was exceedingly appeared at the subsurface of the specimens. The brittle fracture zone was not shown any sign of dimpled surface but instead a quasi-cleavage feature was dominant throughout the subsurface.
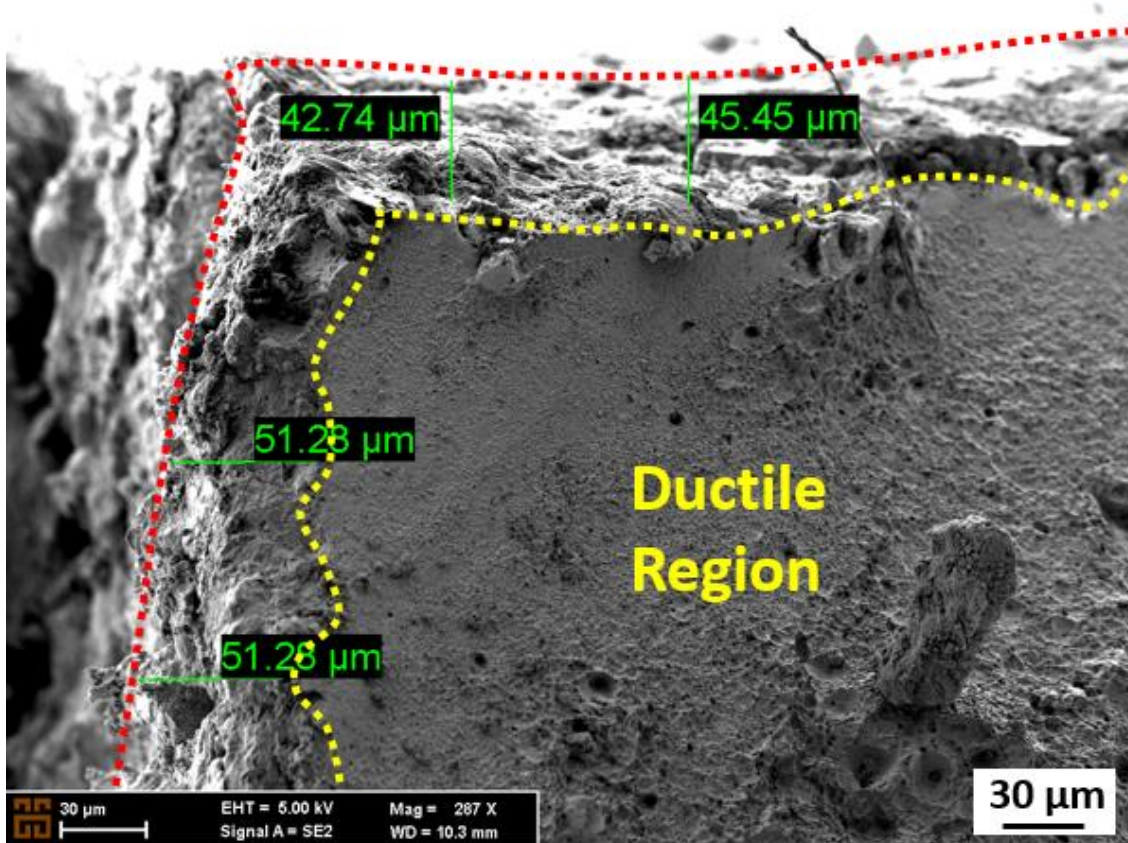
Figure 4.23 Overview of the fracture surface of armor steel-2 and the depth of the hydrogen-affected zone

Figure 4.23 shows the fracture surface and corresponding hydrogen-affected zone of armor steel-2 under a high magnification microscopic image. Similar to the armor steel-1, the central region of the specimen exhibited the signs of ductile fracture characteristics but the side regions of the specimen were significantly deteriorated by cathodic hydrogen charging. The average brittle fracture zone depth was around 47,69 μm, meaning that hydrogen could only reached up to this point. Table 4.6 shows the given parameters used to calculate the hydrogen diffusion coefficient.

Table 4.6 Fick's second law parameters for armor steel-1 and armor steel-2

Material	x (mm)	t (s)	C_x	C_0	C_s
Armor steel-1	0.0443	259200	0.000001	0	1
Armor steel-2	0.0477	259200	0.000001	0	1

In order to find the hydrogen diffusion coefficient, abbreviated as D, Fick's second law in Eq. (4.5) was applied for armor steel-1 as follows;

$$\frac{0.000001 - 0}{1 - 0} = 1 - \text{erf}\left(\frac{0.0443}{2\sqrt{D \times 259.200}}\right)$$

$$erf^{-1}(1 - 0.000001) = \frac{0.0443}{2\sqrt{D \times 259.200}}$$

$$2\sqrt{D \times 259.200} = \frac{0.0443}{3.4589}$$

$$D = 1.58 \times 10^{-10} \; mm^2/s$$

and was applied for armor steel-2 as follows;

$$\frac{0.000001 - 0}{1 - 0} = 1 - \text{erf}\left(\frac{0.0477}{2\sqrt{D \times 259.200}}\right)$$

$$erf^{-1}(1 - 0.000001) = \frac{0.0477}{2\sqrt{D \times 259.200}}$$

$$2\sqrt{D \times 259.200} = \frac{0.0477}{3.4589}$$

$$D = 1.834 \times 10^{-10} \; mm^2/s$$

Hydrogen diffusion coefficients D was found as 1.58×10^{-10} and 1.834×10^{-10} mm^2/s for armor steel-1 and armor steel-2, respectively. Similar diffusion coefficient results were obtained since armor steel-1 and armor steel-2 possess unique microstructures and thus similar diffusivity behavior. After calculating the hydrogen diffusion coefficients from Fick's second law, it was attempted to calculate pre-exponential factor (lattice diffusivity) D_0 from Arrhenius-like equation to make a comparison with published results in the literature. Arrhenius-like formula is as follows;

$$D = D_0 \exp\left(-\frac{E_a}{RT}\right) \tag{4.6}$$

where D_0 is the pre-exponential constant which would be considered as the frequency of attempt, E_a is the effective activation energy which would be considered as the minimum energy needed to overcome a diffusion jump, R is the gas constant and T is the hydrogen-charging temperature in Kelvin. Table 4.7 shows the parameters for armor steel-1 and armor steel-2 used to calculate the pre-exponential factor.

Table 4.7 Arrhenius-like equation hydrogen diffusion parameters for armor steel-1 and armor steel-2

Material	D (mm^2/s)	E_a (J/mol) [116]	R (J/K^{-1}mol^{-1})	T (K)
Armor steel-1	1.58×10^{-10}	45000	8.314	353
Armor steel-2	1.834×10^{-10}	45000	8.314	353

Eq. (4.6) was applied to solve the only unknown D_0 for armor steel-1:

$$1.58 \times 10^{-10} \, mm^2/s = D_0 \times \exp\left(-\frac{45000}{8.314 \times 353}\right)$$

$$D_0 = \frac{1.58 \times 10^{-10} \, mm^2/s}{2.20 \times 10^{-7}}$$

$$D_0 = 7.18 \times 10^{-4} \, mm^2/s$$

and was applied to solve the only unknown D_0 for armor steel-2:

$$1.834 \times 10^{-10} \, mm^2/s = D_0 \times \exp\left(-\frac{45000}{8.314 \times 353}\right)$$

$$D_0 = \frac{1.834 \times 10^{-10} \, mm^2/s}{2.20 \times 10^{-7}}$$

$$D_0 = 8.33 \times 10^{-4} mm^2/s$$

Pre-exponential factor D_0 was found as 7.18 x 10^{-4} and 8.33 x 10^{-4} mm^2/s for armor steel-1 and armor steel-2, respectively. To compare the obtained results D_0 of armor steel-1 and armor steel-2 with literature, a vast number of articles that cover the hydrogen diffusivity of UHSS were searched. The published results in the literature were in accordance with our obtained D_0 pre-exponential factors above [118]. Moreover, hydrogen diffusion profiles of armor steel-1 and armor steel-2 for different charging times at 353K were given in Figure 4.24 and Figure 4.25, respectively.
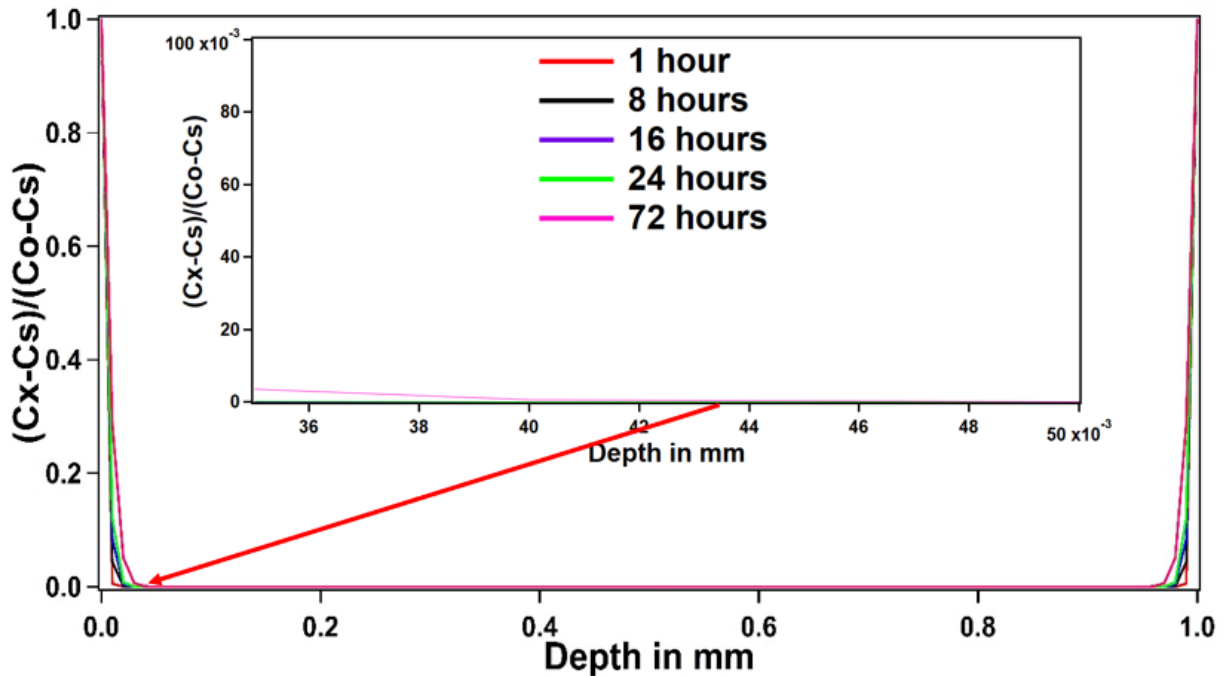
Figure 4.24 Hydrogen diffusion profiles of armor steel-1 for different hydrogen charging times at 353K
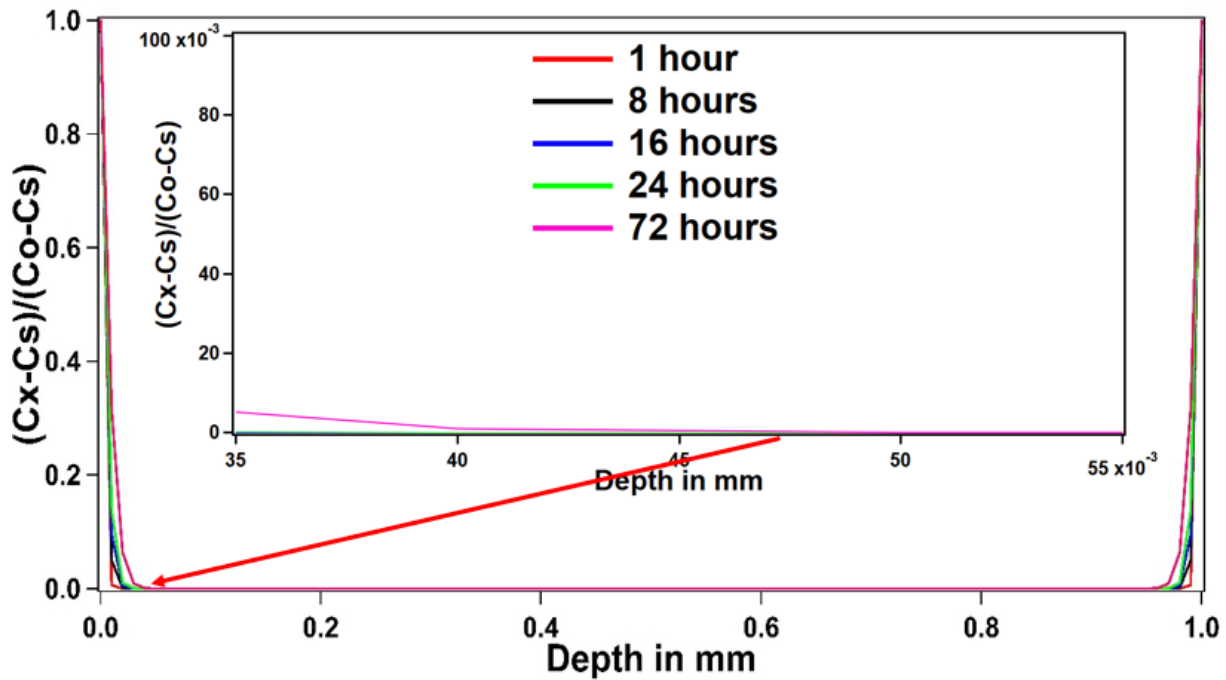
Figure 4.25 Hydrogen diffusion profiles of armor steel-2 for different hydrogen charging times at 353K

4.4 Sensitivity Analysis on Triaxiality Factor and Effect of Hydrogen on Fracture Locus

The stress triaxiality is known as one of the most important factors that governs the occurrence of ductile fracture. In the previous studies performed by Atkins [119], McClintock [120] and Rice [121], it was strongly pointed out that hydrostatic stress remarkably effect the fracture initiation of ductile materials, meaning that it changes with reference to stress state. Allowing considerable amount of deformation without fracturing is the ability of a material called as fracture ductility and equivalent fracture strain parameter smoothly reveals the fracture ductility of materials. Hancock and Mackenzie proposed that equivalent fracture strain could be shown as an exponential function of stress triaxiality. This relationship is called as fracture locus. In this study, the effect of hydrogen on fracture locus of armor steel-1 and armor steel-2 was investigated using uniaxial tensile test method at room temperature. Quasi-static regime was used to perform tensile tests (0,25 mm/min). 5 different sample geometries were used to investigate the fracture locus at different specific stress states. A digital image correlation (DIC) system was utilized to obtain the equivalent fracture strain. Finite element analysis (FEA) based simulations were carried out through plastic deformation to calculate the stress triaxiality factors of samples. Figure 4.26 shows the dimensions of 5 different samples which were

selected to assure of different stress triaxialities and estimate the effect of hydrogen charging on fracture locus.
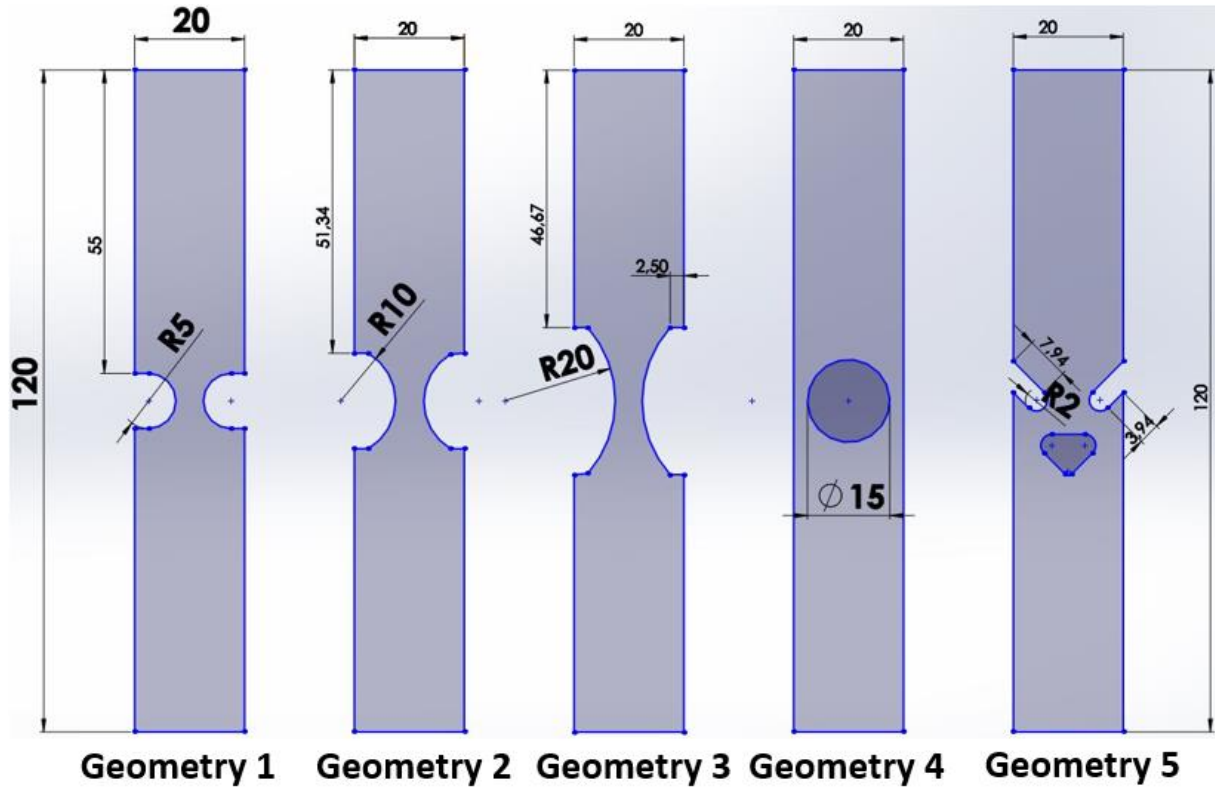
Figure 4.26 Specimen dimensions for tensile tests and fracture locus studies (unit: mm)

Stress triaxiality is often used in fracture mechanics in order to estimate the type of failures (ductile or brittle) in critical applications. In the field of continuum mechanics, stress triaxiality is defined as the ratio of hydrostatic stress to equivalent von Mises stress, which is given in Eq. (4.7).

$$STF = \frac{\sigma_{mean}}{\sigma_{eq}} = \frac{(\sigma_{11}+\sigma_{22}+\sigma_{33})/3}{\sigma_{eq}} \tag{4.7}$$

where σ_{mean}, σ_{eq}, σ_{11}, σ_{22} and σ_{33} represents mean stress (hydrostatic stress), equivalent stress and diagonal components of the Cauchy stress tensor, respectively. As described in the study of Bridgeman, analytical expressions of STF can be created based on the specimen geometry but these assumptions generally become highly controversial due to the usage of questionable parameters such as accurate plastic material behavior. Moreover, as pointed out earlier, STF is not constant during the plastic deformation process and it exhibits a spatial distribution. To overcome this challenge, it is appropriate to apply the FEA based simulations and perform an averaging process for the most critical integration point which is usually placed at the center of the notched cross section. Conducting the FEA based simulations results in the determination of nominal STF values of 5 different geometries in a more scientific manner. Abaqus CAE

software was used to construct the FEA models. These models totally mimicked the tensile test conditions. The equivalent plastic strain and Cauchy stress tensor were obtained using the post-processor to define the evaluation of STF.
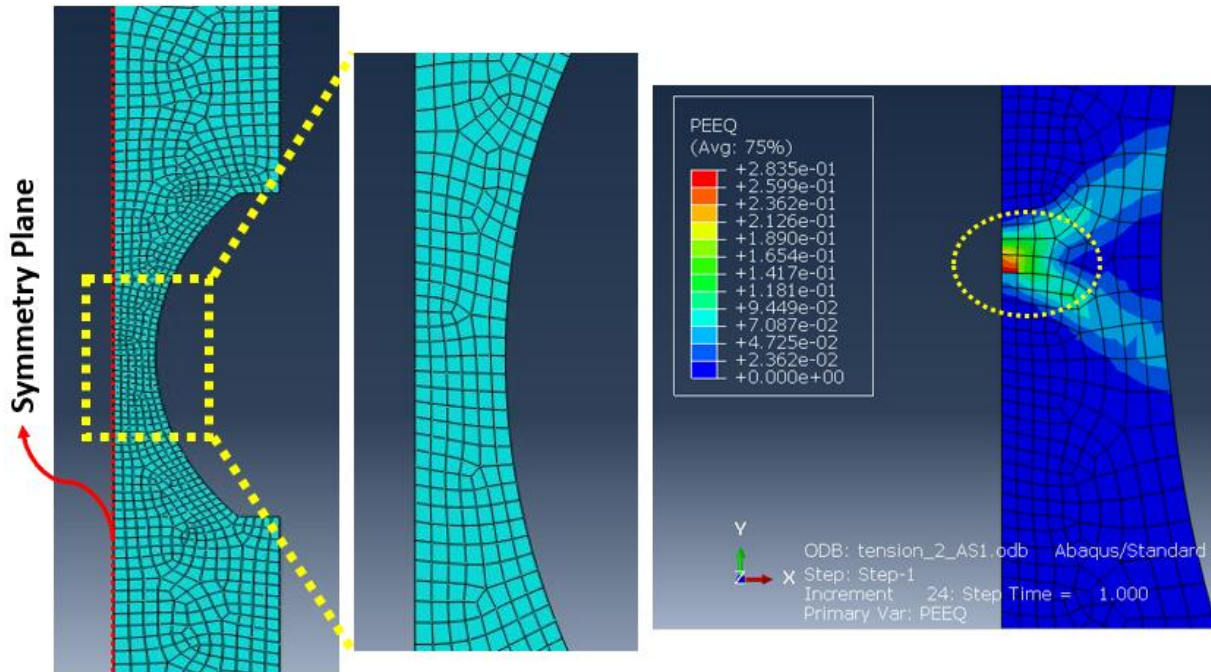
Figure 4.27 An example meshing structure of the specimen having a 20 mm notch radius (geometry-3) and equivalent plastic strain (PEEQ) results

The meshing structure of a specimen having a 20 mm notch radius were given in Figure 4.27. Double-bias seeding method was applied to perform all meshing operations of 5 different notched specimens. Since only central node in the notched cross section is important to calculate STF, the meshing element density increased on the symmetry plane in the direction of displayed arrows via double-bias seeding method. Since the specimens used in tensile tests have a thickness of 1 mm, a 4-node quadrilateral bilinear and reduce integration plane stress elements were used in FEA models. The element size from central node to edges of notched specimen was gradually decreased because the most critical nodes and elements are at the center of notched cross section. Therefore, double-bias meshing method was used to reduce the simulation time. Figure 4.28 shows the flow curve data of armor steel-1 and armor steel-2 which were obtained from uniaxial tensile tests at 0.25 mm/min cross-head displacement speed. These flow curve data were used in FEA based simulations to define the material model.
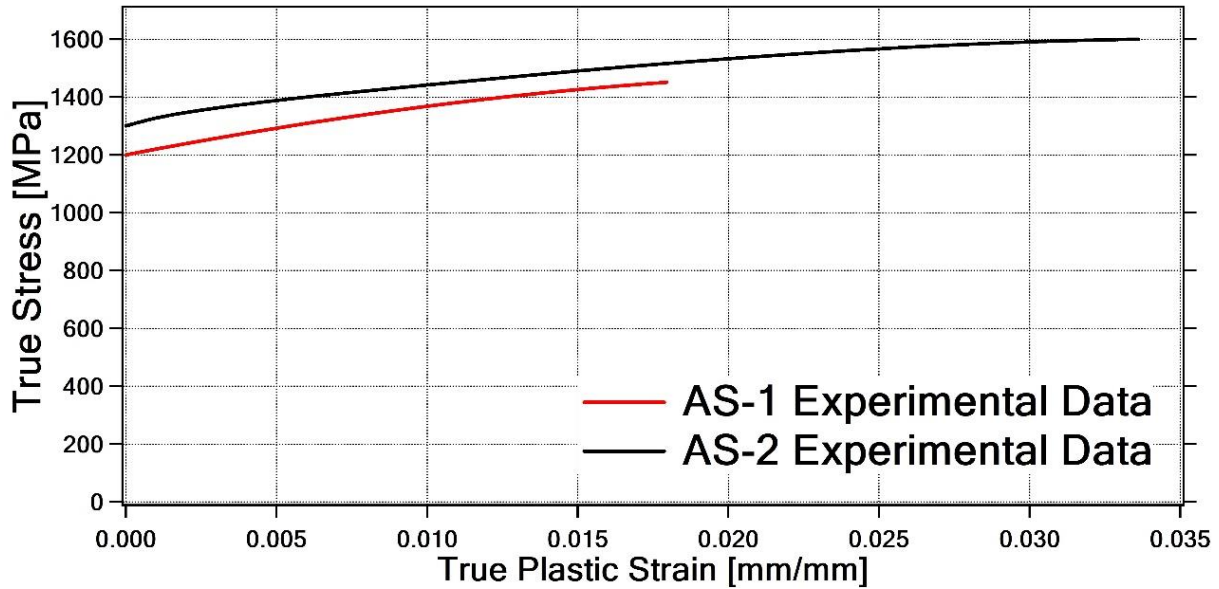
Figure 4.28 True stress-true plastic strain of armor steel-1 and armor steel-2 at 0.25 mm/min cross-head displacement speed.

Figure 4.29 and Figure 4.30 shows the STF evolution versus equivalent plastic strain of armor steel-1 and armor steel-2 for each geometry. In order to calculate the nominal STF values for each tensile specimen, Eq. (4.8) were used as follows;

$$\eta = \left(\frac{1}{\overline{\epsilon_p}}\right) * \int_0^{\overline{\epsilon}} \eta(\overline{\epsilon_p}) * d\overline{\epsilon_p} \qquad \textbf{(4.8)}$$

η represents the STF and $\overline{\epsilon_p}$ represents the equivalent plastic strain. As pointed out earlier, this integration was calculated from 0 to equivalent plastic strain for each sample. The nominal STF values and equivalent fracture strains for as-received and hydrogen charged conditions for each tensile specimen of armor steel-1 and armor steel-2 were tabulated in Table 4.8 and 4.9, respectively.

Table 4.8 Nominal STF and equivalent fracture strain of as-received and hydrogen-charged specimens for armor steel-1

	STF	Equivalent Fracture Strain	
		H-uncharged	H-charged
Geometry 1	0.5488	0.1601	0.1137
Geometry 2	0.4731	0.2041	0.1589
Geometry 3	0.4427	0.2107	0.1791
Geometry 4	0.3822	0.1204	0.1012
Geometry 5	0.2950	0.1337	0.0930

Table 4.9 Nominal STF and equivalent fracture strain of as-received and hydrogen-charged specimens for armor steel-2

	STF	Equivalent Fracture Strain	
		H-uncharged	H-charged
Geometry 1	0.5468	0.1645	0.1065
Geometry 2	0.4962	0.1985	0.1375
Geometry 3	0.4301	0.2226	0.1677
Geometry 4	0.3236	0.1007	0.1375
Geometry 5	0.2434	0.1232	0.0807
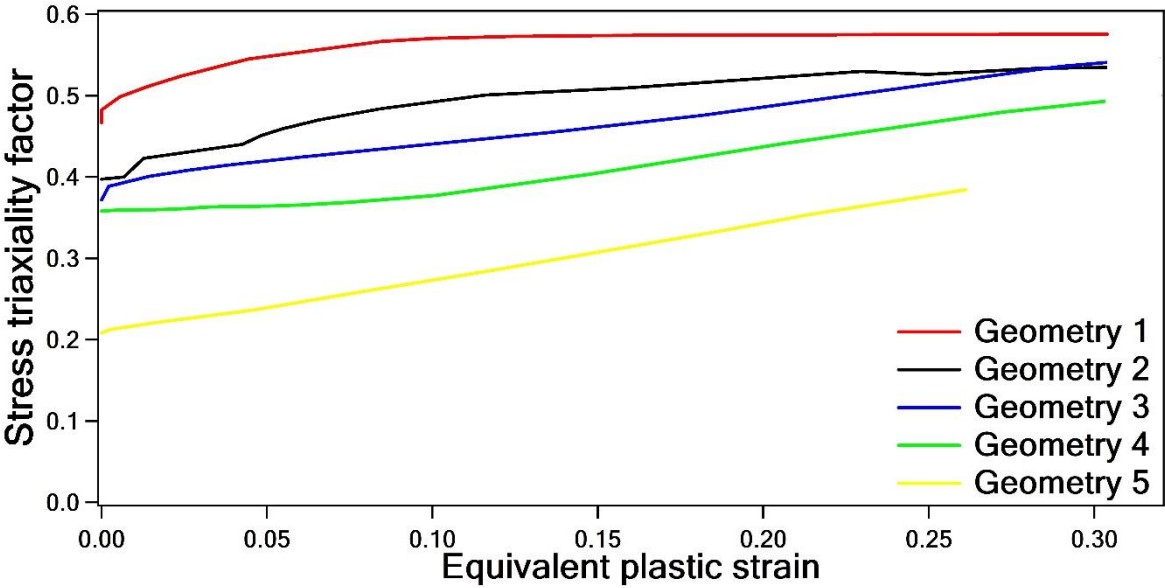
Figure 4.29 Evolution of the STF with respect to equivalent plastic strain for armor steel-1.
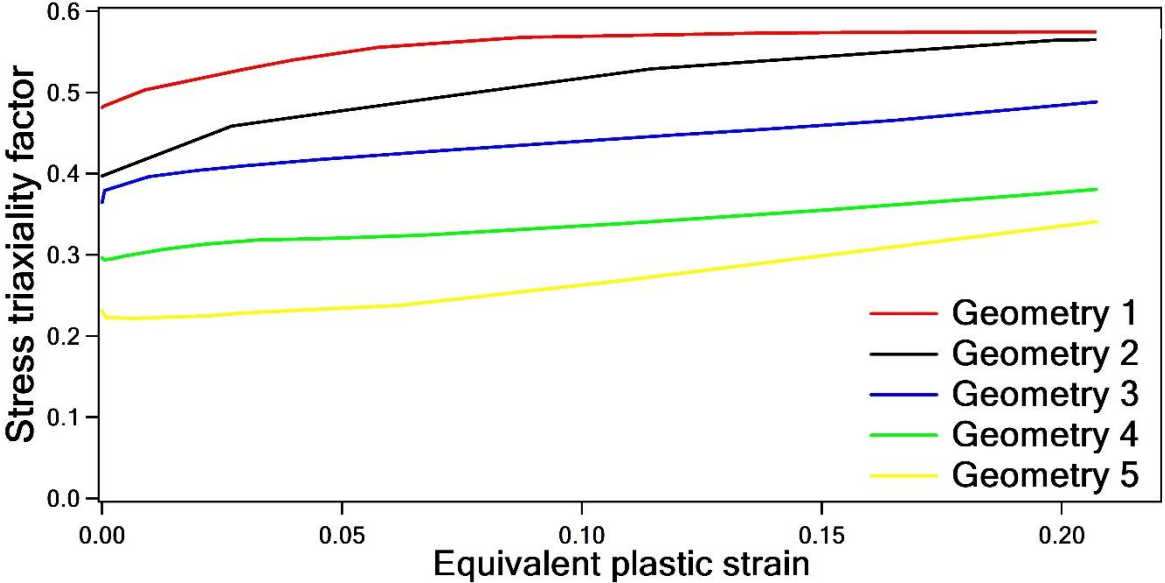
Figure 4.30 Evolution of the STF with respect to equivalent plastic strain for armor steel-2.

For the case of both steels, without the exception of geometry-5, STF moderately increased at the earlier stages of plastic deformation and reached almost a steady-state condition. The time for reaching the nearly steady-state condition was increased as notched radius increased. Since geometry-5 is a tensile-shear specimen, its STF evolution value would be the lowest one among all geometries which corresponds well with the FEA analysis results and literature. Moreover, as shown in Figure 4.26, the notch radius of geometries increases from geometry-1 (5 mm) to geometry-3 (20 mm). Increasing the notch radius progressively decreased the STF values because hydrostatic stress at the notched radius increases as a result of high stress localization and local strain hardening tendency when notch radius is decreased. For that reason, the evaluation of STF values should decrease from geometry-1 to geometry-3 and the STF of geometry-4 should be around 1/3. To sum up, in such circumstances, it is found that our STF values which were achieved from FEA simulations are in good agreement with the theoretical expressions and the published works in the literature [122,123].

Ncorr-a powerful and open-source MATLAB program-was performed to carry out Digital Image Correlation (DIC) analysis in order to compute the equivalent fracture strain for each geometry. A python script was used to calculate the equivalent fracture strain from Lagrangian strains, which will later be explained in detail. Before uniaxial tensile tests were conducted, at the beginning, randomly speckle patterns were produced by spraying the black paint solution onto the white background test specimens. The main purpose of having a white background is to obtain a smooth surface to facilitate tracking of black patterns during analysis. An example of speckle pattern study was given in Figure 4.31.

Figure 4.31 A speckle pattern application with tensile test specimen

The essential motivation of establishing this speckle pattern is to produce most accurate results since the images are used as inputs in Ncorr program. The basic principle of DIC is to obtain the information from the reference image (so-called undistorted image) in the following images (so-called distorted images). All images, including the reference image, were obtained from a video recording taken across the tensile test specimen parallel to the loading direction. Tensile tests were recorded with 4K-60fps Ultra HD resolution until the failure of the specimens. From the video recordings, 120 images were extracted for each geometry by using the DVDVideoSoft Free Studio software. Later on, these images were utilized in Ncorr program and processed by determining the region of interest (ROI) area to track the specific area to reduce the computational time and get rid of tracking unnecessary parts. The outputs of DIC analysis were in-plane Green-Lagrangian (GL) strains as $\epsilon_{xx}, \epsilon_{yy}$ and ϵ_{yx}. Then, principal strains ϵ_{11} and ϵ_{22} were computed from these obtained Green-Lagrangian strains using Eq (4.9):

$$\epsilon_{11,22} = \frac{\epsilon_{xx} + \epsilon_{yy}}{2} \pm \sqrt{\left(\frac{\epsilon_{xx} - \epsilon_{yy}}{2}\right)^2 + \left(\epsilon_{xy}\right)^2} \qquad \textbf{(4.9)}$$

Following after, the true (Hecky) principal strains were obtained using the calculated principal strains as shown in Eq (4.10) (For the details of Eq. (4.10), please refer to [101]):

$$\epsilon_{true} = ln\left(\sqrt{2 * \epsilon_{lang} + 1}\right) \qquad \textbf{(4.10)}$$

ϵ_{33}, the third component of principal true strain, was computed by volume consistency assumption of J2-plasticity theory. In the end, the equivalent fracture strain, ϵ_f, was explicitly calculated from the Von Mises equivalent strain equation as given in Eq (4.11).

$$\epsilon_f = \sqrt{\left(\frac{2}{3}\right) * \left(\epsilon_{11}^2 + \epsilon_{22}^2 + \epsilon_{33}^2\right)} \qquad \textbf{(4.11)}$$

Table 4.10 Step-by-step calculation of equivalent fracture strain with above given equations

	ϵ_{xx} (GL)	ϵ_{xy} (GL)	ϵ_{yy} (GL)	Principal GL Strain (ϵ_{11})	Principal GL Strain (ϵ_{22})	True Principal Strain (ϵ_{11})	True Principal Strain (ϵ_{22})	True Principal Strain (ϵ_{33})	Equivalent Fracture Strain
H-charged	-0.019	0.029	0.115	0.12	-0.026	0.109	-0.026	-0.083	**0.1137520**

H-uncharged	-0.023	0.055	0.166	0.18	-0.038	0.154	-0.039	-0.115	**0.1601061**

Table 4.10 shows an exemplary equivalent fracture strain results for as-received and hydrogen-charged armor steel-1 specimens which were calculated using the abovementioned equations. It starts with computing the GL strains from Ncorr program and ends with the calculation of equivalent fracture strain using Eq. (4.9).
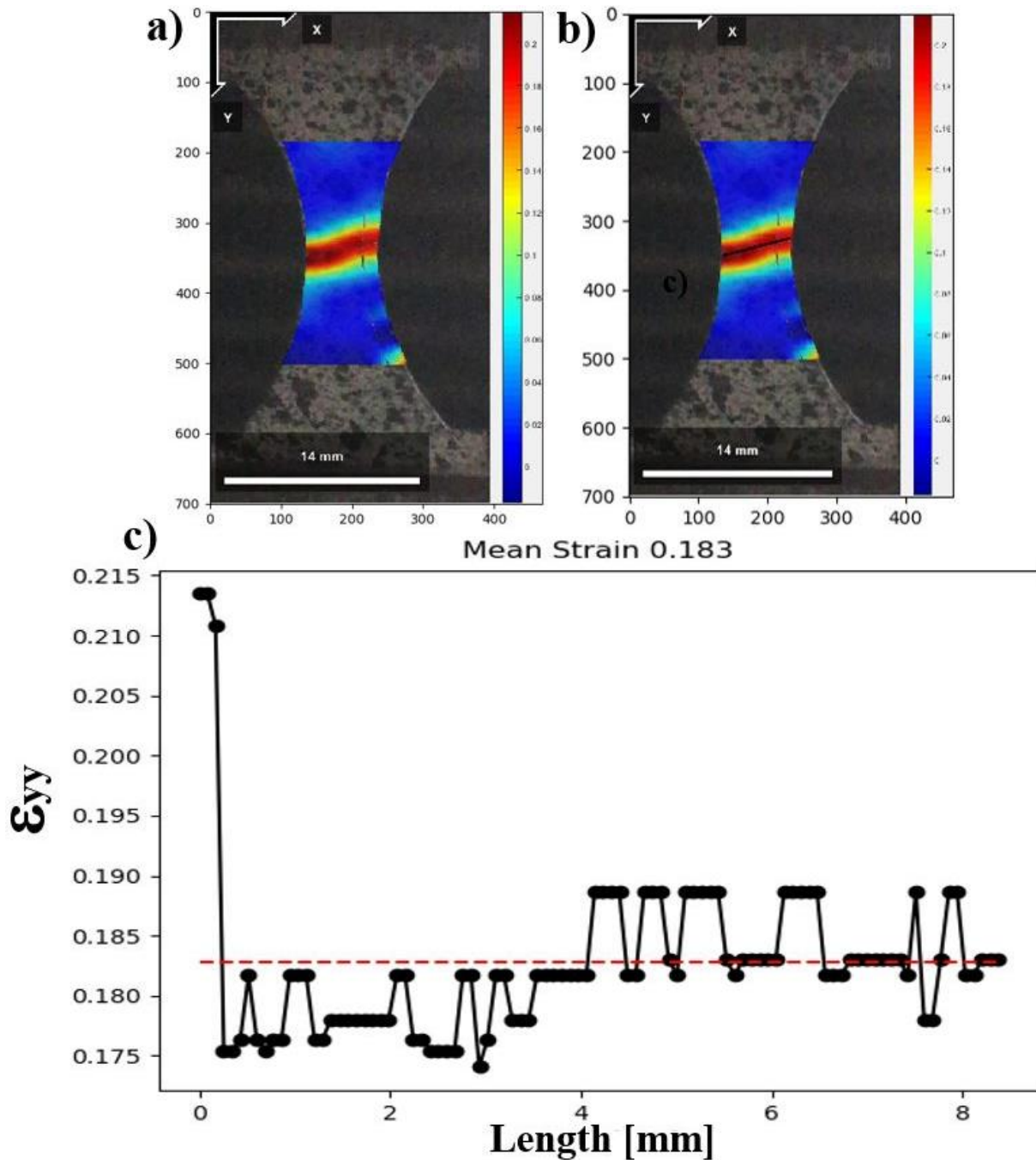
Figure 4.32 a) The reference image taken from post-processor Ncorr study for ϵ_{yy} b) the reference image with HSS line at the centered notch region c) Geometry-3 ϵ_{yy} of each pixel on HSS versus length in mm

As previously mentioned, at the end of Ncorr analysis with reference and distorted images in direction of ROI, reference image which was taken from post-processor Ncorr study was given with colorbar and its upper/lower limits. This python script employed in this study takes strain field and colorbar (rgb decomposition) as input to calculate the mean strain. To do this, highest strained section (HSS), the red region in Figure 4.32a and 4.32b, was marked with black line and the script computed the strain values of each pixel located on the marked black line direction of HSS. Figure 4.32c shows the mean strain calculation of each pixel on HSS for ϵ_{yy}.
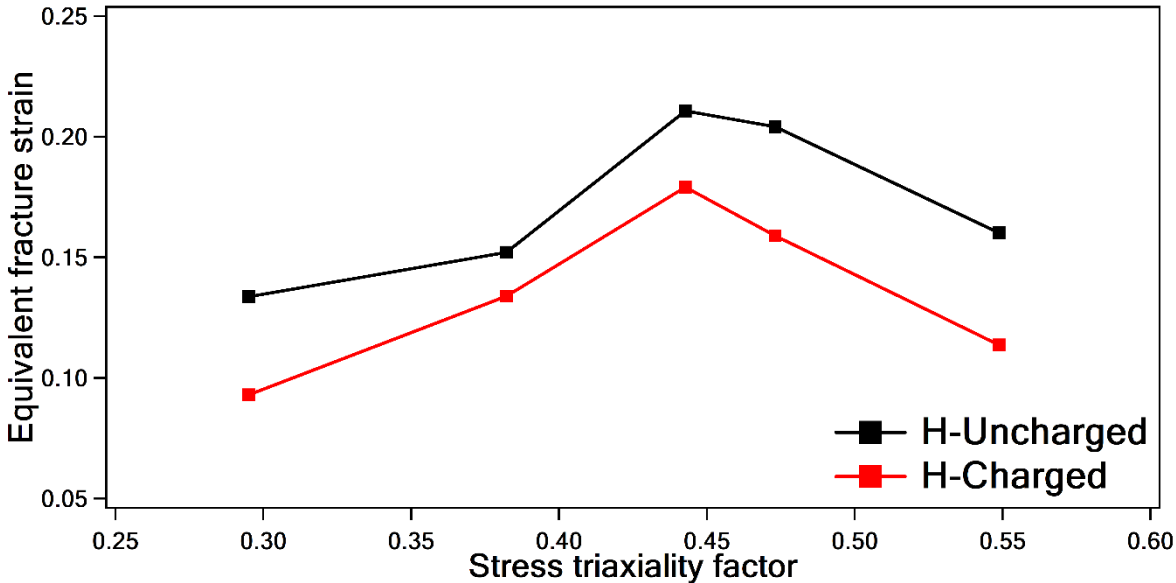
Figure 4.33 Fracture locus of the as-received and hydrogen-charged armor steel-1 specimens
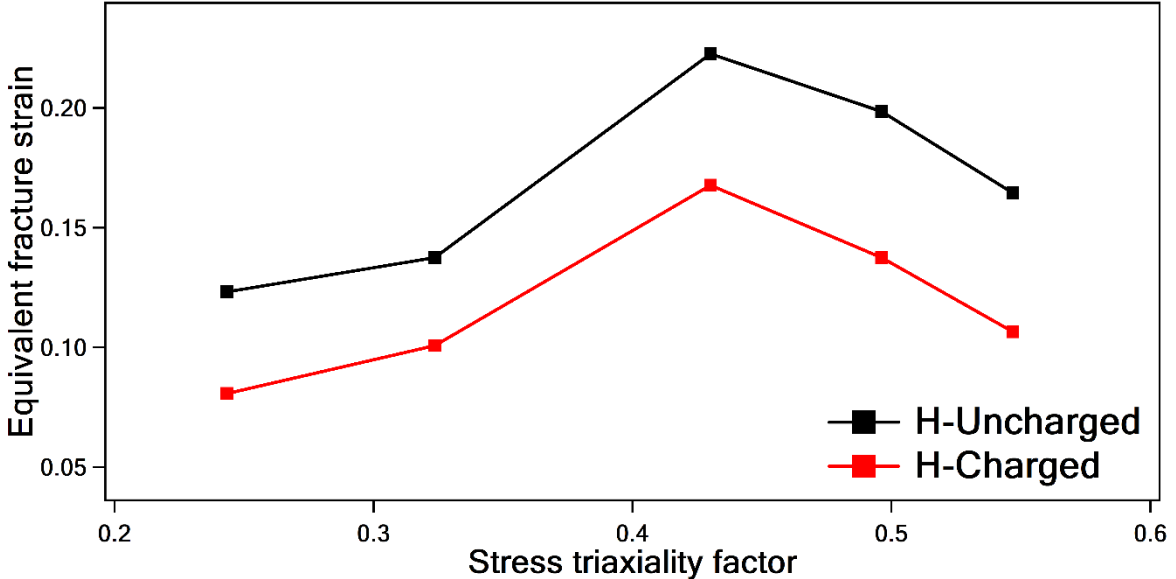
Figure 4.34 Fracture locus of the as-received and hydrogen-charged armor steel-2 specimens

Figure 4.33 and 4.34 shows the fracture locus of armor steel-1 and armor steel-2, respectively. These data were obtained from experimental studies by conducting the uniaxial tensile tests with 5 different geometries at 0.25 mm/min with/out hydrogen-charged samples. Additionally, it should be noted that these graphs were created with the aid of Table 4.8 and 4.9. Since the usage areas of UHSS are comprised of most critical applications such as defense, space and marine, fracture criterion of these kind of steels must properly be applied to predict the safe usage of materials (or structures and components) because they are subjected to various and combined loading modes. The term "fracture locus" defines the relationship between equivalent fracture strain and STF. The fracture locus analysis of armor steel-1 and armor steel-2 explicitly revealed that the presence of hydrogen in microstructure adversely effects the formability of both studied steels since the region under the line graphs of fracture locus provides us plastic deformation prior to fracturing. For the case of hydrogen-charged samples, they were subjected to cathodic hydrogen charging operation for 72 hours at 353K in an aqueous solution. The exposure to hydrogen-rich solution of armor steel-1 and armor steel-2 caused a drastic drop in the average fracture locus by approximately 22% and 30% percent, respectively. This novel finding of the effect of hydrogen on the fracture locus was also obtained in the previous study of author of the thesis and his advisors [101]. When investigated and analyzed the root cause of this abrupt reduction in the fracture locus of hydrogen-charged specimens, the diffusion of hydrogen atoms through microstructure enhanced the microstructural activities and during tensile tests analysis, diffused hydrogen atoms did act as barriers to restrict the movement of dislocations and thus an earlier fracture occurred compared to hydrogen-free specimens. As clearly described in Chapter 3, hydrogen atoms also reduce the cohesive energy between metal atoms and leads to catastrophic failures well below the permissible stress values. Therefore, equivalent fracture strain values decreased due to the earlier fractures of hydrogen-charged specimens. This finding also underlines the importance of reducing the possible risks of HE to confirm the safe usage of these armor steels during some manufacturing processes.
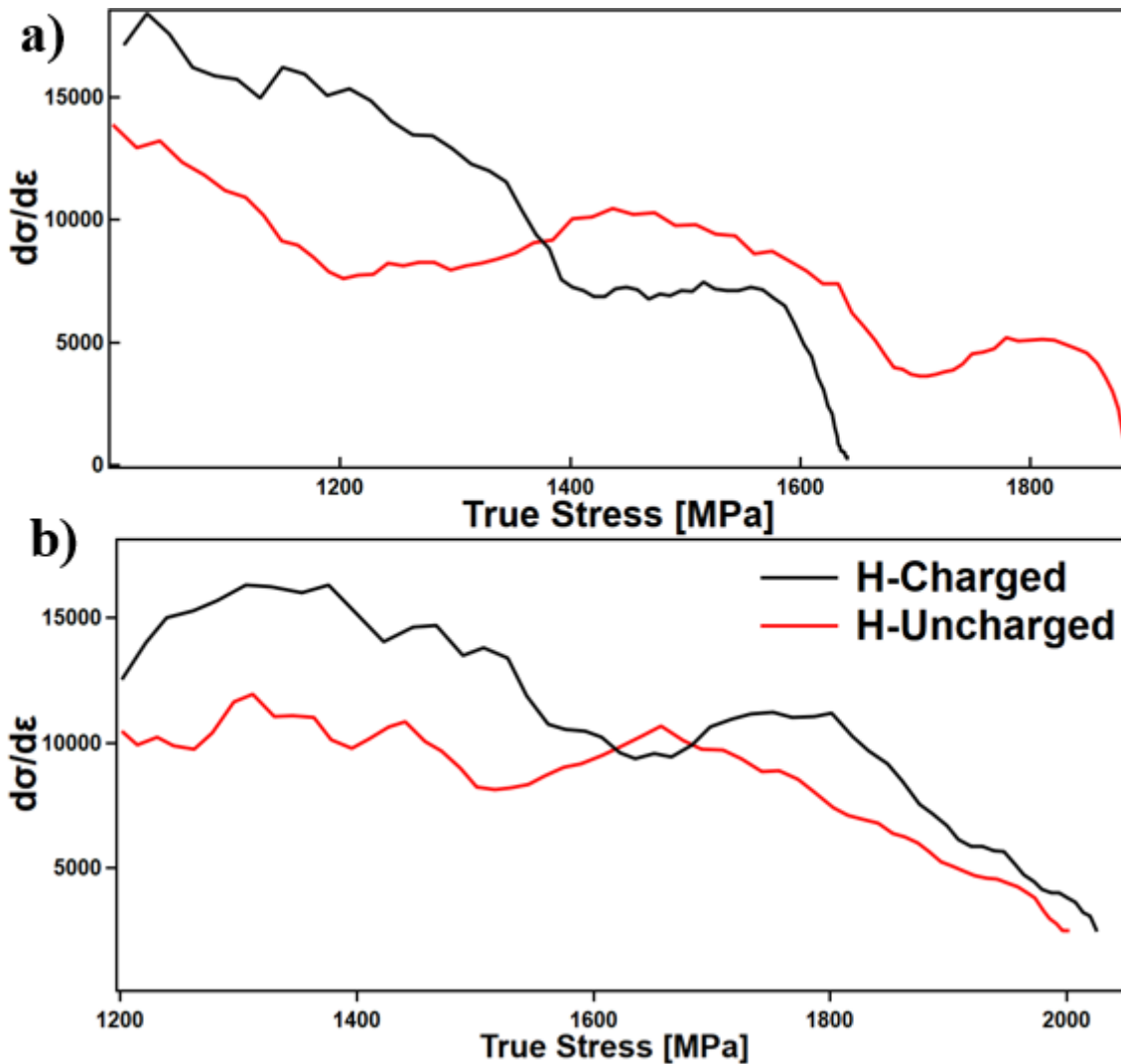
Figure 4.35 Kocks Mecking curves for hydrogen-charged and hydrogen-uncharged specimens at 100 s^{-1} strain rate. a) armor steel-1 b) armor steel-2

Lastly, the Kocks-Mecking curves of the armor steel-2 were given for notched tensile tests in Figure 4.35. The presence of hydrogen creates higher work hardening rate at the earlier stages of plastic deformation but after a while, hydrogen-charged and uncharged specimens possess the same trend.

4.5 Ballistic Tests and Effect of Hydrogen on Ballistic Performance

Ballistic tests are employed for armor steel of plates in order to investigate the impact resistance of armor steels against bullets. The ballistic test results submitted by the manufacturer must be satisfactory by the suppliers, so that armored military vehicles could be trustworthily

produced by defense industry companies. For instance, the manufacturers must guarantee on not to be fractured and perforated of armor steel plates within the range of ballistic limits given in the technical details of each steel. There are several different types of internal and external characteristic features which effect the ballistic performance of armored steel plates such as main alloying elements, type of microstructure, heat treating, the speed of bullet, the angle of shooting, distance, bullet diameter, etc. MIL-DTL-12560 and MIL-DTL-46100 are the most popular two armor steel grades currently in use. Started with World War II, these steel grades have been used but also made some improvements by years to enhance the ballistic resistance of them. In this thesis, ballistic tests were carried out with and without hydrogen-charged conditions to reveal the influences of hydrogen on the mechanical response of armor steel-1 and armor steel-2. As demonstrated in the previous experimental observations in this thesis, hydrogen remarkably degraded the characteristic features of armor steels in a negative way. Since ballistic performance of armor steels is of utmost importance for armored military vehicle producers, ballistic tests were performed with as-received and hydrogen charged specimens. Specimens were continuously subjected to hydrogen in the electrolyte solution at 353K for 72 hours to ensure the diffusion and progress of hydrogen atoms towards the inner side of microstructure. Figure 4.36 shows the specimens used in the experimental investigations for ballistic tests and Figure 4.37 shows the dimensions of armor steels used in the experimental investigations of ballistic tests. The dimensions of specimens used in ballistic tests were selected relatively bigger than other specimens used in another experimental investigations because of making easier the bullet to find the target.
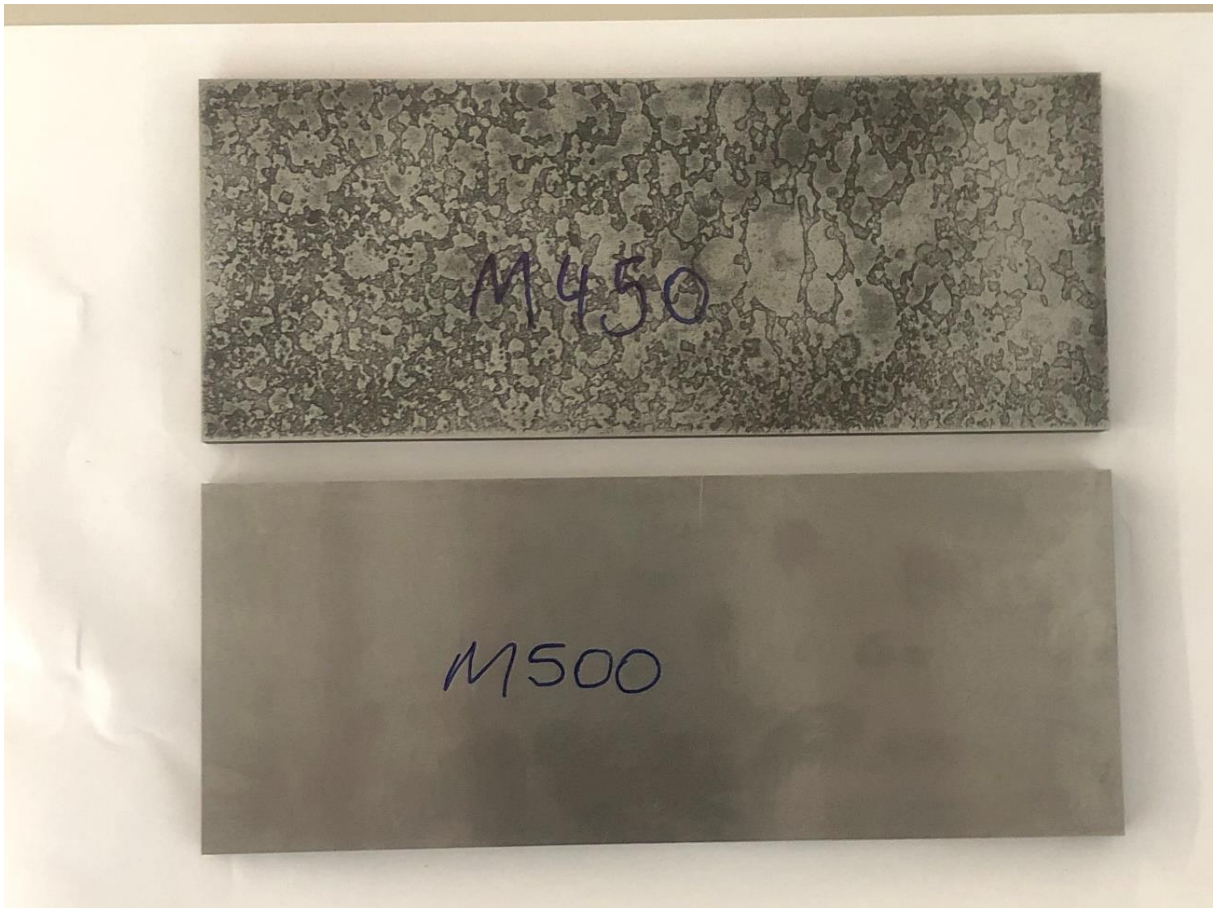
Figure 4.36 Armor steel-1 (above) and armor steel-2 (below) ballistic test specimens
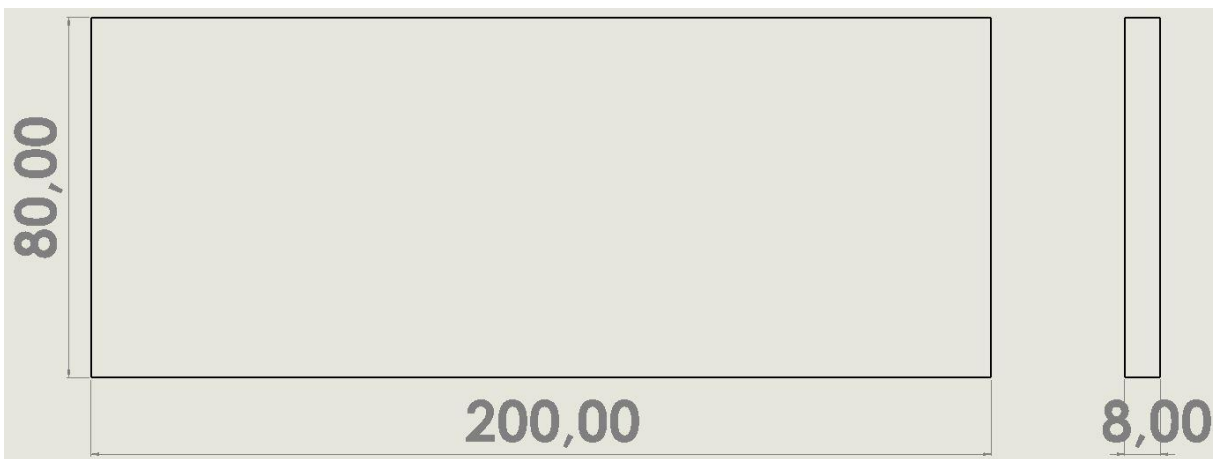
Figure 4.37 The dimensions of armor steel-1 and armor steel-2 ballistic test specimens in mm.

Figure 4.38 demonstrates the ballistic test set-up prior to experiments were performed. In order to minimize the potential slippage during the test shooting, specimens were tightly clamped to each corner using a fixture.
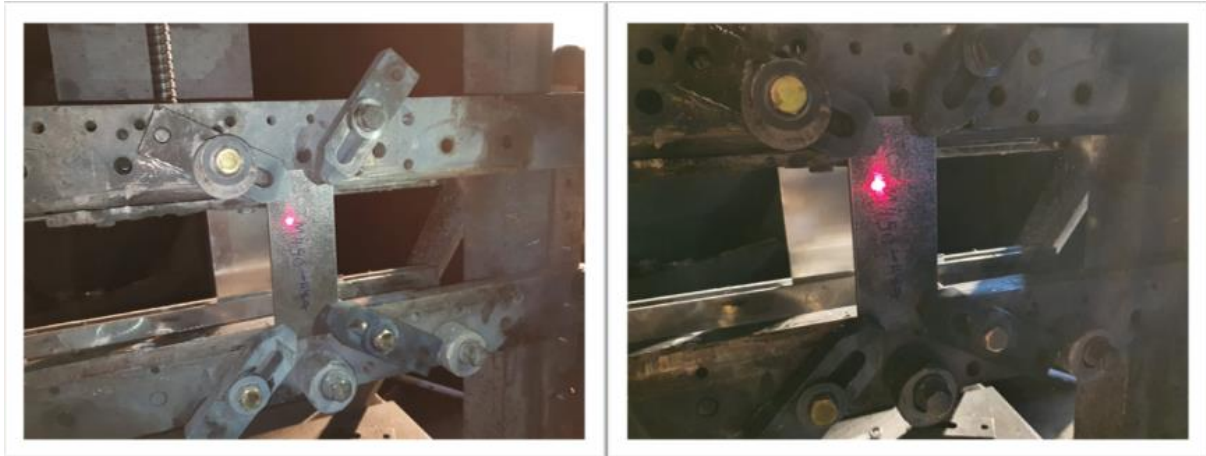
Figure 4.38 The ballistic test experimental set-up

To begin with, ballistic tests were carried out to reveal the effect of hydrogen on the ballistic performance and penetration behavior of armor steel-1 and armor steel-2. Hydrogen-induced mechanical degradation of UHSSs is almost inevitable when subjected to hydrogen-rich environments and thus, investigating the ballistic performance of armor steels with and without hydrogen presence conditions would shed light on the change in the mechanical properties when exposed to hydrogen. At first, as-received and hydrogen charged armor steel-2 specimens were investigated for the ballistic performance. The target specimens were firmly mounted on the rigid frame from the corners to reduce the slipping of the samples and two shoots were performed on each target specimen at room temperature. A standard ammunition of 7.62-mm APM2 armor piercing projectile was used to perform the experiments and firing obliquity was arranged to 30º. It is consisted of a jacket made gilding material, a lead nose element, lead base filler and a core which is made of very strong steel R_c62. This strong core provides very high penetration capability to target specimen. The ballistic test investigations of armor steel-1 and armor steel-2 were performed using MIL-DTL-12560 and MIL-DTL-46100 standards, respectively. Figure 4.39 shows the overview of ballistic test specimens after the experimental studies. All ballistic test specimens were subjected to at least 2 shoots to ensure the data consistency. For the hydrogen-charged armor steel-2 specimen, 4 shoots were carried out to figure out the ballistic behavior in detail. MIL-DTL-12560 and MIL-DTL-46100 military standards were used to determine the tests parameters.
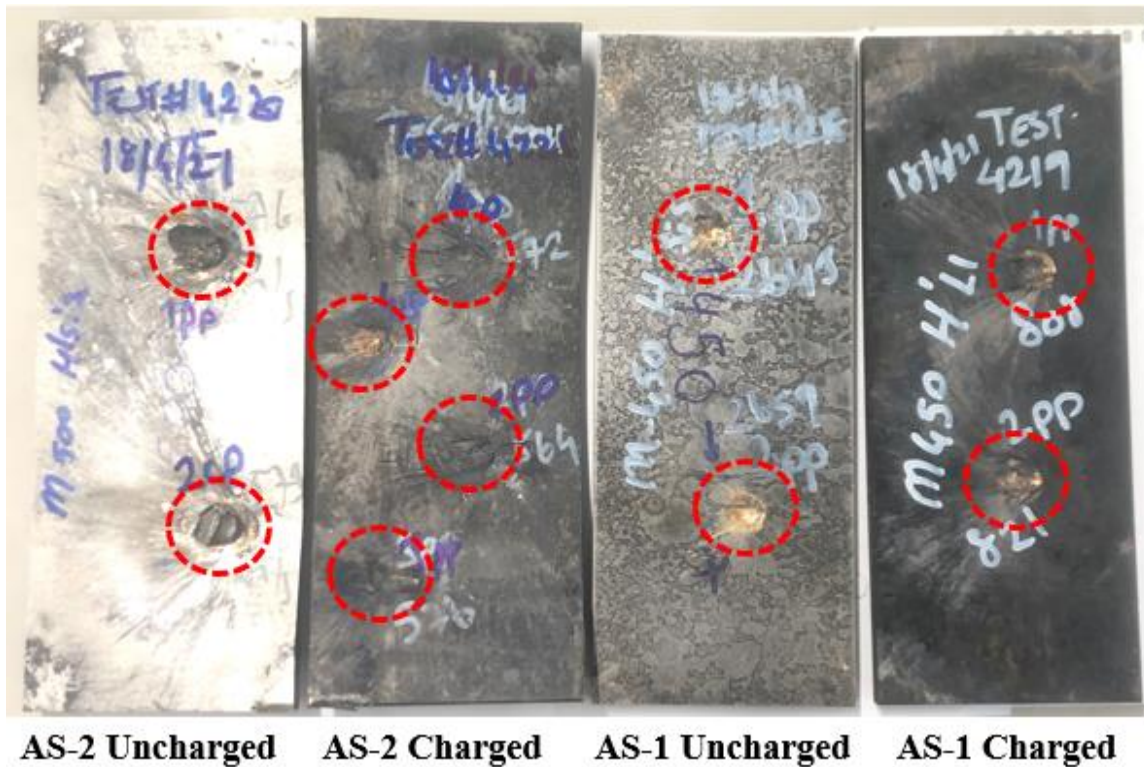
Figure 4.39 Front face overview of all ballistic test specimens showing the shooting regions in red dotted round shapes

Figure 4.40 shows the overview of front faces and close views of armor steel-1 plates after the ballistic tests with and without hydrogen charged conditions. The amount of gunpowder in ballistic experiments was between 2.80 gr and 2.84 gr. While the strike velocities of the bullets for as-received specimen were determined as 2643 and 2659 fps which corresponds to 806 m/s and 810 m/s, it was 2651 and 2692 fps which corresponds to 808 m/s and 820 m/s, respectively. For both cases of armor steel-1, the bullets were not be able perforate the armor plates but partially penetrated through the plate. Moreover, the damage on the hydrogen-charged steel plate was more distinct because bigger craters were formed as a result of penetration of the bullets.

Figure 4.40 The images of as-received (above) and hydrogen-charged (below) armor plates after the ballistic tests

To quantify the damage evaluation of both hydrogen-charged and uncharged conditions, 3D optical scanning analysis were performed as shown in Figure 4.41. The depth of the craters was investigated using 3D scan technique to characterize the damage evaluation during the ballistic tests.

Figure 4.41 3D Optical Scanning device used to evaluate the damage area

Figure 4.42 shows the 3D optical scanning results of armor steel-1 plates with and without hydrogen-charged conditions. The results clearly demonstrated the damage evaluation where

the bullets hit the target specimens. When examining the damage sites closely, 3D optical device allowed to measure the depth of the craters.
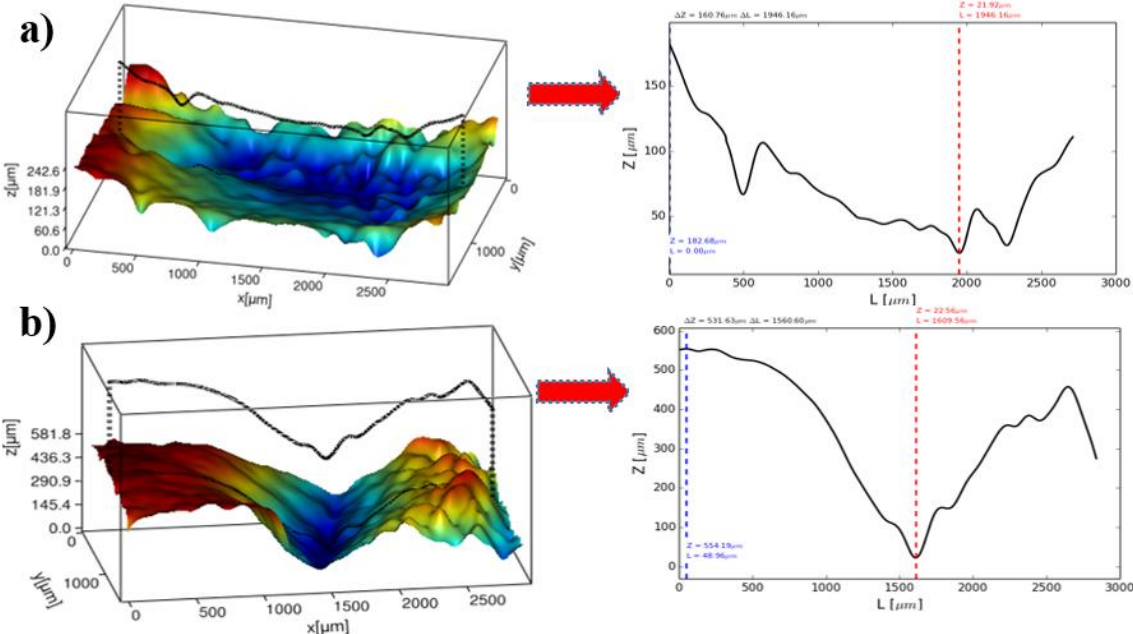
Figure 4.42 3D scan analysis results of armor steel-1 a) as-received b) hydrogen-charged

The depths of the craters for as-received and hydrogen-charged steel plates were found as 160.76 μm and 531.63 μm, respectively. The bullets were not perforated thorough the target specimen for both conditions but created a more than three times bigger crater on hydrogen-charged steel plate in comparison with as-received steel plate. This might be attributed to the fact that hydrogen lowered the cohesive energy between metal atoms and thus decreased the fracture resistance of steel plates which led to bigger holes over the surface.

4.6 Fractographic Analysis on Impact Failures

Fractography is a widely used technique in materials science to carry out the failure analysis in the fracture surface of materials. It shed light on the essential causes of fractures of structural components in service environments. Investigating the characteristic features of fracture surfaces under high-resolution electron microscopy could assist researchers to figure out the type of failures that materials experience when subjected to internal and external loads. Two different types of fracture modes exist as ductile fracture and brittle fracture. While ductile fracture mode allows for larger plastic deformations when subjected to critical loads, brittle fracture occurs at earlier stages of stress levels (sometimes in the elastic region in the stress-strain graph) and leads to lower load-bearing capacity. It is undesirable for metallic materials

to exhibit a brittle type of fracture when operating in a service environment because they are mostly designed for satisfying moderate ductility and tensile strength values. Accordingly, the armor steel-1 and armor steel-2 possess ductile fracture behavior when subjected to various mechanical loads and stresses in service. Besides, these armor sheet plates must possess high toughness characteristic against sudden shock reaction forces such as mine explosions. However, as outlined in previous sub-sections, atomic and molecular hydrogen significantly changes the nature of AHSS and makes them brittle. Armored combat vehicles manufactured by armor steel-1 and armor steel-2 operate in rough terrains and hydrogen-rich environments. Besides that, hydrogen could be diffused through metallic materials when they are in the liquid phase and could be trapped during the solidification process. For that reason, the presence of hydrogen poses a risk for metallic materials at every stage from the production of metallic material to the service environment. A vast number of studies were performed to show the effect of hydrogen on the fracture surface of AHSSs and published in the literature to unveil the remarkable change in the fracture surfaces carried out by high-resolution images [124–126]. Experimental studies in our mechanical tests clearly revealed the detrimental effect of hydrogen on the mechanical responses of armor steel-1 and armor steel-2. For instance, a decrease of about one-fifth was observed in the tensile tests with armor steels in the sub-section 4.2.1. Moreover, toughness values considerably reduced around 25% in CVN impact tests in the sub-section 4.2.5. Pre-charging the specimens by cathodic hydrogen charging process for 72 hours led hydrogen atoms to adsorb on the specimen surface at first and then diffuse through the crystal lattice in the microstructure. As the movement of hydrogen atoms through the microstructure was accelerated by the temperature, it reduced the cohesive energy between metal atoms and also piled up at interstitial sites which create a stress field. These stress fields expand the metal lattice and inevitable cracks occur. The fractographic analysis with armor steel-1 and armor steel-2 were carried out with as-received and hydrogen-charged specimens used in the CVN impact tests in experimental studies.

Figure 4.43 shows the in-situ SEM images of as-received armor steel-1 specimens carried out after the CVN impact tests. Figure 4.43b and 4.43d are the magnified images taken from the fracture surfaces of 4.43a and 4.43c (indicated by yellow dotted square), respectively. The fracture surface morphologies of as-received specimens exhibited a typical ductile fracture manner with nano- and micro-sized voids, dimples and primary cracks. These small and uniform dimples are formed during the plastic deformation when fragile particles-such as inclusions and precipitates-fracture as a result of applied force. Micro-void coalescence (MVC) is a well-accepted mechanism used for the explanation of ductile fracture in metallic materials.

This mechanism proposes that ductile fracture starts with the nucleation of voids. As plastic deformation proceeds and the stress increases, these voids are nucleated when inclusions and precipitates are fractured. Later on, nucleated voids are combined in the center to form larger voids and thus voids are growth which causes a large crack. In the end, the occurrence of fracture is inevitable because the growth of voids increases after necking when the material cannot resist the applied forces. It is important to note that the fracture that occurs in the ductile fracture process is not caused by the growth of a single crack, but by the combination of cracks.
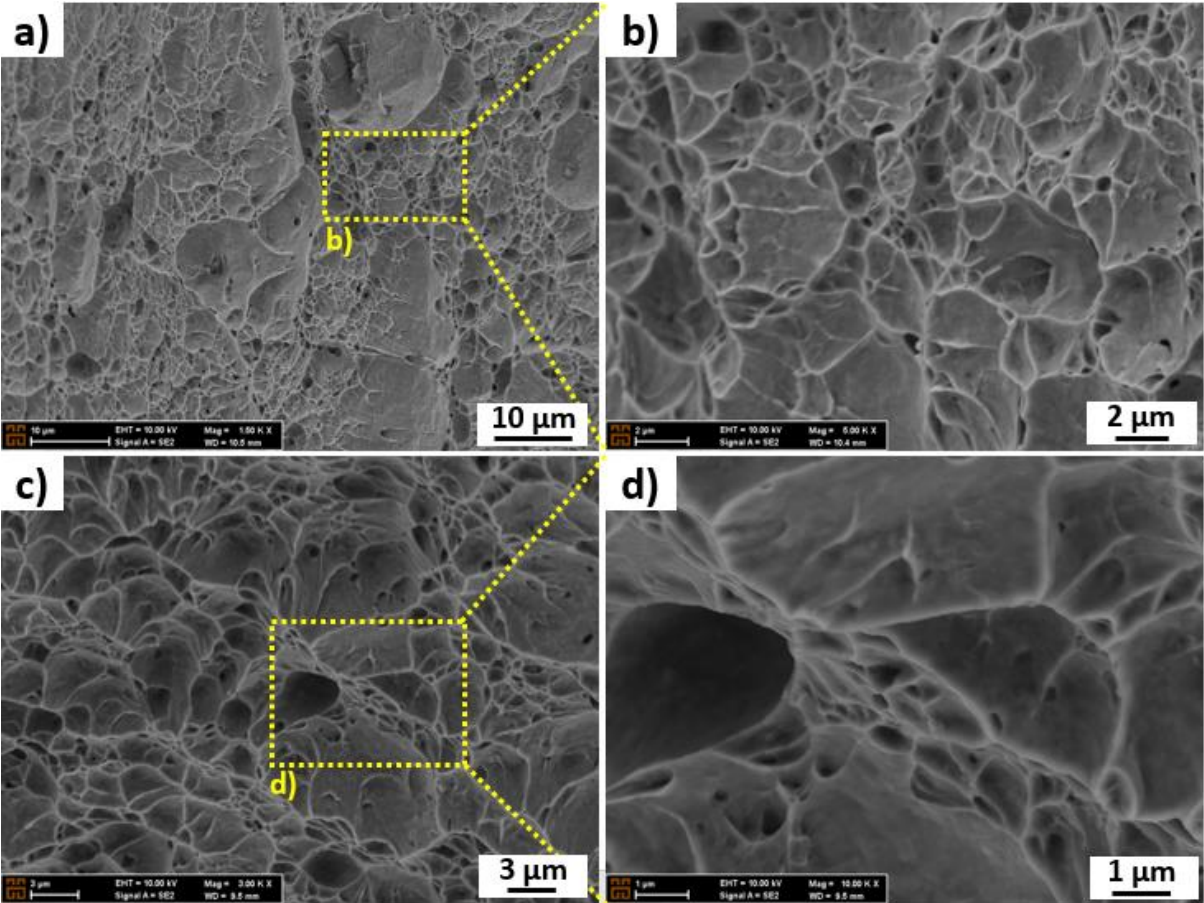
Figure 4.43 Fracture surface overview of armor steel-1 without hydrogen-charging condition.

Figure 4.44 demonstrates the fracture morphologies of hydrogen-charged armor steel-1 specimens carried out after the CVN impact tests. Figure 4.44b is the magnified image taken from the left-center of Figure 4.44a. As overviewed in the previous sections, the presence of hydrogen alters the mechanical properties and corresponding fracture mode from ductile to brittle fracture especially for high strength steels and high hydrogen concentration conditions. Deep cracks along with the uniform dimples were observed in the fracture surface of armor steel-1 specimens in the presence of high hydrogen concentrations. Moreover, while the volume fraction of dimples over the fracture surface was decreased as a result of cathodic hydrogen

charging, the volume fraction of cracks was remarkably increased. The increase in the volume fracture of deep cracks could be attributed to the fact that diffused hydrogen atoms reduced the cohesive strength between the bonds of metal atoms and led to the rupturing of the bonds at relatively low-stress levels. Additionally, segregated hydrogen atoms at interstitial and extraordinary sites significantly enhanced the stress applied on the grain walls and caused the crack propagation at that region. Figure 4.44d possesses the length of the deep crack as nearly 50 μm. The fracture surface of hydrogen-charged specimens consisted of this kind of deep cracks with lengths ranging from between 1 and around 100 μm. Figure 4.44c shows the distinct division of ductile and brittle regions. While the edges of the specimens showed brittle-like fracture features, the central region of armor steel-1 exhibited a ductile fracture manner because hydrogen could not be able to reach up to the center of the specimens. It makes sense because more time is needed for hydrogen atoms to reach the central regions and also it is obvious that hydrogen embrittlement is a process meaning that the risk of embrittlement due to hydrogen increases as time passes. Hydrogen reaches up to around 1.3 mm in depth which is well-consisted with the published studies in the literature. 24, 48 and 72 hours are common hydrogen charging durations for the performed studies but it is not a sufficient time for hydrogen atoms to move through the central regions.

Figure 4.44 Fracture surface overview of armor steel-1 with the hydrogen-charging condition.

Figure 4.45 and Figure 4.46 show the fracture surfaces of as-received and hydrogen-charged armor steel-2 specimens carried out after the CVN impact tests. Since armor steel-1 and armor steel-2 possess similar microstructural features, it wouldn't be surprising to observe similar fracture morphological behavior. A dimpled fracture surface was observed in the SEM images taken from armor steel-2 as-received specimens. Nano- and micron-size dimples cover almost the whole surface which is a prominent sign of transgranular fracture. In this type of fracture, the initiated cracks grow through the grains which consume more energy than intergranular fracture. For the case of hydrogen-charged specimens, the fracture morphology of armor steel-2 was quite similar with armor steel-1 since the existence of deep cracks became visible under higher magnifications. In addition to that, the size of the crack formed along the fracture surface was quite distinct. The length of the cracks taken from two different fracture surface of specimens was around 1.1 mm, 1.8 mm and 4 mm. Intergranular fracture occurs as a result of diffused hydrogen atoms by decrease the cohesive energy between metal atoms and thus initiated cracks reduce the impact energy that the material needs to carry in normal

conditions. The transition zone between ductile and brittle surface is also given in Figure 4.46a. Hydrogen could be able to reach up to almost 1 mm for armor steel-2.

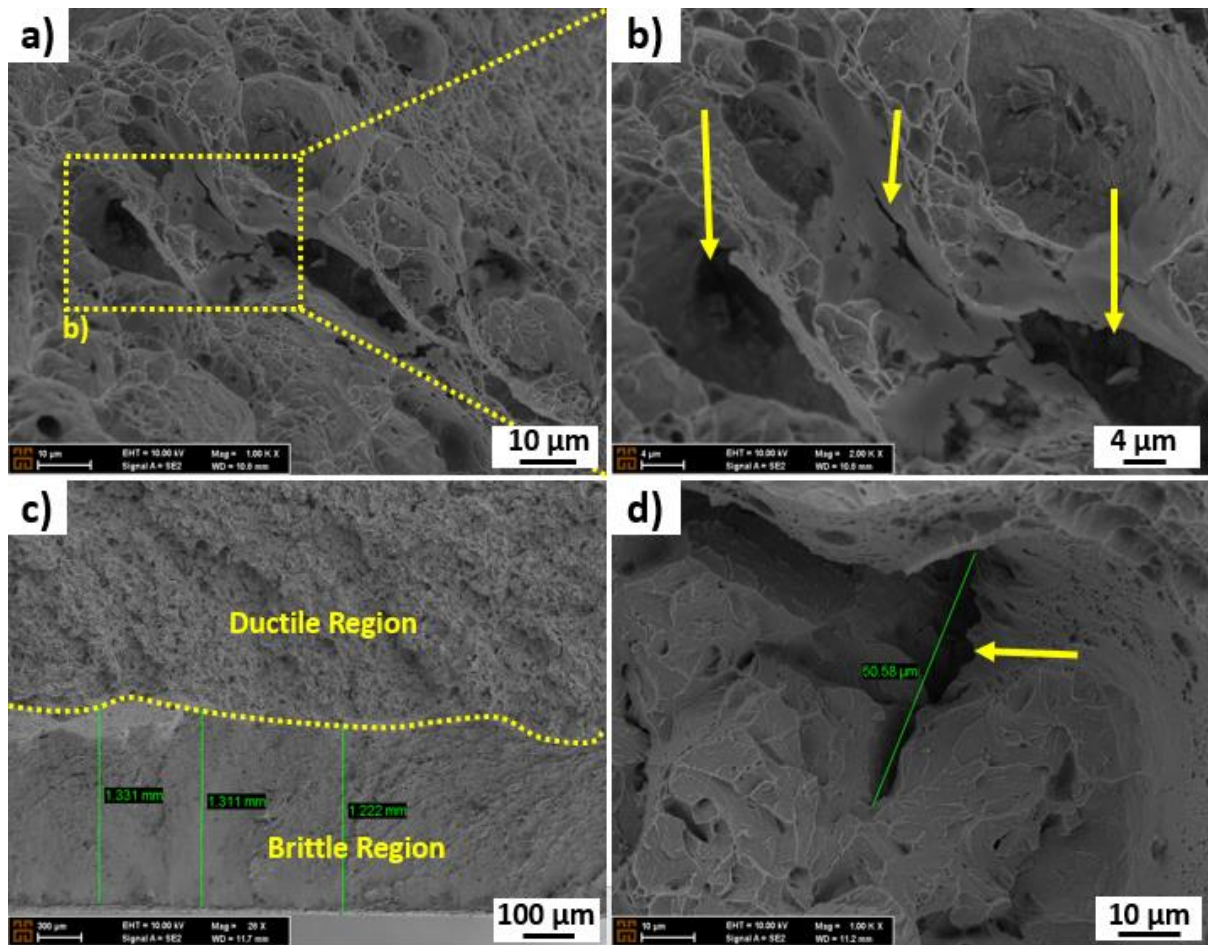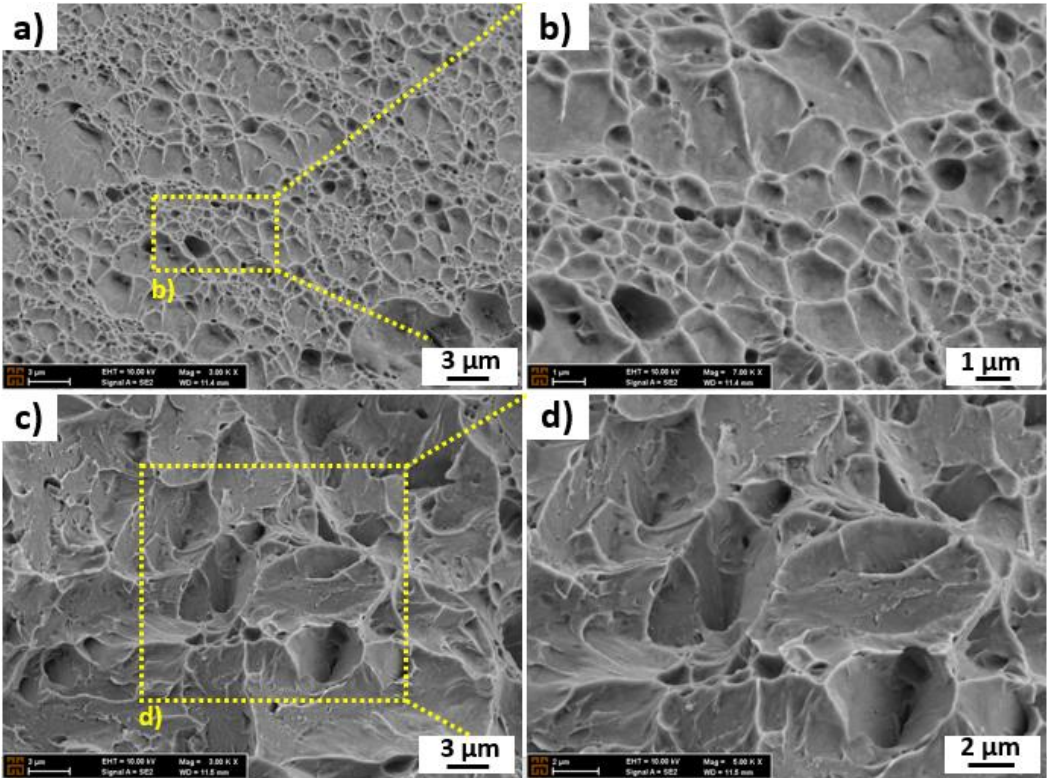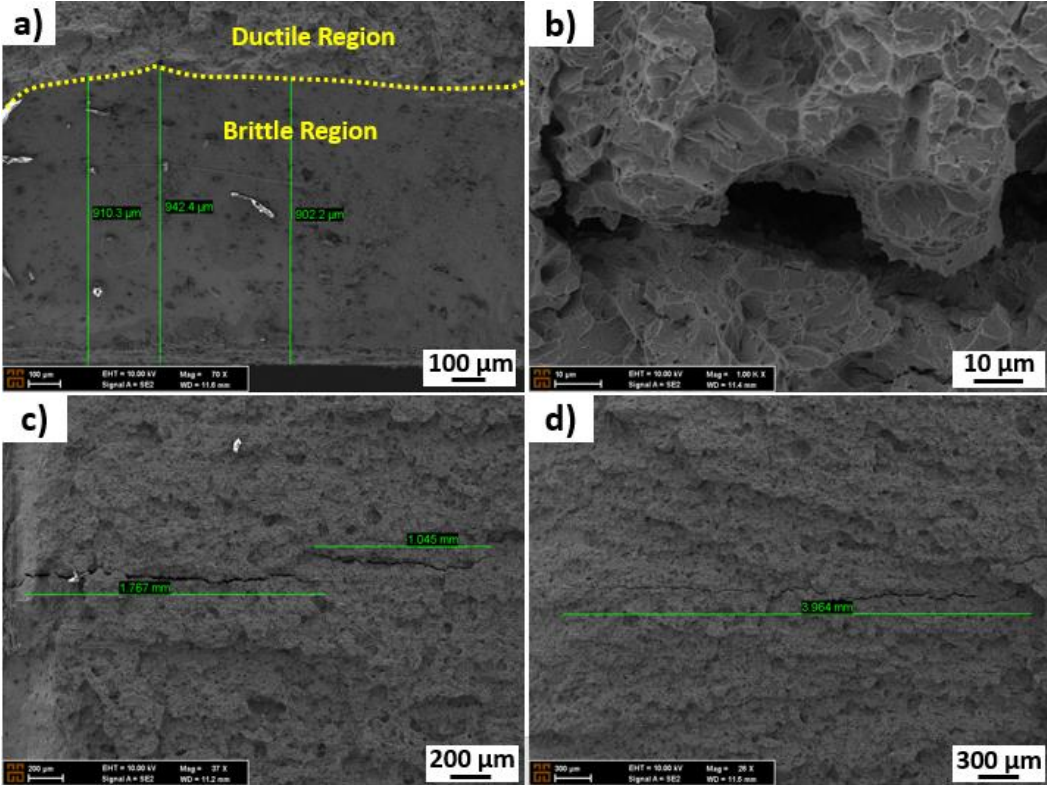**Figure 4.45 Fracture surface overview of armor steel-2 without hydrogen-charging condition.**

Figure 4.46 Fracture surface overview of armor steel-2 with hydrogen-charging condition.

Chapter 5

5. Conclusions and Future Prospects

5.1 Conclusions

In this thesis, the hydrogen embrittlement behavior of armor steels used in the hull protection of armored combat/wheeled vehicles was investigated by experimental methods. First of all, cathodic hydrogen charging set-up was successfully established and all the specimens were charged with hydrogen at 353K for 72 hours to be used in experimental studies. Various mechanical tests-including tension, compression, micro- and macro-hardness, CVN impact, ballistic tests-were performed to unveil the adverse effects of hydrogen on the mechanical properties of armor steels used in the production of armored combat and wheeled vehicles of FNSS. In addition to that, hydrogen bake-out process was carried out for both armor steel-1 and armor steel-2 to remove the diffused hydrogen atoms out of microstructure by improving the suggested optimization parameters (temperature and duration) in ASTM B850 – 98(2015) standard which is used to reduce the risk of hydrogen embrittlement. Moreover, hydrogen content measurements were performed with as-received and hydrogen-charged specimens using inert gas fusion technique to ensure that samples were saturated with hydrogen prior to experimental investigations. To determine the macroscopic effect of hydrogen on the ballistic performance, ballistic tests were also performed with and without hydrogen charged specimens. Fractographic analysis was carried out by SEM to observe the significant change on the fracture surfaces of as-received and hydrogen charged specimens due to hydrogen. The experimental results clearly showed that hydrogen presence in the microstructure of specimens considerably changed the mechanical properties of armor steel-1 and armor steel-2. The load-bearing capacity of both armor steels was reduced more than 25% in CVN impact test experiments. Similarly, the reduction in the total elongation of armor steel-1 and armor steel-2 was between 15% and 20% in tensile tests and the ductility of specimens was significantly reduced up to 40% in high strain rate tests. To sum up, armor steels which conform to MIL-DTL-12560 (armor steel-1) and MIL-DTL-46100 (armor steel-2) was subjected to hydrogen-rich environment to determine hydrogen embrittlement behavior by experimental methods and the

results clearly indicated that the mechanical properties of armor steels used in the protection of armored vehicles produced by FNSS negatively affected when exposed to hydrogen-rich environments. Hydrogen bake-out process was employed to reduce the risk of hydrogen embrittlement and corresponding bake-out process parameters were successfully optimized for both armor steels.

5.2 Societal Impact and Contribution to Global Sustainability

As previously outlined, this thesis is a SAYP project supported by the Undersecretariat of Defense Industries of Turkey. This special program was launched in 2012 and it has mainly three following aims; (i) to provide the information transfer between industry companies and universities, (ii) To establish a graduate thesis study at universities which will be in line with the needs and priority areas of defense industry companies, (iii) To train postgraduate students to be qualified as research and development personnel in defense industry. Therefore, the purpose of the SAYP project is to provide both knowledge transfer and train personnel for the defense industry by carrying out the studies requested by the defense industry companies with the graduate students, as well as the university-industry cooperation. Within the scope of SAYP, we have investigated the hydrogen embrittlement behavior of armor steels used by FNSS defense industry company. During the production process of armored combat vehicles, these UHSS steels are cracked in welding, plate bending and laser cutting operations. Before this thesis studies, there was no any experimental data to comment on the unexpected cracks occurred during manufacturing processes. To characterize the hydrogen embrittlement behavior, various mechanical tests were performed with two different armor steels with and without hydrogen charged conditions. By doing so, it was revealed that the existence and/or the diffusion of tiny amount of hydrogen atoms through microstructure significantly reduced the mechanical properties of high-strength armor steels. To reduce the risk of hydrogen embrittlement, hydrogen bake-out process was performed and process parameters were successfully optimized. The outputs of the thesis will be used by FNSS company to prevent the catastrophic brittle failures of their armor steels in the production process of armored vehicles. Therefore, it will be lessening the financial losses of FNSS occurred due to deleterious effect of hydrogen embrittlement.

5.3 Future Prospects

In this study, hydrogen embrittlement behavior of armor steels was investigated using various mechanical test methods to determine the susceptibility of armor steel-1 and armor steel-2 which are used in the manufacturing of armored vehicles by FNSS. Moreover, hydrogen bake-out operation was performed for both steels to minimize the risk of hydrogen embrittlement by heating the specimens to higher temperatures and keep for a length of time to drive the settled and accumulated hydrogen atoms out of microstructure prior to operating in-service environments. It is a common knowledge that

hydrogen adversely effects most important metals, steels and alloy systems and reduces the ductility and the load-bearing capacity which results in the catastrophic brittle failures well below its permissible stress values. Therefore, hydrogen embrittlement phenomenon is one of the greatest concerns for designers, manufacturers and industries that use high strength susceptible metallic materials. The defense industry companies also have to deal with this phenomenon closely and take the necessary precautions. Within this context, this thesis study aimed to reveal the hydrogen embrittlement behavior of two different armor steels used by FNSS and observe the changes in the mechanical properties and characteristic features of them. As a future work, the investigation of the hydrogen embrittlement behavior of other high strength steels and alloys used in the production of armored vehicles by defense industry companies would be carried out. Moreover, numerical modeling and simulation of hydrogen embrittlement will be an effective future work when supported with the experimental studies.

BIBLIOGRAPHY

[1] S.K. Dwivedi, M. Vishwakarma, Effect of hydrogen in advanced high strength steel materials, Int. J. Hydrogen Energy. 44 (2019) 28007–28030. doi:10.1016/j.ijhydene.2019.08.149.

[2] E. Billur, B. Makine, I.O. Yilmaz, S. Erzincanlioglu, Mechanical properties of trip aided bainitic ferrite (tbf) steels in production and service conditions, Hittite J. Sci. Eng. 5 (2019) 231–237. doi:10.17350/HJSE19030000100.

[3] S.N. Green, Do we need a new strategy to prevent terrorist attacks on the United States ?, Cent. Strateg. Int. Stud. (2016) 1–8. https://www.csis.org/analysis/do-we-need-new-strategy-prevent-terrorist-attacks-united-states (accessed November 15, 2020).

[4] Crises are fueling the global arms trade: SIPRI report | In Depth | DW | 09.03.2020, (2020). https://www.dw.com/en/crises-are-fueling-the-global-arms-trade-sipri-report/a-52688298 (accessed November 15, 2020).

[5] N. Altun, Determination of Level of the Defense Expenditures: A Theoretical Discussion, Res. J. Polit. Econ. Manag. 5 (2017).

[6] O. BAYRAM, Savunma Sanayinin Gelişiminin İhracat-İthalat Dengesi Üzerindeki Etkileri, Güvenlik Strat. Derg. 16 (2020) 163–188. doi:10.17752/guvenlikstrtj.719977.

[7] Top 100 | Defense News, News about defense programs, business, and technology, (2020). https://people.defensenews.com/top-100/ (accessed November 15, 2020).

[8] A. Karakus, TÜRK SAVUNMA SANAYİİNİN GELİŞİMİ, TÜRKİYE'NİN SAVUNMA HARCAMALARININ BOYUTLARI VE BAZI NATO ÜLKELERİ İLE KARŞILAŞTIRMALI EKONOMETRİK ANALİZİ, 2006.

[9] A. Mevlutoglu, Commentary on Assessing the Turkish defense industry : structural issues and major challenges Commentary on Assessing the Turkish defense industry : structural issues and major challenges, Def. Stud. 2436 (2017) 0. doi:10.1080/14702436.2017.1349534.

[10] E. Konca, A Comparison of the Ballistic Performances of Various Microstructures in MIL-A-12560 Armor Steel, Metals (Basel). 10 (2020).

[11] P.K. Jena, B. Mishra, M. Rameshbabu, A. Babu, A.K. Singh, K. Sivakumar, T.B. Bhat, Effect of heat treatment on mechanical and ballistic properties of a high strength armour steel International Journal of Impact Engineering Effect of heat treatment on mechanical and ballistic properties of a high strength armour steel, Int. J. Impact Eng. (2010). doi:10.1016/j.ijimpeng.2009.09.003.

[12] Y. Murakami, T. Kanezaki, P. Sofronis, Hydrogen embrittlement of high strength steels: Determination of the threshold stress intensity for small cracks nucleating at nonmetallic inclusions, Eng. Fract. Mech. 97 (2013) 227–243. doi:10.1016/j.engfracmech.2012.10.028.

[13] G. Lovicu, M. Bottazzi, F. D'aiuto, M. De Sanctis, A. Dimatteo, C. Santus, R. Valentini, Hydrogen embrittlement of automotive advanced high-strength steels, Metall. Mater. Trans. A Phys. Metall. Mater. Sci. 43 (2012) 4075–4087. doi:10.1007/s11661-012-1280-8.

[14] J. Schmitt, T. Iung, Comptes Rendus Physique New developments of advanced high-strength steels for automotive applications, Comptes Rendus Phys. 19 (2018) 641–656. doi:10.1016/j.crhy.2018.11.004.

[15] X. Zhang, Y. Chen, J. Hu, Recent advances in the development of aerospace materials,

Prog. Aerosp. Sci. 97 (2018) 22–34. doi:10.1016/j.paerosci.2018.01.001.

[16] R. Kanno, Advances in steel materials for innovative and elegant steel structures in Japan-a review, Struct. Eng. Int. 26 (2016) 242–253. doi:10.2749/101686616X14555428759361.

[17] O. Barrera, D. Bombac, Y. Chen, T.D. Daff, E. Galindo-Nava, P. Gong, D. Haley, R. Horton, I. Katzarov, J.R. Kermode, C. Liverani, M. Stopher, F. Sweeney, Understanding and mitigating hydrogen embrittlement of steels: a review of experimental, modelling and design progress from atomistic to continuum, J. Mater. Sci. 53 (2018) 6251–6290. doi:10.1007/s10853-017-1978-5.

[18] M.L. Martin, M.J. Connolly, F.W. Delrio, A.J. Slifka, Hydrogen embrittlement in ferritic steels, Appl. Phys. Rev. 7 (2020). doi:10.1063/5.0012851.

[19] Q. Xu, J. Zhang, Novel Methods for Prevention of Hydrogen Embrittlement in Iron, Sci. Rep. 7 (2017) 1–9. doi:10.1038/s41598-017-17263-8.

[20] T. Fras, C.C. Roth, D. Mohr, Fracture of high-strength armor steel under impact loading, Int. J. Impact Eng. 111 (2018) 147–164. doi:10.1016/j.ijimpeng.2017.09.009.

[21] N. Kılıç, S. Bedir, A. Erdik, B. Ekici, A. Tas, M. Güden, Ballistic behavior of high hardness perforated armor plates against 7 . 62 mm armor piercing projectile, Mater. Des. 63 (2014) 427–438. doi:10.1016/j.matdes.2014.06.030.

[22] N. Kılıç, B. Ekici, Ballistic resistance of high hardness armor steels against 7 . 62 mm armor piercing ammunition, Mater. Des. 44 (2013) 35–48. doi:10.1016/j.matdes.2012.07.045.

[23] Ş.. ATAPEK, ZIRH ÇELİKLERİNİN FİZİKSEL METALURJİK ESASLAR DOĞRULTUSUNDA GELİŞTİRİLMESİ VE KARAKTERİZASYONU, (2006) 141.

[24] M. Balakrishnan, V. Balasubramanian, G. Madhusudhan Reddy, Effect of PTA hardfaced interlayer thickness on ballistic performance of shielded metal arc welded armor steel welds, J. Mater. Eng. Perform. 22 (2013) 806–814. doi:10.1007/s11665-012-0338-5.

[25] M.. DOGRUGIDEN, FARKLI KAYNAK METOTLARI İLE BİRLEŞTİRİLEN ZIRH ÇELİKLERİNİN KIRILMA TOKLUK DEĞERLERİNİN İNCELENMESİ, (2019). http://repositorio.unan.edu.ni/2986/1/5624.pdf.

[26] S. Kurt, FARKLI KAYNAK AĞZI AÇISI ve GEOMETRİLERİN DE GERÇEKLEŞTİRİLEN KAYNAKLARIN MIL-A 46100 ZIRH ÇELİĞİ MİKROYAPISINA ve MEKANİK ÖZELLİKLERİNE ETKİSİNİN DENEYSEL ve SAYISAL OLARAK İNCELENMESİ, (2015).

[27] S. Endo, N. Nakata, Development of Thermo-Mechanical Control Process (TMCP) and high performance steel in JFE Steel, JFE Tech. Rep. 20 (2015) 1–7.

[28] K. Nishioka, K. Ichikawa, Progress in thermomechanical control of steel plates and their commercialization, Sci. Technol. Adv. Mater. 13 (2012). doi:10.1088/1468-6996/13/2/023001.

[29] C.F. Kuang, J. Li, S.G. Zhang, J. Wang, H.F. Liu, A.A. Volinsky, Effects of quenching and tempering on the microstructure and bake hardening behavior of ferrite and dual phase steels, Mater. Sci. Eng. A. 613 (2014) 178–183. doi:10.1016/j.msea.2014.06.100.

[30] X. Tao, C. Li, L. Han, J. Gu, Microstructure evolution and mechanical properties of X12CrMoWVNbN10-1-1 steel during quenching and tempering process, Integr. Med. Res. 5 (2015) 45–57. doi:10.1016/j.jmrt.2015.06.001.

[31] E. Konca, A Comparison of the Ballistic Performances of Various Microstructures in MIL-A-12560 Armor Steel, Metals (Basel). 10 (2020) 446. doi:10.3390/met10040446.

[32] P.K. Jena, K.S. Kumar, V.R. Krishna, A.K. Singh, T.B. Bhat, Studies on the role of microstructure on performance of a high strength armour steel, Eng. Fail. Anal. 15 (2008) 1088–1096. doi:10.1016/j.engfailanal.2007.11.011.

[33]   E.J. Pavlina, C.J. Van Tyne, Correlation of Yield Strength and Tensile Strength with Hardness for Steels, J. Mater. Eng. Perform. 17 (2008) 888–893. doi:10.1007/s11665-008-9225-5.

[34]   S.A. Salihu, Assessment of Advanced High Strength Steels used in Auto Industry – A Review, Int. J. Sci. Res. Sci. 2 (2016) 565–571.

[35]   T. DENİZ, BALLISTIC PENETRATION OF HARDENED STEEL PLATES, (2010).

[36]   P. Pedeferri, Hydrogen-Induced Damage, (2018) 275–295. doi:10.1007/978-3-319-97625-9_14.

[37]   M.B. Djukic, V. Sijacki Zeravcic, G.M. Bakic, A. Sedmak, B. Rajicic, Hydrogen damage of steels: A case study and hydrogen embrittlement model, Eng. Fail. Anal. 58 (2015) 485–498. doi:10.1016/j.engfailanal.2015.05.017.

[38]   E. Ohaeri, U. Eduok, J. Szpunar, Hydrogen related degradation in pipeline steel: A review, Int. J. Hydrogen Energy. 43 (2018) 14584–14617. doi:10.1016/j.ijhydene.2018.06.064.

[39]   N. Saini, C. Pandey, M.M. Mahapatra, Effect of diffusible hydrogen content on embrittlement of P92 steel, Int. J. Hydrogen Energy. 42 (2017) 17328–17338. doi:10.1016/j.ijhydene.2017.05.214.

[40]   X.C. Ren, Q.J. Zhou, G.B. Shan, W.Y. Chu, J.X. Li, Y.J. Su, L.J. Qiao, A Nucleation Mechanism of Hydrogen Blister in Metals and Alloys, Metall. Mater. Trans. A. 39 (2008) 87–97. doi:10.1007/s11661-007-9391-3.

[41]   A. Trautmann, G. Mori, M. Oberndorfer, S. Bauer, C. Holzer, C. Dittmann, Hydrogen Uptake and Embrittlement of Carbon Steels in Various Environments, Materials (Basel). 13 (2020) 1–16.

[42]   V. Demetriou, J.D. Robson, M. Preuss, R. Morana, Effect of hydrogen on the mechanical properties of alloy 945X (UNS N09945) and influence of microstructural features, Mater. Sci. Eng. A. 684 (2017) 423–434. doi:10.1016/j.msea.2016.12.088.

[43]   N.D. Adasooriya, W. Mekonnen, E. Holm, T. Årthun, V. Hansen, K. Gunnar, T. Hemmingsen, Effect of hydrogen on mechanical properties and fracture of martensitic carbon steel under quenched and tempered conditions, Mater. Sci. Eng. A. 803 (2021) 140495. doi:10.1016/j.msea.2020.140495.

[44]   W.H. JOHNSON, On Some Remarkable Changes Produced in Iron and Steel by the Action of Hydrogen and Acids, Nature. 11 (1875) 393–393. doi:10.1038/011393a0.

[45]   O. Reynolds, On the effect of acid on the interior of iron wire, J. Franklin Inst. 99 (1875) 70–72. doi:10.1016/0016-0032(75)90215-x.

[46]   M.B. Djukic, G.M. Bakic, V.S. Zeravcic, A. Sedmak, B. Rajicic, Hydrogen embrittlement of industrial components: Prediction, prevention, and models, Corrosion. 72 (2016) 943–961. doi:10.5006/1958.

[47]   J. Song, W.A. Curtin, A nanoscale mechanism of hydrogen embrittlement in metals, Acta Mater. 59 (2011) 1557–1569. doi:10.1016/j.actamat.2010.11.019.

[48]   A. Barnoush, H. Vehoff, Recent developments in the study of hydrogen embrittlement : Hydrogen effect on dislocation nucleation, Acta Mater. 58 (2010) 5274–5285. doi:10.1016/j.actamat.2010.05.057.

[49]   S. V Brahimi, S. Yue, K.R. Sriraman, Alloy and composition dependence of hydrogen embrittlement susceptibility in high-strength steel fasteners, Philos. Trans. R. Soc. A Math. Phys. Eng. Sci. 375 (2017) 20160407. doi:ttps://doi.org/10.1098/rsta.2016.0407.

[50]   B.A. Pundt, Hydrogen in Nano-sized Metals **, Adv. Eng. Mater. 6 (2004) 11–21. doi:10.1002/adem.200300557.

[51]   M.B. Djukic, G.M. Bakic, V. Sijacki Zeravcic, A. Sedmak, B. Rajicic, The synergistic action and interplay of hydrogen embrittlement mechanisms in steels and iron: Localized plasticity and decohesion, Eng. Fract. Mech. 216 (2019) 106528.

doi:10.1016/j.engfracmech.2019.106528.

[52] S.K. Dwivedi, M. Vishwakarma, Hydrogen embrittlement in different materials: A review, Int. J. Hydrogen Energy. 43 (2018) 21603–21616. doi:10.1016/j.ijhydene.2018.09.201.

[53] Q. Liu, Q. Zhou, J. Venezuela, M. Zhang, A. Atrens, Hydrogen influence on some advanced high-strength steels, Corros. Sci. 125 (2017) 114–138. doi:10.1016/j.corsci.2017.06.012.

[54] J.C. Villalobos, S. Serna, A general overview of hydrogen embrittlement, (2020) 139–168. doi:10.1016/B978-0-12-818332-8.00006-5.

[55] E.O. Vilar, J.P. Carrasco, D.F. Arau, A critical review of mathematical models used to determine the density of hydrogen trapping sites in steels and alloys, Int. J. Hydrogen Energy. 39 (2014) 12194–12200. doi:10.1016/j.ijhydene.2014.06.036.

[56] P.C. Rivera, V.P. Ramunni, P. Bruzzoni, Hydrogen trapping in an API 5L X60 steel, Corros. Sci. 54 (2012) 106–118. doi:10.1016/j.corsci.2011.09.008.

[57] M. Vrbek, K., Lamut, J., Marolt, M., & Knap, Changes in Hydrogen Content During Steelmaking, Arch. Metall. Mater. 60 (2015) 295–299. doi:10.1515/amm-2015-0047.

[58] Q. Liu, Q. Zhou, J. Venezuela, M. Zhang, J. Wang, A. Atrens, A review of the influence of hydrogen on the mechanical properties of DP, TRIP, and TWIP advanced high-strength steels for auto construction, Corros. Rev. 34 (2016) 127–152. doi:10.1515/corrrev-2015-0083.

[59] Q. Liu, A. Atrens, A critical review of the influence of hydrogen on the mechanical properties of medium-strength steels, Corros. Rev. 31 (2013) 85–103. doi:10.1515/corrrev-2013-0023.

[60] A. Lasia, D. Gregorie, General Model of Electrochemical Hydrogen Absorption into Metals, J. Electrochem. Soc. 142 (1995) 3393–3399. doi:10.1149/1.2050267.

[61] J. Sezgin, A. Montouchet, G. Perrin, K. Wolski, N. Eos, Modelling of hydrogen induced pressurization of internal cavities, Int. J. Hydrogen Energy. 42 (2017) 15403–15414. doi:10.1016/j.ijhydene.2017.04.106.

[62] T.P. Perng, J.K. Wu, A brief review note on mechanisms of hydrogen entry into metals, Mater. Lett. 57 (2003) 3437–3438. doi:10.1016/S0167-577X(03)00095-8.

[63] Y. Duan, W. Liu, Y. Ma, Q. Cai, W. Zhu, J. Li, Microstructure characterization and tensile properties of hot isostatic pressed China ultrahigh strength steel, J. Mater. Res. Technol. 9 (2020) 15192–15201. doi:10.1016/j.jmrt.2020.10.013.

[64] Z. Lv, L. Qian, S. Liu, L. Zhan, S. Qin, Preparation and Mechanical Behavior of Ultra-High Strength Low-Carbon Steel, Materials (Basel). 13 (2020) 459.

[65] T. Schaffner, A. Hartmaier, V. Kokotin, M. Pohl, Analysis of hydrogen diffusion and trapping in ultra-high strength steel grades, J. Alloys Compd. 746 (2018) 557–566. doi:10.1016/j.jallcom.2018.02.264.

[66] D.P. Escobar, K. Verbeken, L. Duprez, M. Verhaege, Evaluation of hydrogen trapping in high strength steels by thermal desorption spectroscopy, Mater. Sci. Eng. A. 551 (2012) 50–58. doi:10.1016/j.msea.2012.04.078.

[67] M.A. V Devanathan, Z. Stachurski, The Adsorption and Diffusion of Electrolytic Hydrogen in Palladium, Proc. R. Soc. A. 270 (1962) 90–102. doi:10.1098/rspa.1962.0205.

[68] D. Rudomilova, G. Luckeneder, Techniques for investigation of hydrogen embrittlement of advanced high strength steels, Corros. Rev. 36 (2018) 413–434.

[69] T. Zakroczymski, Adaptation of the electrochemical permeation technique for studying entry , transport and trapping of hydrogen in metals, Electrochim. Acta. 51 (2006) 2261–2266. doi:10.1016/j.electacta.2005.02.151.

[70] Q. Liu, M. Zhang, Q. Zhou, A. Atrens, Hydrogen trapping in some advanced high

strength steels, Corros. Sci. 111 (2016) 770–785. doi:10.1016/j.corsci.2016.05.046.

[71] K. Verbeken, Analysing hydrogen in metals: bulk thermal desorption spectroscopy (TDS) methods 2, Woodhead Publ. Ser. Met. Surf. Eng. 1 (2012) 27–55. doi:10.1533/9780857095374.1.27.

[72] M. Dadfarnia, P. Sofronis, T. Neeraj, Hydrogen interaction with multiple traps : Can it be used to mitigate embrittlement ?, Int. J. Hydrogen Energy. 36 (2011) 10141–10148. doi:10.1016/j.ijhydene.2011.05.027.

[73] C.F. Dong, Z.Y. Liu, X.G. Li, Y.F. Cheng, Effects of hydrogen-charging on the susceptibility of X100 pipeline steel to hydrogen-induced cracking, Int. J. Hydrogen Energy. 34 (2009) 9879–9884. doi:10.1016/j.ijhydene.2009.09.090.

[74] S.P. Lynch, Hydrogen embrittlement (HE) phenomena and mechanisms, Stress Corros. Crack. Theory Pract. (2011) 90–130. doi:10.1533/9780857093769.1.90.

[75] O. Barrera, A.C.F. Cocks, Computational modelling of hydrogen embrittlement in welded structures, Philos. Mag. 93 (2013) 2680–2700. doi:10.1080/14786435.2013.785638.

[76] T.E.D.B. Flanagan, N.B. Mason, The Effect of Stress on Hydride Precipitation, Scr. Metall. 15 (1981) 109–112.

[77] H.K. Birnraum, Hydrogen Embrittlement of a Titanium: In Situ Tem Studies, Acta Metall. 36 (1988) 111–124.

[78] S. Lynch, Hydrogen embrittlement phenomena and mechanisms, Corros. Rev. 30 (2012) 105–123. doi:10.1515/corrrev-2012-0502.

[79] L.. Pfeil, The Effect of Occluded Hydrogen on the Tensile Strength of Iron, Proc. R. Soc. A. 112 (1926) 182–195. doi:10.1098/rspa.1926.0103.

[80] C.J. Mcmahon, Hydrogen-induced intergranular fracture of steels, Eng. Fract. Mech. 68 (2001) 773–788.

[81] J. Song, W.A. Curtin, Atomic mechanism and prediction of hydrogen embrittlement in iron, Nat. Mater. 12 (2013) 145–151. doi:10.1038/nmat3479.

[82] R.A. Oriani, A Mechanistic Theory of Hydrogen Embrittlement of Steels, Berichte Der Bunsengesellschaft Für Phys. Chemie. 76 (1972) 848–857.

[83] W.W. Gerberich, P.G. Marsh, J.W. Hoehn, Hydrogen Induced Cracking Mechanisms — Are There Critical Experiments?, 1994.

[84] A. Tehranchi, W.A. Curtin, The role of atomistic simulations in probing hydrogen e ff ects on plasticity and embrittlement in metals, Eng. Fract. Mech. 216 (2019) 106502. doi:10.1016/j.engfracmech.2019.106502.

[85] H.Y. Song, L. Zhang, M.X. Xiao, Molecular dynamics simulation of effect of hydrogen atoms on crack propagation behavior of α -Fe, Phys. Lett. A. 380 (2016) 4049–4056. doi:10.1016/j.physleta.2016.10.019.

[86] H.K. Birnraum, P. Sofronis, Hydrogen-enhanced localized plasticity--a mechanism for hydrogen- related fracture, Mater. Sci. Eng. A. 176 (1994) 191–202.

[87] I.M. Robertson, The effect of hydrogen on dislocation dynamics, Eng. Fract. Mech. 68 (2001) 671–692.

[88] M. Kappes, M. Iannuzzi, R.M. Carranza, Hydrogen Embrittlement of Magnesium and Magnesium Alloys :A Review, J. Electrochem. Soc. 160 (2013) 168–178. doi:10.1149/2.023304jes.

[89] P.J. Ferreria, I.M. Robertson, H.K. Birnbaum, Hydrogen Effects on The Interaction Between Dislocation, Acta Mater. 46 (1998) 1749–1757.

[90] G. Lu, Q. Zhang, N. Kioussis, E. Kaxiras, Hydrogen-Enhanced Local Plasticity in Aluminum : An Ab Initio Study, Phys. Rev. Lett. 87 (2001) 1–4. doi:10.1103/PhysRevLett.87.095501.

[91] J. Han, J. Nam, Y. Lee, Acta Materialia The mechanism of hydrogen embrittlement in

intercritically annealed medium Mn TRIP steel, Acta Mater. 113 (2016) 1–10. doi:10.1016/j.actamat.2016.04.038.

[92] M. Hatano, M. Fujinami, K. Arai, H. Fujii, M. Nagumo, Hydrogen embrittlement of austenitic stainless steels revealed by deformation microstructures and strain-induced creation of vacancies, Acta Mater. 67 (2014) 342–353. doi:10.1016/j.actamat.2013.12.039.

[93] M. Koyama, C.C. Tasan, E. Akiyama, K. Tsuzaki, ScienceDirect Hydrogen-assisted decohesion and localized plasticity in dual-phase steel, Acta Mater. 70 (2014) 174–187. doi:10.1016/j.actamat.2014.01.048.

[94] A. Laureys, T. Depover, R. Petrov, K. Verbeken, Materials Characterization Microstructural characterization of hydrogen induced cracking in TRIP-assisted steel by EBSD, Mater. Charact. 112 (2016) 169–179. doi:10.1016/j.matchar.2015.12.017.

[95] S.P. Lynch, Environmentally Assisted Cracking: Overview of Evidence for an Adsorption-Induced Process, Acta Metall. 36 (1988) 2639–2661.

[96] S.P. Lynch, Metallographic Contributions to Understanding Mechanisms of Environmentally Assisted Cracking, Metallography. 23 (1989) 147–171.

[97] A. Pundt, R. Kirchheim, Hydrogen in Metals: Microstructural Aspects, Annu. Rev. 36 (2006) 555–608. doi:10.1146/annurev.matsci.36.090804.094451.

[98] K.A. Nibur, D.F. Bahr, B.P. Somerday, Hydrogen effects on dislocation activity in austenitic stainless steel, Acta Mater. 54 (2006) 2677–2684. doi:10.1016/j.actamat.2006.02.007.

[99] P.K. Pradhan, P.R. Dash, Micro void coalescence of ductile fracture in mild steel during tensile straining, Frat. Ed Integrità Strutt. 6 (2012) 51–60. doi:10.3221/IGF-ESIS.19.05.

[100] P. Fayek, S. Esser, V. Quiroz, C.D. Kim, Investigation of the pressure dependent hydrogen solubility in a martensitic stainless steel using a thermal agile tubular autoclave and thermal desorption spectroscopy, Metals (Basel). 11 (2021) 1–10. doi:10.3390/met11020231.

[101] B. Bal, B. Çetin, F.C. Bayram, E. Billur, Effect of hydrogen on fracture locus of Fe–16Mn–0.6C–2.15Al TWIP steel, Int. J. Hydrogen Energy. 45 (2020) 34227–34240. doi:10.1016/j.ijhydene.2020.09.083.

[102] M. Enomoto, L. Cheng, H. Mizuno, Y. Watanabe, T. Omura, J. Sakai, K. Yokoyama, H. Suzuki, R. Okuma, Hydrogen Absorption into Austenitic Stainless Steels Under High-Pressure Gaseous Hydrogen and Cathodic Charge in Aqueous Solution, Metall. Mater. Trans. E. 1 (2014) 331–340. doi:10.1007/s40553-014-0034-5.

[103] B. Bal, B. Okdem, F.C. Bayram, M. Aydin, A detailed investigation of the effect of hydrogen on the mechanical response and microstructure of Al 7075 alloy under medium strain rate impact loading, Int. J. Hydrogen Energy. 45 (2020) 25509–25522. doi:10.1016/j.ijhydene.2020.06.241.

[104] M.R. Louthan, Hydrogen embrittlement of metals: A primer for the failure analyst, J. Fail. Anal. Prev. 8 (2008) 289–307. doi:10.1007/s11668-008-9133-x.

[105] M. Elboujdaini, R.W. Revie, Metallurgical factors in stress corrosion cracking (SCC) and hydrogen-induced cracking (HIC), J. Solid State Electrochem. 13 (2009) 1091–1099. doi:10.1007/s10008-009-0799-0.

[106] S.P. Lynch, Gaseous Hydrogen Embrittlement of Materials in Energy Technologies: The Problem, its Characterisation and Effects on Particular Alloy Classes, 2012. doi:10.1533/9780857093899.2.274.

[107] I.M. Robertson, P. Sofronis, A. Nagao, M.L. Martin, S. Wang, D.W. Gross, K.E. Nygren, Hydrogen Embrittlement Understood, Metall. Mater. Trans. B Process Metall. Mater. Process. Sci. 46 (2015) 1085–1103. doi:10.1007/s11663-015-0325-y.

[108] F.G. Wei, K. Tsuzaki, Hydrogen trapping phenomena in martensitic steels, in: Gaseous

Hydrog. Embrittlement Mater. Energy Technol. Probl. Its Characterisation Eff. Part. Alloy Classes, 2012: pp. 493–525. doi:10.1533/9780857093899.3.493.

[109] J.W. Watson, Y.Z. Shen, M. Meshii, Effect of Cathodic Charging on the Mechanical Properties of Aluminum, Metall. Trans. A. 19 (1988) 2299–2304.

[110] S.A.A.L. Duheisat, An Investigation of Mechanical Degradation of Pure Copper by Hydrogen, Contemp. Eng. Sci. 7 (2014) 165–178.

[111] X. Yang, B. Zhang, Material embrittlement in high strain-rate loading, Int. J. Extrem. Manuf. 1 (2019). doi:10.1088/2631-7990/ab263f.

[112] R. Silverstein, D. Eliezer, B. Glam, Hydrogen Effect on Duplex Stainless Steels at Very High Strain Rates, Energy Procedia. 107 (2017) 199–204. doi:10.1016/j.egypro.2016.12.172.

[113] B. Bal, B. Okdem, F.C. Bayram, M. Aydin, A detailed investigation of the effect of hydrogen on the mechanical response and microstructure of Al 7075 alloy under medium strain rate impact loading, Int. J. Hydrogen Energy. (2020). doi:10.1016/j.ijhydene.2020.06.241.

[114] M. Tajally, Z. Huda, H.H. Masjuki, A comparative analysis of tensile and impact-toughness behavior of cold-worked and annealed 7075 aluminum alloy, Int. J. Impact Eng. 37 (2010) 425–432. doi:10.1016/j.ijimpeng.2009.08.009.

[115] D. Pérez Escobar, T. Depover, L. Duprez, K. Verbeken, M. Verhaege, Combined thermal desorption spectroscopy, differential scanning calorimetry, scanning electron microscopy and X-ray diffraction study of hydrogen trapping in cold deformed TRIP steel, Acta Mater. 60 (2012) 2593–2605. doi:10.1016/j.actamat.2012.01.026.

[116] D. Pérez Escobar, K. Verbeken, L. Duprez, M. Verhaege, Evaluation of hydrogen trapping in high strength steels by thermal desorption spectroscopy, Mater. Sci. Eng. A. 551 (2012) 50–58. doi:10.1016/j.msea.2012.04.078.

[117] N. Winzer, O. Rott, R. Thiessen, I. Thomas, K. Mraczek, T. Höche, L. Wright, M. Mrovec, Hydrogen diffusion and trapping in Ti-modified advanced high strength steels, Mater. Des. 92 (2016) 450–461. doi:10.1016/j.matdes.2015.12.060.

[118] T. Schaffner, A. Hartmaier, V. Kokotin, M. Pohl, Analysis of hydrogen diffusion and trapping in ultra-high strength steel grades, J. Alloys Compd. 746 (2018) 557–566. doi:10.1016/j.jallcom.2018.02.264.

[119] A.G. Atkins, Fracture in forming, J. Mater. Process. Technol. 56 (1996) 609–618. doi:10.1016/0924-0136(95)01875-1.

[120] F.A. McClintock, A Criterion for Ductile Fracture by the Growth of Holes, J. Appl. Mech. 35 (2016) 363.

[121] J.R. Rice, D.M. Tracey, On the ductile enlargement of voids in triaxial stress fields*, J. Mech. Phys. Solids. 17 (1969) 201–217. doi:10.1016/0022-5096(69)90033-7.

[122] Y. Bai, X. Teng, T. Wierzbicki, On the application of stress triaxiality formula for plane strain fracture testing, J. Eng. Mater. Technol. Trans. ASME. 131 (2009) 0210021–02100210. doi:10.1115/1.3078390.

[123] S. Basu, A.A. Benzerga, On the path-dependence of the fracture locus in ductile materials: Experiments, Int. J. Solids Struct. 71 (2015) 79–90. doi:10.1016/j.ijsolstr.2015.06.003.

[124] A. Nagao, M. Dadfarnia, B.P. Somerday, P. Sofronis, R.O. Ritchie, Hydrogen-enhanced-plasticity mediated decohesion for hydrogen-induced intergranular and "quasi-cleavage" fracture of lath martensitic steels, J. Mech. Phys. Solids. 112 (2018) 403–430. doi:10.1016/j.jmps.2017.12.016.

[125] J. Venezuela, Q. Liu, M. Zhang, Q. Zhou, A. Atrens, A review of hydrogen embrittlement of martensitic advanced high-strength steels, Corros. Rev. 34 (2016) 153–186. doi:10.1515/corrrev-2016-0006.

[126] R. Valentini, M.M. Tedesco, S. Corsinovi, L. Bacchi, M. Villa, Investigation of mechanical tests for hydrogen embrittlement in automotive PHS steels, Metals (Basel). 9 (2019) 934. doi:10.3390/met9090934.

CURRICULUM VITAE

BSc, Abdullah Gul University-Mechanical Engineering (06/2018), Kayseri/Turkey

MSc, Abdullah Gul University-Advanced Materials and Nanotechnology (05/2021)

Research Associate - The Researcher Training Program for Defense Industry (SAYP)

Email: ferdicaner.bayram@agu.edu.tr

Mobile no: 00905317078544

Summary

➢ Committed, dynamic and versatile prospective Ph.D. student (currently thesis master's degree student) with 5 years of lab experience in materials characterization, microstructure property relationship, hydrogen embrittlement and digital image correlation leading to 4 published papers in well-known journals

➢ Excellent team member and determined, eager and strong personality that involved in prestigious scientific projects (TUBITAK&SAYP projects in TURKEY and Collaborative Research Centre 1153 Project A in Germany) as a research associate and motivated to be a part/member of active research labs with big aims/projects.

➢ Creative and self-motivated individual with easy-integration in a multicultural environment with a unique combination of detail-oriented mindset, driven personality, analytical skills and proven ability to beat tight deadlines by working in a fast-paced work environment leading to the completed project reports and articles published in prestigious journals.

Education

M.Sc., Advanced Materials, Abdullah Gul University, Kayseri/TURKEY 2018 - 2021

Prep. S, English for Academic Purposes, English Language Center, NJ/USA 07/2014 – 09/2014

B.Sc., Mechanical Engineering, Abdullah Gul University, Kayseri/TURKEY 2013 - 2018

Publications

1. Burak Bal, Bilge Okdem, **Ferdi Caner Bayram**, Murat Aydin, A detailed investigation of the effect of hydrogen on the mechanical response and microstructure of Al 7075 alloy under medium strain rate impact loading, International Journal of Hydrogen Energy, IF: 4.93 https://doi.org/10.1016/j.ijhydene.2020.06.241
2. Burak Bal, Baris Cetin, **Ferdi Caner Bayram**, Eren Billur, Effect of hydrogen on fracture locus of Fe-16Mn-0.6C-2.15Al TWIP steel, International Journal of Hydrogen Energy, IF: 4.93 https://doi.org/10.1016/j.ijhydene.2020.09.083

3. Susanne Elisabeth Thürer, Julius Peddinghaus, Norman Heimes, **Ferdi Caner Bayram**, Burak Bal, Johanna Uhe, Bernd-Arno Behrens, Hans Jürgen Maier, Christian Klose, Lateral angular coextrusion: geometrical and mechanical properties of compound profiles, Metals, IF: 1.7 https://doi.org/10.3390/met10091162

4. Ferdi Caner Bayram, Mehmet Fazil Kapcı, Adile Yuruk, Burak Bal, Ismail Alper Isoglu, Investigations of strain rate, size and crack length effects on the mechanical response of PCL electrospun membranes. In press